

UC Santa Barbara

UC Santa Barbara Electronic Theses and Dissertations

Title

Light Activated Delivery of Biomolecules Using Hollow Gold Nanoshells: From Increasing Therapeutic Efficiency to Protein Tracking using VIPERnano

Permalink

<https://escholarship.org/uc/item/4fb3j6z4>

Author

Morgan, Erin Nicole

Publication Date

2019

Peer reviewed|Thesis/dissertation

UNIVERSITY OF CALIFORNIA

Santa Barbara

Light Activated Delivery of Biomolecules Using Hollow Gold Nanoshells: From Increasing
Therapeutic Efficiency to Protein Tracking using VIPER^{nano}

A dissertation submitted in partial satisfaction of the
requirements for the degree Doctor of Philosophy
in Chemistry

by

Erin Nicole Morgan

Committee in charge:

Professor Norbert O. Reich, Chair

Professor Peter Ford

Professor Irene Chen

Professor Cyrus Safinya

June 2019

The dissertation of Erin Nicole Morgan is approved.

Cyrus Safinya

Irene Chen

Peter Ford

Norbert Reich, Committee Chair

June 2019

ACKNOWLEDGEMENTS

The research conducted in this thesis was only possible thanks to the help and collaboration with many individuals. First, I would like to thank Dr. Norbert Reich for his support throughout my PhD Career as my PhD advisor. His extreme enthusiasm for data and science communication were great motivators for my success as a graduate student. His constant eagerness to learn lead him to a sabbatical in Oregon where he sparked two very fruitful collaborations for our lab and my dissertation material. One with a lab at OHSU led by Dr. Kimberly Beatty and graduate student Julia Doh on the VIPER^{nano} protein tracking experiments. I am grateful for their contribution to this project and communication throughout the project's research. The second collaboration at OSU with Dr. Siva Kolluri's lab on delivery of NuBCP peptide with our hollow gold nanoshells. Special thanks to Martin Pearce and John Gamble for their assistance in the zebrafish embryo experiments that were crucial for this project's success. I'd like to thank the undergraduate researchers I've had a pleasure of working with, Jenny Wang and Shannon Moreno for their assistance with experiments as well as their company alongside the highs and lows of research in their years here at UCSB. I am very thankful for the help and great research collaboration with Shannon Moreno, a former undergraduate researcher and Thibault Vitale, a visiting master's student from France. With their assistance, I was able to complete the exciting research on dual wavelength release included in this thesis. I would also like to the graduate and undergraduate students that shared many memories in the Reich Lab throughout the years including Jonathan Sandoval, Hanson Huang, Nick Davis, Jason Carmody, Mathilde Zoch, Dominik Wupperfeld, and Camilo Guzman. A special thanks to Dean Morales and Xiao Huang for their unwavering support as mentors both during their PhD studies and long after. Finally, I would like to thank my moral support system, my family and my friends here in

Santa Barbara. To Victoria and Alisa, friends from the first day of our first year as graduate students at UCSB, your support of friendship was encouraging through rough patches endured throughout our PhD careers and contributed greatly to my sanity as a graduate student. My dad, for inspiring me to pursue a PhD, my mom for always picking up the phone when I needed advice, and my siblings for their constant support. Finally, to my Fiancé, Alex and our two cats Piggy and Quilo, you have supported and encouraged me from day one reminding me of my capabilities and constantly believing in me.

VITA OF ERIN NICOLE MORGAN
June 2019

EDUCATION

Doctor of Philosophy in Chemistry, Department of Chemistry and Biochemistry, University of Santa Barbara, USA, June 2019
Bachelor of Science in Chemistry, ACS certified, Iona College, NY, May 2013

PROFESSIONAL EMPLOYMENT

Graduate Student Researcher with Dr. Norbert Reich <i>University of California, Santa Barbara</i>	01/2014- 05/2019
Teaching Assistant, Department of Chemistry General Chemistry and Biochemistry Laboratory <i>University of California, Santa Barbara</i>	09/2014- 12/2018
Research Assistant to Dr. Allen Padwa <i>Metabolix Inc.</i>	Summer 2010 & Winter 2012
Summer Intern <i>Bruker Optics</i>	Summer 2012

PRESENTATIONS

- “In vivo targeting of BCL-2 phenotypic conversion through hollow gold nanoshell delivery in chemoresistant H460 lung cancer cells”, Keystone Symposia: Delivering Therapeutics Across Biological Barriers, Dublin, Ireland, 2019
- “Controlling the Genome: Light activated delivery of Gene Editing proteins and siRNA allows for up and down regulation of the genome using gold nanoparticles”, Keystone Symposia: Genome Engineering, Victoria, Canada, 2019
- “Light Directed Delivery of Proteins and Peptides: Gene Editing Cas9 and NuBCP Peptide Targeting BCL-2 in Resistant Cancer Cells”, ASBMB, San Diego, 2018
- “Spatial and Temporal Control of mRNA Delivery Using Hollow Gold Nanoshells, UC Systemwide Bioengineering Symposium, UCLA, 2017
- “Characterization of native and model proteins by Near-Infrared Spectroscopy”, NY ACS 61th URS, CUNY, NY, April 27, 2013
- “Characterization of Native and Model Proteins by Near-Infrared Spectroscopy”, The 4th Annual URD, Iona College. April 16, 2013

PUBLICATIONS

- Morgan, E.; Gamble, J. T.; Pearce, M. C.; Elson, D. J.; Tanguay, R. L.; Kolluri, S. K.; Reich, N. O. Improved in Vivo Targeting of BCL-2 Phenotypic Conversion through Hollow Gold Nanoshell Delivery. *Apoptosis Int. J. Program. Cell Death* 2019.
- Morgan, E.; Doh, J.; Beatty, K.; Reich, N.O. VIPERnano: An improved live cell protein tracking technology. *Nano Letters*. Manuscript submitted
- Morgan, E.; Wupperfeld, D.; Morales, D. P.; Reich, N. O. Shape Matters: Gold Nanoparticle Shape Impacts the Biological Activity of SiRNA Delivery. *Bioconjug. Chem.* 2019.
- Morgan, E.; Moreno, S; Vital, T; Huang, X; Reich, N.O. Controlling the Genome: up and down-regulation with gold nanorods and near infrared light. *ACS Applied Materials and Interfaces*. Manuscript in preparation.
- Morales, D. P.; Morgan, E. N.; McAdams, M.; Chron, A. B.; Shin, J. E.; Zasadzinski, J. A.; Reich, N. O. Light-Triggered Genome Editing: Cre Recombinase Mediated Gene Editing with Near-Infrared Light. *Small* 2018, 14 (30), 1800543.

ABSTRACT

Light Activated Delivery of Biomolecules Using Hollow Gold Nanoshells: From Increasing
Therapeutic Efficiency to Protein Tracking using VIPER^{nano}

by

Erin Nicole Morgan

Intracellular delivery of biomolecules is hindered by both the size and charge of the biomolecule. While a number of delivery methods are available for genetic material, few are available for larger biomolecules like peptides and proteins. The delivery of these biomolecules are often limited to viral transfections of the genetic material which can lead to off-target gene editing due to prolonged expression of a protein within a cell. We developed and studied a delivery method for poly-histidine tagged proteins and peptides of variable sizes and charges for transient protein expression with light control via hollow gold nanoshells (HGNs). The construct of our delivery system involves a thiolated strand (nucleic acid or PEG based) containing an NTA attached to the particle's gold surface. A his-tagged protein or peptide of interest is attached to the HGN via copper-NTA affinity. Endosomal uptake of these particles is mediated through an orthogonal strand containing a cell penetrating peptide (CPP). Protein release and endosomal disruption is achieved after irradiation with a focused femtosecond pulsed-laser of biologically benign near-infrared light. This thesis evaluates a variety of areas, from increasing the therapeutic efficacy of an apoptotic peptide to visualization of protein movement using live cell imaging with VIPER^{nano}.

TABLE OF CONTENTS

I. INTRODUCTION.....	1
A. PROTEIN THERAPEUTICS.....	1
B. PROTEIN TRACKING.....	2
C. PLASMONIC NANOPRTICLES FOR BIOMOLECULE DELIVERY.....	4
D. REFERENCES.....	5
II. IMPROVED IN VIVO TARGETING OF BCL-2 PHENOTYPIC CONVERSION THROUGH HOLLOW GOLD NANOSHELL DELIVERY.....	11
A. ABSTRACT.....	11
B. INTRODUCTION.....	11
C. MATERIALS AND METHODS.....	13
D. RESULTS.....	19
E. DISCUSSION.....	28
F. CONCLUSION.....	30
G. REFERENCES.....	30
III. VIPERNANO: IMPROVED LIVE CELL PROTEIN TRACKING.....	35
A. ABSTRACT.....	35
B. INTRODUCTION.....	35
C. RESULTS AND DISCUSSION.....	37
D. CONCLUSIONS.....	48
E. MATERIALS AND METHODS.....	48
F. REFERENCES.....	53
IV. CONTROLLING THE GENOME: UP AND DOWN-REGULATION WITH GOLD NANORODS AND NEAR INFRARED LIGHT.....	59

A. ABSTRACT.....	59
B. INTRODUCTION.....	59
C. RESULTS AND DISCUSSION.....	61
D. CONCLUSIONS.....	67
E. EXPERIMENTAL SECTION.....	68
F. REFERENCES.....	74
V. SHAPE MATTERS: GOLD NANOPARTICLE SHAPE IMPACTS THE BIOLOGICAL ACTIVITY OF SIRNA DELIVERY.....	77
A.	
ABSTRACT.....	77
B. INTRODUCTION.....	77
C. RESULTS AND DISCUSSION.....	80
D. CONCLUSIONS.....	91
E. EXPERIMENTAL PROCEDURES.....	91
F. REFERENCES.....	99
VI. DETAILED EXPERIMENTAL PROCEDURES.....	105
A. CONFOCAL AND TWO PHOTON MICROSCOPY.....	105
AI. INTRODUCTION.....	105
AII. INTERNALIZATION EXPERIMENTS.....	106
AIII. RELEASE EXPERIMENTS.....	108
AIV. VISUALIZATION USING THE LEICA SP8.....	109
B. CRIPSR CAS9 DELIVERY.....	111
BI. INTRODUCTION.....	111
BII. INVITRO CLEAVAGE ASSAY.....	114

BIII. GFP KNOCKOUT STUDIES.....	115
BIV. INTERNALIZATION AND RELEASE STUDIES WITH CAS9-CY3.....	115
BV. REFERENCES.....	116

LIST OF FIGURES

- Figure II-1.** Optimization of NuBCP Loading onto HGNs. A. Ratio of Biotin:FAM complement strands on HGN-STV-TAT particles determines 1:9 particles allow for maximal loading of NuBCP with 3 μ M initial peptide concentration. B. Increase in loading of NuBCP-Cy5 on 32 pM particles with increasing initial concentrations of NuBCP. NuBCP loading is determined by Cy5 fluorescence in KCN etch of washed HGN-NuBCP pellet.....20
- Figure II-2.** Orthogonal surface chemistry of internalization peptide Streptavidin TAT and therapeutic peptide NuBCP on a HGNs. b. Size distribution of nanoparticles during coating steps. HGN particles have a Z-average diameter of 58 nm; HGN-DNA-, 79 nm; HGN-DNA-TAT, 141 nm; HGN-DNA-TAT-NuBCP, 190 nm. Image to the right displays TEM image of HGN-DNA-TAT. Scale bar 100 nm. c. Illustration of the delivery of HGN-NuBCP into a cancer cell. 1) Hollow gold nanoparticles coated in NuBCP (purple hexagon) are taken into the cell by internalization peptide Streptavidin TAT (red semi-circle) mediated endocytosis. 2) Irradiation with NIR 800nm light, releases NuBCP from nanoparticle and endosome into the cytosol. 3) NuBCP binds to the Bcl-2 loop domain and converts Bcl-2 (green) into a pro-apoptotic protein which inhibits anti-apoptotic proteins (orange) and activates other pro-apoptotic proteins (blue) on the mitochondria. 4) Activated pro-apoptotic proteins facilitate mitochondrial outer membrane permeabilization, initiating apoptosis, and results in cell death.....21
- Figure II-3.** Release of Cy5 labeled NuBCP shows laser dependent release. a. An increase in laser power leads to an increase in NuBCP release from HGN loaded with 900 nM NuBCP. Percent release is shown above bar graphs and determined by the percentage of peptide released into the supernatant after laser irradiation. Total peptide loaded is determined by KCN etch of the no laser pellet. b. Dark field microscopy demonstrates cellular internalization of gold nanoparticles (orange light scattering) only when TAT peptide is present on the particle surface. c. Release of FAM labeled DNA and Cy5 labeled NuBCP in HeLa cells using two photon microscope for NIR laser irradiation. Release of both DNA and peptide is shown from diffusion of dye labels throughout the cell after laser irradiation.....23
- Figure II-4.** (a) MDA-MB-231 cells were treated with 3.2 pM HGN, 3.2 pM HGN-NuBCP and were then irradiated with an 800 nm 5 kHz laser at 1 W as cells flowed through a borosilicate microcapillary tube at 100 μ L/min. 500 nM and 3 μ M NuBCP indicate the final concentration of NuBCP delivered in cell media via HGNs or in media alone for NuBCP only. Note the NuBCP only control was not treated with laser. Cell viability of MDA-MB231 cells was observed 96 hrs after laser irradiation. (b) Bcl-2 is expressed in both MDA-MB-231 and H460 R-PAC cells. Western Blot analysis of MDA-MB-231 and H460 R-PAC indicates levels of Bcl-2 and GAPDH is used as a loading control. (c) Laser dependent release of NuBCP-Cy5 in H460 cells with JC-1 assay shows mitochondrial destabilization as green fluorescence increases from the JC-1 monomer upon irradiation with two-photon 800 nm laser.....24
- Figure II-5.** Irradiation of H460 cells without NuBCP in the presence of HGN does not cause mitochondria depolarization. Irradiation of HGN in H460 cells with JC-1 assay does not show an increase in green fluorescence from the JC-1 monomer upon laser irradiation with 800 nm laser equipped 2 photon microscope indicating the mitochondria membranes remain intact post laser irradiation without NuBCP on the HGNs. No fluorescence is observed in the

Cy5 channel due to no peptide on the HGNs. Confirmation of particles in cells through Z-stack slice of 800 nm irradiation which shows the surface resonance light scattering produced by the HGN internalized in the H460 cells. The white resonant light scattering is demonstrated through the white puncta visualized throughout the cells in the Z-stack slice during 800 nm irradiation.....25

Figure II-6. (a) Effect of HGN-NuBCP-9 on survival and development of Zebrafish embryos. Treatment with vehicle (PBS-Tween 0.01%) and HGN-NuBCP-9 10 μ M in embryo media. Survivorship was assessed by counting the number of live versus dead fish in each group (n=30 all groups). (b) H460 derived paclitaxel line is resistant to 10 nM paclitaxel treatment. Percentage viability is calculated relative to vehicle treatment. Data is representative of three independent assays done in triplicate. Two-way ANOVA with Sidak's multiple comparisons post-test, ****P<0.0001. Log2 fold change of cell area for vehicle (c), HGN (e) and HGN-NuBCP (g) exposed H460 PacR cells in xenografts after no exposure (-Laser) or exposure (+Laser) to two-photon NIR laser. Data normalized to no laser control; Vehicle (- Laser) N = 20, (+ Laser) N = 20; HGN: (- Laser) N = 20, (+ Laser) N = 19. HGN-NuBCP: (- Laser) N = 19, (+ Laser) N = 20. Representative figures zebrafish xenografts for vehicle (d), HGN (f) and HGN-NuBCP (h) treatment groups at 1 and 4 day post injection (dpi) with transplanted H460 PacR cells (Red); 10x magnification.....27

Figure III-1. VIPERnano relies on much smaller fluorescent protein tags. (A) Nucleosome (PDB ID: 1kx5) with H2B-GFP (GFP PDB ID: 2yog) shows the DNA (tan) wrapped around the octamer of histone proteins (light blue) including the two H2B proteins (dark blue) fused to GFP (green). (B) H2B-GFP fusion monomer with size markers for GFP (27 kDa) and H2B (15 kDa) (C) H2B-CoilE fusion monomer with size markers for CoilE (5.2 kDa) and H2B (15 kDa). Structure prediction for CoilE peptide model with PEPFOLD3 24,25.....38

Figure III-2. Particle assembly strategy and size analysis (a) VIPER technology strategy. A target protein is genetically tagged with the CoilE peptide. The tagged protein can then be labeled by dimerization with a CoilR peptide conjugated to a fluorescent dye delivered with a HGN. (b) Illustration of HGN construct with 1:1 loading of thiol-PEG-NTA (CoilR-Cy5 strand): Thiol-PEG-biotin (Internalization strand). The biotin terminated PEG was labeled with streptavidin TAT for internalization while the orthogonal NTA terminated strand allowed for CoilR-Cy5 loading. (c) Dynamic light scattering size distribution of nanoparticles at different stages of synthesis and conjugation step.....39

Figure III-3. (a) Schematic of HGN-CoilR-Cy5 (magenta) internalization and release from the endosome with NIR light colocalizes with cellular targets (e.g., H2B-CoilE-mEmerald and Mito-CoilE-mEmerald). (b) Streptavidin-TAT coating on nanoparticles allows for internalization of HGN-CoilR-Cy5 into HeLa cells observed by Cy5 fluorescence and light scattered from the gold nanoparticles with dark field microscopy (orange puncta).....41

Figure III-4. Light activated release of CoilR-Cy5 from HGN is NIR light activated. (a) Release of CoilR-Cy5 from 32 pM HGNs quantified by fluorescence intensity observed in the supernatant solution after NIR irradiation and centrifugation. Samples were centrifuged and their pellets were analyzed for total peptide loading with KCN etch and fluorescence detection. (b) HeLa cells were treated with HGN-CoilR-Cy5 and irradiated using a two-photon microscope at 800 nm. Release of CoilR-Cy5 upon NIR irradiation is demonstrated

by the diffusion of CoilR-Cy5 across HeLa cells as the peptide was released from the endosomal membrane into the cytosol. The blue boxes indicate region of interests (ROIs) selected to demonstrate CoilR-Cy5 diffusion through pixel distribution plots. (c) Magnification of selected ROIs demonstrating CoilR-Cy5 peptide diffusion from fluorescent puncta after NIR laser irradiation. (d) Smoothed pixel distribution plot (2nd order, 80 neighbors) where an increase in gray value demonstrates the increase in Cy5 fluorescence observed in an averaged plot from N = 4 before laser irradiation (black trace) and N= 4 after laser irradiation (magenta trace).....43

Figure III-5. (a) Confocal imaging of HeLa cells transfected with Mito-CoilE-mEmerald 24 hours post laser irradiation of a region of interest (ROI) with internalized HGN-CoilR shows specific labeling (white merge) of cellular mitochondria (Mito-CoilE-mEmerald in green) with CoilR-Cy5 (magenta) increases with higher laser irradiation power. Two-photon NIR excitation at full power was 2.4 W. (b) Overlay of mEmerald and Cy5 in high resolution fluorescence microscopy of CoilR-Cy5 in HeLa cells with H2B-CoilE-mEmerald over 10 seconds shows peptide movement only in irradiated samples (top image) and little to no movement in non-irradiated samples (bottom image) N=3 for both laser conditions.....45

Figure III-6. Live tracking of cellular dynamics using HGN-CoilR (a) HeLa cells transfected with Mito-CoilE-mEmerald were treated with 3.2 pM HGN-CoilR and irradiated using a two-photon microscope at 800 nm. 24 hours post laser irradiated images were collected over a period of 2.5 hours to demonstrate the ability to track mitochondria movement over time. Each photo is a combination of 100 images taken as a time lapse to generate one NanoJ-SRRF high resolution image. (b) HeLa cells transfected with H2B-CoilE-mEmerald were treated with 3.2 pM HGN-CoilR and irradiated. The cells were later re-localized using gridded culture dishes 24 and 48 hours post laser irradiation to observe the separate of two nuclei using the CoilR peptide. (c) Time lapse imaging of (a) demonstrating dynamic movement of mitochondria with both CoilR and mEmerald. White scale bar in images corresponds to 8 μm.....47

Figure IV-1. Illustration of the mechanism of the selective release. Upon irradiation with a 700 nm laser the GNR releases the Cre recombinase on the surface while the siRNA stays bound on the NBs. Upon irradiation with a 1100 nm laser, the NBs release siRNA targeting GFP from the surface of the particle.....62

Figure IV-2. Selective release of gold nanoparticle cargo. a) UV-vis absorbance spectra show different absorbance peaks for both types of particles. b) TEM images of GNR and NB. Scale bar represents 100 nm. c) cell free experiment with GNR and NB displays a selective release of FAM-DNA cargo dependent on the wavelength of NIR excitation. d) Selective release of FAM-DNA from GNR internalized in HeLa cells where focused cells were irradiated with 800 nm (orange box) and another set was irradiated with 1020 nm (blue box) using two-photon excitation. Diffusion of the puncta shown in area irradiated with 800 nm only.....64

Figure IV-3. a) Gene editing by the Cre recombinase after release from the GNRs followed by the knockdown effect after release of the GFP siRNA from the NBs. b) Up and down regulation of GFP as measured by flow cytometry compared to 1 % in cell only control. HeLa reporter cells with both sets of particles but with no laser irradiation, 1.4 % ; 48 hours after 800 nm treatment, 11.2 % ; and 96 hours after 800 nm and 48 hours after 1150 nm, 3.2 %. c) Up and down regulation of GFP visualized by fluorescent microscopy. I) Cells containing

both particles and irradiated with both laser wavelengths show efficient Cre release after 800 nm laser and almost total down regulation after 1150 nm laser as demonstrated by GFP fluorescence. II) Cells containing both GNR and NB and irradiated with only 800 nm light retain green fluorescence III) Cells with only GNR particles and irradiated only with 800 nm light show green fluorescence IV) Cells containing both particles and are not irradiated with either NIR wavelengths remain non fluorescent. Scale bar represents 100 μm67

Figure V-1. Characterization of hollow gold nanoshells (HGNS), hollow gold nanocages (HGNC), and gold nanorods (GNR). Transmission electron microscope (TEM) imaging of gold nanoparticles depicts characteristic hollow structures of HGNS and HGNC as evidenced by the decreased electron density at the centers of the particles, while GNR are confirmed to be rod-like. TEM images (JEOL 1230 TEM) are accompanied by UV-Vis absorption spectra showing primary plasmon peaks at ~ 750 nm for each class of nanoparticle. Average size of each gold nanoparticle is ~ 45 nm (TEM scale bar is 100 nm, $n = 20$).....81

Figure V-2. Optimization of siRNA loading onto each kind of gold nanoparticle. (a) Total siRNA loaded onto 3.2 pM particles determined by KCN etch after Method 1 and Method 2. (b) Using method 1 for absorption of RNA onto GNR surface results in a UV-Vis spectrum where the 500 nm peak is much larger than the ideal surface plasmon peak at 800 nm. (c) Longer incubation times with RNA for GNR leads to a doubling in the amount of RNA loaded onto the surface of the particle.....83

Figure V-3. HGNS show the highest level of loading and absolute quantity of siRNA release compared to HGNC and GNR with Qubit assay. (a) Total siRNA loaded onto 3.2 pM particles determined after dissolved with a solution containing KCN after initial loading of 3 μM siRNA (1,000 X the max loading capacity of siRNA calculated). (b) Release of loaded siRNA from 3.2 pM gold nanoparticles after exposure to 800 nm femtosecond pulsed NIR laser light. Percent release from each particle is indicated above each bar ($n = 6$).....84

Figure V-4. HGNS and HGNC show comparable and superior gene knockdown efficiencies over GNR. (a) Flow cytometry histograms of internalization efficiencies of the different gold nanoparticles into HeLa cells as described by changes in fluorescence profiles due to Cy3 labeled particle uptake. Percentage of cells with Cy3 internalized shown for each type of gold nanoparticle was determined via flow cytometry. (b) Quantitative determination of the decreased GFP expression after knockdown in HeLa-GFP cells via flow cytometry. Percent decrease in GFP expression determined from number of cells not fluorescent three days after treatment of HeLa-GFP cells with a particle concentration of 3.8×10^{-12} M (solid bar) or 7.6×10^{-12} M (striped bar). (c) Spatially controlled knockdown of GFP using NIR excitation by confocal microscopy. GFP-fluorescence (green) and bright-field (grey) microscopy images of HeLa-GFP cells three days after siRNA release (yellow square) for GFP-knockdown treated with the different gold nanoparticles. Scale bar in the microscopy images is 100 μm86

Figure V-5. Further characterization of different gold nanoparticles demonstrating DNA loading and enhancement effect of GNR on cy3 fluorescence. (a) Particle concentration of the different gold nanoparticles with double-stranded DNA attached onto the particle surface. All conversions shown in particles per mL are for samples where the maximum absorbance at 800 nm was 1 absorbance unit, as measured with a UV-vis spectrophotometer using a 1 cm

pathlength cuvette. The variance is shown as standard error of the mean. The values were determined using the NanoSight NS300. (b) Loading of the different gold nanoparticles functionalized with DNA. (c) Dark-field microscopy images show the internalization of the gold nanoparticles from the orange colored light scattered from the gold nanoparticles. The cy3-fluorescence shows the internalization of the gold particles from the red fluorescence observed from the DNA strand attached to the gold nanoparticles. Scale bar in the microscopy images are 100 μm88

Figure V-6. Spatially controlled knockdown of GFP using NIR excitation by confocal microscopy. GFP-fluorescence (green) and bright-field (grey) microscopy images of HeLa-GFP cells before irradiation (two columns on the left) and three days after siRNA release (yellow square) for GFP-knockdown treated with the different gold nanoparticles (two columns on the right). Merged images used to show the GFP knockdown after 72 h. Scale bar in the microscopy images is 100 μm90

Figure VI-1. Cy5 and GFP Z-stack show optical focal planes separate depending on dye used. The fluorescent bead imaged had both FAM and Cy5 attached to the surface of the particle. In the bottom image, a single HeLa cell expressing MITO-CoilE-GFP with CoilR-Cy5 shows separate layers for the two dyes.....106

Figure VI-2. Three different particle constructs for Cas9/sgRNA delivery. I. Delivery of sgRNA to HeLa-Cas9 cell line involves a thiolated protector group that would hybridize to the sgRNA and later would be delivered into cells expressing Cas9 for light triggered activation of the CRISPR/Cas9 system. II. Delivery of Cas9/sgRNA with thiol linker works similarly to I however the ribonucleoprotein (RNP) complex is used for delivery of both Cas9 as well as the sgRNA. III. Delivery of NLS-Cas9/sgRNA with His-Tagged Cas9 complexed to sgRNA involves attachment of the 6xHis tag on Cas9 for delivery and association of the sgRNA with the Cas9 for delivery of the system.....112

Figure IV-3. Modified figure from Jain et. al. A. Effect of length and position of protectors using the in vitro cleavage assay with Cas9 and target DNA strand described in Jain et. al. B. Effect of length and position of protectors using flow cytometry analysis of GFP fluorescence gene knockdown. The protectors highlighted in blue indicate “poor protectors” that allow for gene knockdown when hybridized to sgRNA. Red protectors do not allow for gene knockdown and are comparable to the control sgRNA that does not target the DNA template. C. a list of ordered thiolated oligos for testing loading onto the HGNs for delivery.....114

I. INTRODUCTION

A. PROTEINS AS THERAPEUTICS

The study and use of protein therapeutics for medical treatments as increased dramatically since the first ever recombinant protein therapeutic, human insulin, over 25 years ago².

Prior to this, the majority of new therapeutics were small molecule drugs that affect biological pathways. Protein therapeutics can be categorized into proteins with enzymatic activity, proteins that block, stimulate or tag their molecular targets, vaccines and diagnostics². They have a number of advantages over small molecule therapeutics. The first of which is specificity, with protein therapeutics, the action of the protein itself is very specific and therefore less likely to interfere with normal biological processes causing off-target effects. If the protein therapeutic interacts with another protein for therapeutic effect, the area of contact could be much larger than a small-molecule binding pocket, potentially increasing the specificity of the protein therapeutic for the drug target of interest. Protein therapeutics also have the ability to simply replace a protein coded by a mutagenic or deficient gene thereby avoiding gene therapy².

Small-molecule therapeutics however, still have advantages over protein therapeutics such as long term stability, scalability for manufacturing and intracellular availability³.

The last of which is the largest barrier for protein therapeutics. Current protein therapeutics are limited to extracellular protein targets due to their inability to cross the cellular membrane. This lead to the fusion of proteins to internalization peptides that allow for endocytic uptake of the protein of interest for intracellular delivery.

Intracellular delivery using protein fusions to cell penetrating peptides (CPP) like poly arginine often result in endosomal entrapment⁴ resulting in prevention of the drug

reaching the cytosol and therefore reducing efficacy of the therapeutic. It was found that although the CPP fusion proteins allowed for efficient cellular uptake, their endosomolytic activity was very poor⁵. This was demonstrated when an organic fluorophore was attached to a CPP and observed through fluorescent microscopy, a punctate distribution of the fluorophore inside cells was observed indicating endosomal entrapment⁶. Some delivery techniques take advantage of the acidification of the endosome overtime for release of their cargo from the endosome. In these instances, endosomal escape is achieved through the addition of peptides that can disrupt the endosomes at an acidic pH, such as a class of peptides called PMAPs (pH dependent membrane-active peptides⁷. Unfortunately, these peptide fusions have a significant impact on the localization of the protein therapeutic⁷. This was illustrated by a HA2-TAT-mCherry construct⁸. Interestingly, the fusion allowed for endosomal lysis (as shown by distribution of fluorescent dextran internalized with the protein constructs) however the mCherry fused protein retained in the endosomes. It is hypothesized that the lipophilicity of the PMAPs required for disruption of the endosomal membranes may alter the trafficking and function of the attached cargo⁸. This as well as the overall toxicity of many of the PMAPs has limited the therapeutic window of protein therapeutics. In this work we will demonstrate the delivery of protein therapeutics using hollow gold nanoshells which have potential to overcome many of the barriers present in current protein therapeutics.

B. PROTEIN TRACKING

The visualization and tracking of proteins through fluorescence microscopy has transformed cell biology⁹. Antibody-based methods form the basis of many such studies, yet require specific reagents and many proteins are not amenable to this approach; the reliance on cell fixation forms another barrier^{10,11}. Fluorescent protein (FP) fusion tags

provided an enormous improvement by allowing the tracking of proteins in live cells, with new colored variants finding applications for bioimaging and protein tracking¹¹⁻¹⁴. However, FP fusion tags rely on proteins that in many cases are larger than the protein of interest, which can alter protein function, trafficking, stability and localization between the target protein and partner molecules^{15,16}. More recently, smaller peptide epitopes consisting of ~ 10 amino acids like FLAG have been explored as suitable alternatives to the large sized FPs¹⁷. However, these methods still require membrane permeabilization, fixation and incubation with anti-FLAG antibodies, which limits their capabilities for live cell imaging.

The work demonstrated in this thesis enabled the expansion of smaller sized coiled coil probes for protein tracking in live cells. Coiled coil protein tagging involves the endogenous expression of a fusion peptide to a protein of interest (POI) which is labeled by incubation and heterodimerization with a second peptide conjugated to an organic fluorophore¹⁸⁻²¹. Previous use of this technology, versatile interacting peptides (VIP) tags was used to label both extracellular and intracellular proteins^{20,21}. The VIP tags are smaller than fusion protein tags, around 5-7 kDa compared to 30 kDa in size, however require membrane permeabilization and fixation of cells for intracellular POIs²⁰. The technology was expanded to live cell imaging with VIPER (using Coil E as the fusion peptide and Coil R-Cy5 as the delivered secondary coil). In this case, extracellular targets like the transferrin receptors were targeted and internalization was visualized over a period of time. The VIPER technology advanced the coiled coil platform however, delivery of the labeling peptide continued to hinder the advancement to live cell imaging with smaller fusion tags. This work demonstrates delivery of the Coil R-Cy5 labeling

peptide using our HGN platform to introduce small fusion peptide tags for intracellular protein tracking for live cell imaging.

C. PLASMONIC NANOPARTICLES FOR BIOMOLECULE DELIVERY

Gold nanoparticles are inorganic particles that can exist in a variety of shapes and sizes. This work will cover hollow gold nanoshells as well as gold nanorods, nanobones and cages. Gold nanoparticles are often seen as attractive for their biocompatibility and easy surface functionalization²². Surface functionalization is achieved with a covalent gold-thiol bond between a sulfhydryl (SH) functional group on the cargo and the gold on the surface of the particle²³. Successful loading of thiolated RNA, DNA and, polyethylene glycol (PEG) strands are demonstrated throughout the chapters of this thesis.

Gold nanoparticles are also an attractive delivery vehicle due to their tunable surface plasmon resonance (SPR). The oscillating electromagnetic field of light induces a coherent oscillation of free electrons on the gold surface of the particle. The amplitude of that oscillation reaches a maximum at a specific wavelength of light, termed the SPR²⁴. The wavelength of SPR for the gold nanoparticles can be tuned to a specific wavelength based on the overall size, structure and shape of the particle²⁵. The particles in this thesis are ~ 45 nm in diameter and absorb in the near infrared (NIR) region of the electromagnetic spectrum. This research aims to use particles that absorb in the NIR region of light where biological samples are essentially “transparent”^{26,27}. Light controlled systems commonly use high energy light in the ultraviolet (UV) region to allow for release of their cargo, which is often damaging to cell viability due to the amount of energy absorbed by the tissue and therefore should be avoided for potential

therapeutic applications²⁷. The NIR light tuned to the SPR of the gold particles allows for cleavage of gold thiol bond using pulsed (femto and picosecond) lasers²⁸ .

Mentioned previously, major barriers in delivery of biologics are the efficiency of uptake into cells as well as endosomal release²⁹. The particles discussed in this work use an internalization peptide, the trans-activator of transcription (TAT) peptide which allows for efficient internalization of the particles into a variety of cell lines ^{30,31}. Once endocytosed, the particles remain in the endosomes until released using the NIR light. The localized heating caused by the oscillation of the surface electrons allows for cleavage of the gold-thiol bond which releases the cargo from the particle. The localized heating, which does not affect the overall temperature of the cell, allows for release of the particles from the endosome. The heat generated at the surface of the particle vaporizes a minute amount of water forming vapor nanobubbles surrounding the gold particles^{32,33}. The collapse of these nanobubbles causes a mechanical force that ruptures the endosomal membranes, allowing for release of the cargo from the endosome into the cytosol of the cell ³⁴. The use of NIR light with gold nanoparticles allows for spatiotemporal control of cargo release since only samples irradiated with NIR light will release their payload.

D. REFERENCES

- (1) Qiu Zhao, Q.; Boxman, A.; Chowdhry, U. Nanotechnology in the Chemical Industry – Opportunities and Challenges. *J. Nanoparticle Res.* **2003**, *5* (5/6), 567–572. <https://doi.org/10.1023/B:NANO.0000006151.03088.cb>.
- (2) Leader, B.; Baca, Q. J.; Golan, D. E. Protein Therapeutics: A Summary and Pharmacological Classification. *Nat. Rev. Drug Discov.* **2008**, *7*, 21.

(3) Kintzing, J. R.; Filsinger Interrante, M. V.; Cochran, J. R. Emerging Strategies for Developing Next-Generation Protein Therapeutics for Cancer Treatment. *Trends Pharmacol. Sci.* **2016**, *37* (12), 993–1008. <https://doi.org/10.1016/j.tips.2016.10.005>.

(4) Li, H.; Nelson, C. E.; Evans, B. C.; Duvall, C. L. Delivery of Intracellular-Acting Biologics in pro-Apoptotic Therapies. *Curr. Pharm. Des.* **2011**, *17* (3), 293–319.

(5) Richard, J. P.; Melikov, K.; Vives, E.; Ramos, C.; Verbeure, B.; Gait, M. J.; Chernomordik, L. V.; Lebleu, B. Cell-Penetrating Peptides: A REEVALUATION OF THE MECHANISM OF CELLULAR UPTAKE. *J. Biol. Chem.* **2003**, *278* (1), 585–590. <https://doi.org/10.1074/jbc.M209548200>.

(6) Al-Taei, S.; Penning, N. A.; Simpson, J. C.; Futaki, S.; Takeuchi, T.; Nakase, I.; Jones, A. T. Intracellular Traffic and Fate of Protein Transduction Domains HIV-1 TAT Peptide and Octaarginine. Implications for Their Utilization as Drug Delivery Vectors. *Bioconjug. Chem.* **2006**, *17* (1), 90–100. <https://doi.org/10.1021/bc050274h>.

(7) Erazo-Oliveras, A.; Muthukrishnan, N.; Baker, R.; Wang, T.-Y.; Pellois, J.-P. Improving the Endosomal Escape of Cell-Penetrating Peptides and Their Cargos: Strategies and Challenges. *Pharmaceuticals* **2012**, *5* (11), 1177–1209. <https://doi.org/10.3390/ph5111177>.

(8) Lee, Y.-J.; Johnson, G.; Peltier, G. C.; Pellois, J.-P. A HA2-Fusion Tag Limits the Endosomal Release of Its Protein Cargo despite Causing Endosomal Lysis. *Biochim. Biophys. Acta BBA - Gen. Subj.* **2011**, *1810* (8), 752–758. <https://doi.org/10.1016/j.bbagen.2011.05.013>.

(9) Sigal, Y. M.; Zhou, R.; Zhuang, X. Visualizing and Discovering Cellular Structures with Super-Resolution Microscopy. *Science* **2018**, *361* (6405), 880–887. <https://doi.org/10.1126/science.aau1044>.

- (10) Nagarkar-Jaiswal, S.; Lee, P.-T.; Campbell, M. E.; Chen, K.; Anguiano-Zarate, S.; Cantu Gutierrez, M.; Busby, T.; Lin, W.-W.; He, Y.; Schulze, K. L.; et al. A Library of MiMICs Allows Tagging of Genes and Reversible, Spatial and Temporal Knockdown of Proteins in *Drosophila*. *eLife* **2015**, *4*. <https://doi.org/10.7554/eLife.05338>.
- (11) Wang, Y.; Shyy, J. Y.-J.; Chien, S. Fluorescence Proteins, Live-Cell Imaging, and Mechanobiology: Seeing Is Believing. *Annu. Rev. Biomed. Eng.* **2008**, *10* (1), 1–38. <https://doi.org/10.1146/annurev.bioeng.010308.161731>.
- (12) Pakhomov, A. A.; Martynov, V. I. GFP Family: Structural Insights into Spectral Tuning. *Chem. Biol.* **2008**, *15* (8), 755–764. <https://doi.org/10.1016/j.chembiol.2008.07.009>.
- (13) Wu, B.; Piatkevich, K. D.; Lionnet, T.; Singer, R. H.; Verkhusha, V. V. Modern Fluorescent Proteins and Imaging Technologies to Study Gene Expression, Nuclear Localization, and Dynamics. *Curr. Opin. Cell Biol.* **2011**, *23* (3), 310–317. <https://doi.org/10.1016/j.ceb.2010.12.004>.
- (14) Frommer, W. B.; Davidson, M. W.; Campbell, R. E. Genetically Encoded Biosensors Based on Engineered Fluorescent Proteins. *Chem. Soc. Rev.* **2009**, *38* (10), 2833. <https://doi.org/10.1039/b907749a>.
- (15) Costantini, L. M.; Snapp, E. L. Fluorescent Proteins in Cellular Organelles: Serious Pitfalls and Some Solutions. *DNA Cell Biol.* **2013**, *32* (11), 622–627. <https://doi.org/10.1089/dna.2013.2172>.
- (16) Jensen, E. C. Use of Fluorescent Probes: Their Effect on Cell Biology and Limitations. *Anat. Rec. Adv. Integr. Anat. Evol. Biol.* **2012**, *295* (12), 2031–2036. <https://doi.org/10.1002/ar.22602>.

- (17) Kanca, O.; Bellen, H. J.; Schnorrer, F. Gene Tagging Strategies To Assess Protein Expression, Localization, and Function in *Drosophila*. *Genetics* **2017**, *207* (2), 389–412. <https://doi.org/10.1534/genetics.117.199968>.
- (18) Kawano, K.; Yano, Y.; Omae, K.; Matsuzaki, S.; Matsuzaki, K. Stoichiometric Analysis of Oligomerization of Membrane Proteins on Living Cells Using Coiled-Coil Labeling and Spectral Imaging. *Anal. Chem.* **2013**, *85* (6), 3454–3461. <https://doi.org/10.1021/ac400177a>.
- (19) Wang, J.; Yu, Y.; Xia, J. Short Peptide Tag for Covalent Protein Labeling Based on Coiled Coils. *Bioconjug. Chem.* **2014**, *25* (1), 178–187. <https://doi.org/10.1021/bc400498p>.
- (20) Doh, J. K.; White, J. D.; Zane, H. K.; Chang, Y. H.; López, C. S.; Enns, C. A.; Beatty, K. E. VIPER Is a Genetically Encoded Peptide Tag for Fluorescence and Electron Microscopy. *Proc. Natl. Acad. Sci.* **2018**, *115* (51), 12961–12966. <https://doi.org/10.1073/pnas.1808626115>.
- (21) Zane, H. K.; Doh, J. K.; Enns, C. A.; Beatty, K. E. Versatile Interacting Peptide (VIP) Tags for Labeling Proteins with Bright Chemical Reporters. *ChemBioChem* **2017**, *18* (5), 470–474. <https://doi.org/10.1002/cbic.201600627>.
- (22) Li, J.; Xue, S.; Mao, Z.-W. Nanoparticle Delivery Systems for SiRNA-Based Therapeutics. *J. Mater. Chem. B* **2016**, *4* (41), 6620–6639. <https://doi.org/10.1039/C6TB01462C>.
- (23) Boisselier, E.; Astruc, D. Gold Nanoparticles in Nanomedicine: Preparations, Imaging, Diagnostics, Therapies and Toxicity. *Chem. Soc. Rev.* **2009**, *38* (6), 1759. <https://doi.org/10.1039/b806051g>.
- (24) Kreibig, U.; Vollmer, M. *Optical Properties of Metal Clusters*; 1995.

- (25) Cobley, C. M.; Chen, J.; Cho, E. C.; Wang, L. V.; Xia, Y. Gold Nanostructures: A Class of Multifunctional Materials for Biomedical Applications. *Chem Soc Rev* **2011**, *40* (1), 44–56. <https://doi.org/10.1039/B821763G>.
- (26) Prevo, B.; Esakoff, S.; Mikhailovsky, A.; Zasadzinski, J. A. Scalable Routes to Gold Nanoshells with Tunable Sizes and Response to Near-Infrared Pulsed Laser Irradiation. *Small* **2008**, *4*, 1183–1195.
- (27) Weissleder, R. A Clearer Vision for in Vivo Imaging. *Nat. Biotechnol.* **2001**, *19* (4), 316–317. <https://doi.org/10.1038/86684>.
- (28) Thibaudau, F. Ultrafast Photothermal Release of DNA from Gold Nanoparticles. *J. Phys. Chem. Lett.* **2012**, *3* (7), 902–907. <https://doi.org/10.1021/jz3001213>.
- (29) Park, H.-J.; Shin, J.; Kim, J.; Cho, S.-W. Nonviral Delivery for Reprogramming to Pluripotency and Differentiation. *Arch. Pharm. Res.* **2014**, *37* (1), 107–119. <https://doi.org/10.1007/s12272-013-0287-z>.
- (30) Ramsey, J. D.; Flynn, N. H. Cell-Penetrating Peptides Transport Therapeutics into Cells. *Pharmacol. Ther.* **2015**, *154*, 78–86. <https://doi.org/10.1016/j.pharmthera.2015.07.003>.
- (31) Rizzuti, M.; Nizzardo, M.; Zanetta, C.; Ramirez, A.; Corti, S. Therapeutic Applications of the Cell-Penetrating HIV-1 Tat Peptide. *Drug Discov. Today* **2015**, *20* (1), 76–85. <https://doi.org/10.1016/j.drudis.2014.09.017>.
- (32) Lukianova-Hleb, E. Y.; Volkov, A. N.; Lapotko, D. O. Laser Pulse Duration Is Critical For the Generation of Plasmonic Nanobubbles. *Langmuir* **2014**, *30* (25), 7425–7434. <https://doi.org/10.1021/la5015362>.
- (33) Lukianova-Hleb, E. Y.; Belyanin, A.; Kashinath, S.; Wu, X.; Lapotko, D. O. Plasmonic Nanobubble-Enhanced Endosomal Escape Processes for Selective and Guided

Intracellular Delivery of Chemotherapy to Drug-Resistant Cancer Cells. *Biomaterials* **2012**, *33* (6), 1821–1826. <https://doi.org/10.1016/j.biomaterials.2011.11.015>.

(34) Wu, G.; Mikhailovsky, A.; Khant, H. A.; Fu, C.; Chiu, W.; Zasadzinski, J. A. Remotely Triggered Liposome Release by Near-Infrared Light Absorption via Hollow Gold Nanoshells. *J. Am. Chem. Soc.* **2008**, *130* (26), 8175–8177. <https://doi.org/10.1021/ja802656d>.

II. IMPROVED IN VIVO TARGETING OF BCL-2 PHENOTYPIC CONVERSION THROUGH HOLLOW GOLD NANOSHELL DELIVERY

A. Abstract

Although new cancer therapeutics are discovered at a rapid pace, lack of effective means of delivery and cancer chemoresistance thwart many of the promising therapeutics. We demonstrate a method that confronts both of these issues with the light-activated delivery of a Bcl-2 functional converting peptide, NuBCP-9, using hollow gold nanoshells. This approach has shown not only to increase the efficacy of the peptide 30-fold in vitro but also has shown to reduce paclitaxel resistant H460 lung xenograft tumor growth by 56.4%.

B. Introduction

Despite many advances, cancer is still a leading cause of death worldwide. Traditional chemotherapy is based largely on small molecule anti-cancer drugs which, although effective, have severe drawbacks including lack of specificity, high toxicity and often result in drug resistance, precluding continued use [1,2]. The recently developed biologics have improved specificity, in some cases targeting tumors that develop resistance to small molecule therapies [3]. Resistant cancer cells often remain after initial chemotherapy treatment causing tumor recurrence. These resistant cancer cells can be specifically targeted through delivery of a pro-apoptotic peptide, fused with a poly arginine cell penetrating peptide [4]. Although delivery

of pro-apoptotic peptides have shown great promise as new therapeutics, major delivery obstacles still thwart their progress in the therapeutic pipeline.

Intracellular delivery of apoptotic peptides through fusion to cell penetrating peptides like poly arginine, often results in endosomal entrapment [5]. This prevents the drug from reaching the cytosol as well as the subcellular target, in this case, the mitochondria [5]. The low efficiency of endosomal escape makes these therapeutic peptides efficient only at micromolar ranges in vitro [4]. Although the IC₅₀ value in vitro cannot be directly correlated to activity of a therapeutic in vivo, therapeutics with an IC₅₀ value > 10 μM are generally considered weak with a lower potential for in vivo application [6]. In order to increase the potency of therapeutics with high potential, a safe yet efficient delivery vehicle is required.

Here we demonstrate a hollow gold nanoparticle (HGN)-based intracellular delivery platform that overcomes many of these challenges. Orthogonal assembly of a Bcl-2 targeting peptide is achieved via thio-gold bonds; treatment of the HGN construct with pulsed near infra-red light results in the release of the Bcl-2 targeted peptide. The Bcl-2 family of proteins regulate cell death via both pro-apoptotic and anti-apoptotic pathways and are now established as promising therapeutic targets in lymphoma and triple negative breast cancer (TNBC) [7,8]. Expression of Bcl-2 in hormone receptor-negative and TNBC cancers is an independent poor prognostic factor and associated with poor outcome in patients treated with anthracycline based adjuvant chemotherapy [9,10]. Upregulation of Bcl-2 is a mechanism of therapeutic resistance in HER2-positive and TNBC which contributes to poor overall survival [11,12].

Current strategies targeting Bcl-2 include peptides derived from the BH3 domain and small molecule inhibitors such as ABT-199 and ABT-737. However, resistance to ABT-199 is linked to upregulation of other anti-apoptotic proteins such as Bcl-xL [13,14]. An alternative approach to target Bcl-2 in TNBC is the use of NuBCP-9 (NuBCP) which is a nine amino acid peptide derived from Nur77 [15,16]. Bcl-2 binding of NuBCP converts it into a pro-apoptotic protein. NuBCPs' action is potentiated by increased Bcl-2 expression and is capable of inhibiting the pro-survival function of Bcl-xl which is linked to ABT-199 resistance mechanisms [17,18]. However, the delivery of NuBCP is problematic due to its biodegradation and short circulation half-life. Prior efforts to improve on NuBCP delivery still required micromolar concentrations [19–21].

The use of gold nanoparticles as a delivery vehicle for peptide delivery, such as NuBCP, has the potential to increase the potency of NuBCP through increased endosomal escape upon near-infrared (NIR) irradiation. The light triggered release of NuBCP also enables specific release in a target area so the resistant cancer cells can be targeted systematically while leaving other tissues untouched.

C. Material and Methods

Hollow gold nanoshell synthesis and dialysis

HGNs were synthesized through a previously described galvanic replacement of silver seed particles [22]. Briefly, the synthesis can be broken into three steps. The first step initializes the silver seed of the particle in a 500 mL solution of 0.2 mM AgNO₃ (Sigma) and 0.5 mM sodium citrate (Sigma) heated to 60 °C. 0.5 mL of 1.0 M NaBH₄ (EMD) was added quickly to reduce the silver solution to create the initial silver seed. The solution remained at

temperature for 2 hours and then left to cool to room temperature. The second step of the synthesis grows the silver particle to the final 45 nm size by the addition of 0.75 mL of 2 M $\text{NH}_2\text{OH}\cdot\text{HCl}$ (Sigma) and 1.75 mL of 0.1 M AgNO_3 . The solution stirred overnight to allow for full growth of the silver particles to be used for template for later galvanic replacement. The third and final step in the synthesis is the galvanic replacement of the sacrificial silver template by the addition of 3.2 mL of 25 mM HAuCl_4 (Sigma) to the heated solution at 60 °C to obtain hollow gold nanoshells ~45 nm in diameter with an absorption peak maximum at 750 nm. The HGNs were dialyzed overnight in sodium citrate buffer (500 mM) with 0.03 % diethyl dicarbonate (DEPC) (Biochemica) in dialysis cassettes (MWCO 20 kDa).

HGNs surface modifications

DNA adsorption.

Thiol-PEG-DNA-amine (C6-S-S-PEG18-5' ACCCTGAAGTTCATCTGCACCACCG 3'-NH₂ (100 μM, Biosearch Technologies) was deprotected through a 20 minute incubation with 12.5 mM Tris(2-carboxyethyl)phosphine hydrochloride (TCEP, Sigma). A chloroform extraction was performed to remove the C6 cap on the 5' end of the oligo. 6 μM of TCEP treated DNA was added to 64 pM HGN. After a brief sonication, 10 mM sodium citrate was added to adjust the pH of the solution to 3.1 in order to allow for low pH DNA adsorption onto the surface of the HGN. After 20 minutes of incubation at a low pH, the pH was raised to 7.4 with 1 M HEPES (Sigma) and the solution was slowly salted to 1M Na⁺ over a period of 20 minutes using 3.0 M sodium chloride (NaCl), 0.3 M sodium citrate (Na₃Cit) pH 7.0 (SSC 20x) with 0.01% Tween-20 and 1 mM MgCl₂. After another 20-minute incubation excess DNA was through two wash steps performed by centrifuging at 10,000 x g for 10

minutes with resuspension and sonication in washing buffer (1mM MgCl₂, 0.01 % Tween-20, 300 mM NaCl and 30 mM Na₃Cit pH 7). After the last wash, the particles were suspended in hybridization buffer (10 mM MgCl₂, 600 mM Na⁺).

Hybridization of complementary DNA

Complementary DNA (2 μM) is added to the HGN-DNA in ratio of 1:9 (5'-biotin to 5'-FAM labeled) to allow for a varied surface modification of the HGN. 0.2 μM Biotin and 1.8 μM DNAComp-FAM are added to hybridization buffer, mixed and then added to 64 pM HGN-DNA to a final concentration of 1 μM complement DNA with 32 pM HGN-DNA and sonicated. The solution is then heated at 70 °C for 2 minutes and held at 45 °C for 30 minutes before washed two times with conjugation buffer (10 mM HEPES, 1mM MgCl₂ and 0.01% Tween-20).

NTA functionalization of HGN-DNA

N-[N_α,N_α-Bis(carboxymethyl)-L-lysine]-12-mercaptododecanamide (NTA) (Sigma) was added to the amine at the 3' end of the dsDNA strand through a 20 minute room temperature incubation with 1 mg/mL NHS-PEG4-maleimide linker (Quanta Biodesign). After 20 minutes the maleimide terminated HGN-DNA particles were washed three times at 4 °C and then suspended in conjugation buffer with 50 μM NTA, sonicated and left at room temperature for 3 hours and then washed three times in PBS with 0.01% Tween-20 (PBST).

Streptavidin and Biotin-TAT functionalization of HGN-NTA

An equal volume of 1mg/mL streptavidin (Prozyme) in PBST was added to 62 pM HGN-NTA and quickly sonicated and vortexed. After 1 hour of incubation at room

temperature the streptavidin coated HGN were centrifuged twice at 10,000 xg for 10 minutes at 4 °C and each time was suspended in PBST. A final concentration of 20 μM biotin-TAT (Anaspec) was added in two steps of equal volume with a 30 minute incubation at room temperature after each addition. The particles were then washed another two times with PBST to remove any excess biotin-TAT and stored at 4 °C until further use.

NuBCP loading onto HGN and quantification of loading

NuBCP was loaded onto the HGN at 1, 3 and 10 μM initial concentration for 32 pM HGN and 500 μM CuCl₂ and incubated for 20 minutes on ice before being washed three times in PBST. Total loading per particle was determined through KCN etch. 32 pM particles were incubated in KCN solution (0.1 M KCN, 1 mM K₃Fe(CN)₆) to dissolve the gold particles and completely release the molecules coating the particle surface. In laser experiments, quantification of peptide released by laser was determined after centrifugation of the lasered sample and removal of the supernatant. The pellet was treated with KCN etch to determine the amount retained on the particle. Quantification of peptide in the supernatant and etched off the pellet was determined using standard linear calibration curves between concentration of Cy5 labeled NuBCP and the corresponding fluorescence intensity detected from the Tecan M200 plate reader. The fluorescence intensity in solution released with KCN etch or laser irradiation was converted to peptide concentration using the calibration curve.

Two-photon microscopy

Cells were plated 24 hours prior at 40,000 cells per well in an 8 well glass slide (Millipore cat no. PEZGS0816) in 200 μL of DMEM + 10% FBS. 500 uM CuCl₂ was added to 25 μL of ~32 pM HGNS (in PBST) prior to addition of NuBCP-Cy5. Particles were sonicated and incubated with 1, 3 and 5 μM NuBCP-Cy5 for 30 min on ice then spun down at

5,000 rcf for 10 min and washed 1X with PBST. HGN-NuBCP-Cy5 particles were then suspended in 200 μ L of DMEM + 10% FBS and sonicated prior to addition to 8 well glass slide for 2 hours at 37°C in 5% CO₂. Cells were washed 2X with PBS and then one drop of PBS was added to each well prior to cover glass addition. Samples were focused on using a 25 x water immersion objective lense and irradiated using a mode locked Ti:sapphire tunable femtosecond pulsed laser (100 fs pulse duration, 80 mHz repetition rate, Mai Tai HP, Newport-Spectra Physics). The excitation source was set to irradiate at 800 nm, 5% NIR laser power and in 0.69 nm slices throughout the cell volume. Images capturing FAM and Cy5 fluorescence were collected before and after laser irradiation.

Cellular Internalization and Imaging

Cells were plated and treated with HGN, HGN+NucBCP (containing no DNA or TAT),HGN-DNA-NucBCP, HGN-DNA-TAT, HGN-DNA-TAT-NucBCP, or no particles as described above and observed on an Olympos BX51 upright compound microscope with a dark field condenser.

Mitochondrial Depolarization Assay of Cancer Therapeutic Resistant H460 cells treated with HGN and HGN-NucBCP

Cells were plated and treated with HGN or HGN-NucBCP as described above. Prior to irradiation, cells were treated with media containing 10 μ g•mL⁻¹ solution of JC-1 dye (ThermoFisher) and incubated for 10 minutes. The cells were washed three times with PBS and treated with the laser conditions outlined above.

Femtosecond Pulse Laser Irradiation of HGN in MDA-MB-231 cells through Microcapillary Device

MDA-MB-231 cells were dissociated from flask using cell dissociation buffer (CDB, Gibco), and washed two times with PBS. 100,000 cells were suspended in media and incubated for 2 hours with HGN and HGN-NuBCP. The cells were washed two times with PBS and divided into 5,000 per tube in 100 μ L and focused through a capillary tube positioned perpendicular to the NIR beam path at a rate of 100 μ L \cdot min⁻¹. Samples without irradiation were passed through the capillary tube with NIR beam path blocked to prevent irradiation of the sample. The samples were collected and plated on a 96 well plate and assayed for viability 96 hours later using the PrestoBlue viability stain according to the manufacturer's protocol on a Tecan M200 plate reader.

Zebrafish Xenograft and Two-photon Laser Exposure

Zebrafish (*Danio rerio*) housing was conducted at the Sinnhuber Aquatic Research Laboratory at Oregon State University in accordance with Institutional Animal Care and Use Committee protocols. Under standard laboratory conditions, adult 5D Tropical zebrafish were maintained at 28 \pm 1 $^{\circ}$ C on a 14hr light/10 hr dark photoperiod in reverse osmosis water with added salt solution (0.6%, Instant Ocean, UnitedPet Group, Inc., Blacksburg, VA, USA). Eggs collected were staged according to Kimmel et al [23]. To prevent pigmentation, zebrafish embryos were maintained in E3 media with phenylthiourea (0.003%, Sigma, USA) starting at 24 hours post fertilization.

Before transplantation, cancer cells were labeled with a CM-DiI cell tracker dye (Thermo Fisher Sci.) according to the manufacturer's protocol and exposed to vehicle (media), HGN 32 pM or HGN-NuBCP 32 pM loaded with 10 μ M treatment. Cells were allowed to incubate with treatment at room temperature for 1hr on a rotator. Cells were then washed with PBS and suspended in DMEM to a concentration of 2x10⁷ cells/mL. Xenograft transplantation occurred as in Pearce et al [4]. Briefly, suspended cells were loaded into a glass needle pulled

from a borosilicate glass pipette by a micropipette puller (Sutter Instrument, Novato, CA). Around 200 cancer cells were transplanted into the yolk of 2-day post fertilization zebrafish by a micro-pressure injector. Xenografts recovered overnight at 34°C without light after transplantation.

For two-photon laser irradiation, zebrafish were immobilized by being anesthetized by emersion in 0.2mg/mL Tricaine E3 media and imbedded in 0.8% (w/v) low melting point agarose on a glass bottom 96-well plate. Zebrafish were irradiated using a mode locked Ti:Sapphire Laser widely tunable femtosecond pulsed laser (140 fs pulse duration, 80 MHz repetition rate, Chameleon Vision Laser, Coherent) using a Zeiss LSM 780 confocal microscope at 20x objective. Zebrafish yolks were irradiated at 800 nm, 6% NIR laser power and in 0.75 nm slices throughout the yolk volume.

For imaging, zebrafish xenografts at 1 and 4-day post injection (dpi) were immobilized as mentioned above and fluorescent cells were captured on a as z-stacks with wide-field settings on a Zeiss LSM 780 confocal microscope with a 10x objective. Using Fiji (ImageJ) software, cancer growth was analyzed by producing a maximum projection image of a median filtered z-stack and calculating the cell area from an Otsu applied threshold [24]. An increase in cell area from 1 to 4dpi was consider cancer growth. Above all the pages must be conceived as a sequence of images with design continuity. The reader should experience the pages as a flow of related events rather than as separate isolated entities.

D. Results

To assemble the HGN-peptide constructs, single strands of thiol-DNA amine were added to the surface of the HGN through low pH mediated adsorption followed by addition of a complementary DNA strand. The complementary DNA strand allows for tracking of the particles (with FAM-tagged DNA) and internalization through a DNA-biotin tag. A ratio of

1:9 (Biotin:FAM) allows for optimal peptide loading onto the HGN (~10,000 peptides per particle) with efficient internalization (Figure II-1a) The biotin strand allows for internalization into cells only after the addition of streptavidin and a biotinylated cell penetrating peptide, TAT (Biotin- YGRKKRRQRRRPQ). The terminal amine on the thiol-DNA anchoring strand was further functionalized with a thiol derivative of nitrilotriacetic acid (NTA) using a NHS-PEG₄-maleimide linker. The NTA on the surface of the particle allows for the His-tagged NuBCP onto the particle in the presence of Cu²⁺ (Figure II-2a).

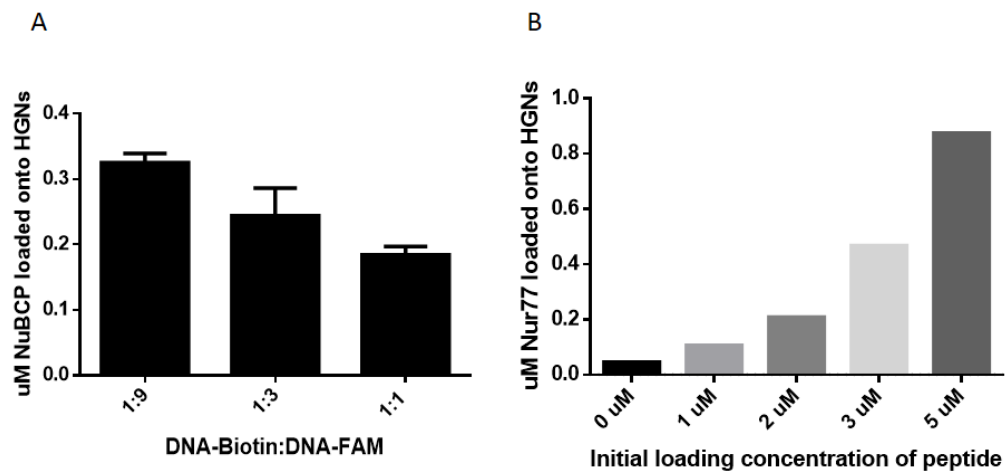


Figure II-1. Optimization of NuBCP Loading onto HGNS. A. Ratio of Biotin:FAM complement strands on HGN-STV-TAT particles determines 1:9 particles allow for maximal loading of NuBCP with 3 μ M initial peptide concentration. B. Increase in loading of NuBCP-Cy5 on 32 pM particles with increasing initial concentrations of NuBCP. NuBCP loading is determined by Cy5 fluorescence in KCN etch of washed HGN-NuBCP pellet.

The average diameter of the final construct increased from 58 nm to 190 nm from citrate capped HGN to the full construct containing NuBCP (Figure II-2b). Figure II-2c demonstrates the delivery of HGN-NuBCP via Streptavidin TAT mediated endocytosis. After irradiation with 800 nm light, NuBCP is released from the HGN and the endosome into the cytosol. Upon release, NuBCP binds to the Bcl-2 loop domain and converts Bcl-2 into a pro-apoptotic protein, which further inhibits anti-apoptotic proteins and activates other pro-

apoptotic proteins on the mitochondria. Finally, activated pro-apoptotic proteins facilitate mitochondrial outer membrane permeabilization, initiating apoptosis, resulting in cell death [16].

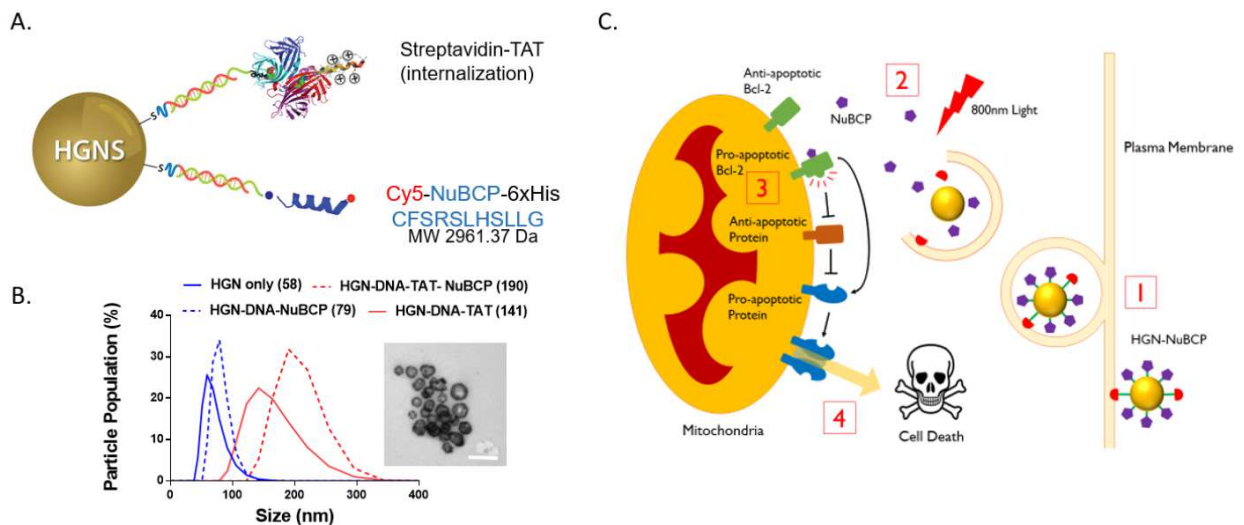


Figure II-2. Orthogonal surface chemistry of internalization peptide Streptavidin TAT and therapeutic peptide NuBCP on a HGNS. b. Size distribution of nanoparticles during coating steps. HGN particles have a Z-average diameter of 58 nm; HGN-DNA-, 79 nm; HGN-DNA-TAT, 141 nm; HGN-DNA-TAT-NuBCP, 190 nm. Image to the right displays TEM image of HGN-DNA-TAT. Scale bar 100 nm. c. Illustration of the delivery of HGN-NuBCP into a cancer cell. 1) Hollow gold nanoparticles coated in NuBCP (purple hexagon) are taken into the cell by internalization peptide Streptavidin TAT (red semi-circle) mediated endocytosis. 2) Irradiation with NIR 800nm light, releases NuBCP from nanoparticle and endosome into the cytosol. 3) NuBCP binds to the Bcl-2 loop domain and converts Bcl-2 (green) into a pro-apoptotic protein which inhibits anti-apoptotic proteins (orange) and activates other pro-apoptotic proteins (blue) on the mitochondria. 4) Activated pro-apoptotic proteins facilitate mitochondrial outer membrane permeabilization, initiating apoptosis, and results in cell death.

In order to verify the HGN-NuBCP construct has laser-controlled release of NuBCP, both cell-free and cell-based release studies were conducted. Cel

I-free treatment shows laser-dependent release of the peptide with up to 22% of the loaded peptide (Figure II-3a). Total loading of the peptide was determined through Cy5 fluorescence following a KCN etch of the washed HGN-NuBCP pellet (Figure II-1b) level of release is typical for peptides and proteins loaded onto HGNs [4]. Cellular internalization of nanoparticles containing TAT was observed via dark field microscopy (orange puncta Figure II-3b). Initial release experiments in HeLa cells using two-photon microscopy also demonstrates internalization of the HGN-peptide constructs visualized as fluorescent puncta within the endosomes as seen in the lower left panel of Figure II-3c. Only after NIR irradiation was release of the FAM labeled DNA as well as the NuBCP-Cy5 observed as the puncta diffused across the cell demonstrating endosomal release (Figure II-3c). Similar experiments were carried out with MDA-MB-231 breast cancer cells that express high levels of Bcl-2 (Figure II-4a,b). Bulk laser experiments used a micro-capillary device to flow the cells with internalized particles through the path of the laser beam to maximize the fraction of cells exposed to irradiation [5]. Cell viability was determined 96 hours after laser irradiation and demonstrated 80% cell viability loss with HGN-NuBCP particles. When MDA-MD-231 cells were treated with three times the amount of the unconjugated NuBCP peptide, the cells remained viable. This indicates the HGN particles are necessary for uptake of the peptide into the cells in order to cause the desired effect. A control involving HGN particles without NuBCP was irradiated with NIR light and a cell viability loss of only 10% was observed likely due to heating caused on the surface of the HGNs. This data demonstrates the requirement for both HGN and NuBCP for effective loss of cancer cell viability.

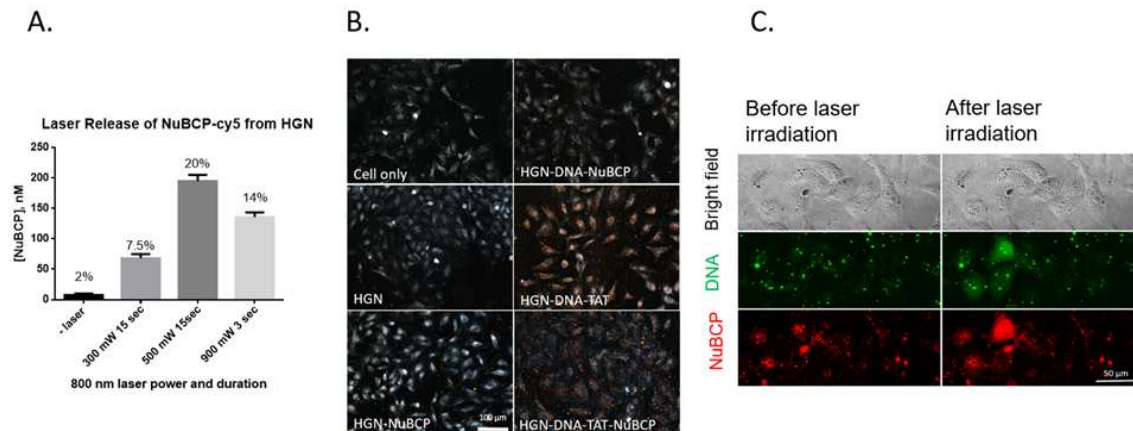


Figure II-3. Release of Cy5 labeled NuBCP shows laser dependent release. a. An increase in laser power leads to an increase in NuBCP release from HGN loaded with 900 nM NuBCP. Percent release is shown above bar graphs and determined by the percentage of peptide released into the supernatant after laser irradiation. Total peptide loaded is determined by KCN etch of the no laser pellet. b. Dark field microscopy demonstrates cellular internalization of gold nanoparticles (orange light scattering) only when TAT peptide is present on the particle surface. c. Release of FAM labeled DNA and Cy5 labeled NuBCP in HeLa cells using two photon microscope for NIR laser irradiation. Release of both DNA and peptide is shown from diffusion of dye labels throughout the cell after laser irradiation.

When an initial concentration of 10 μM NuBCP is incubated with 32 pM HGN, 1.8 μM is actually loaded onto the HGN construct (Figure II-1). After irradiation only 500 nM NuBCP is released from the particles in cell-free studies. This value can be used to estimate the maximum amount of NuBCP released and used for cell studies (50 nM). This data suggests our HGN-NuBCP delivery increases the potency of the peptide by 30-fold compared to previous particle delivery methods [19]. We observe no cell death when MDA-MB-231 cells are treated with the peptide without HGN assembly (Figure II-4a). The HGN-NuBCP in MDA-MB-231 cells showed no significant cell viability loss without laser irradiation indicating either the NuBCP remains attached on the HGN in the cellular endosomes or is degraded after 96 hours.

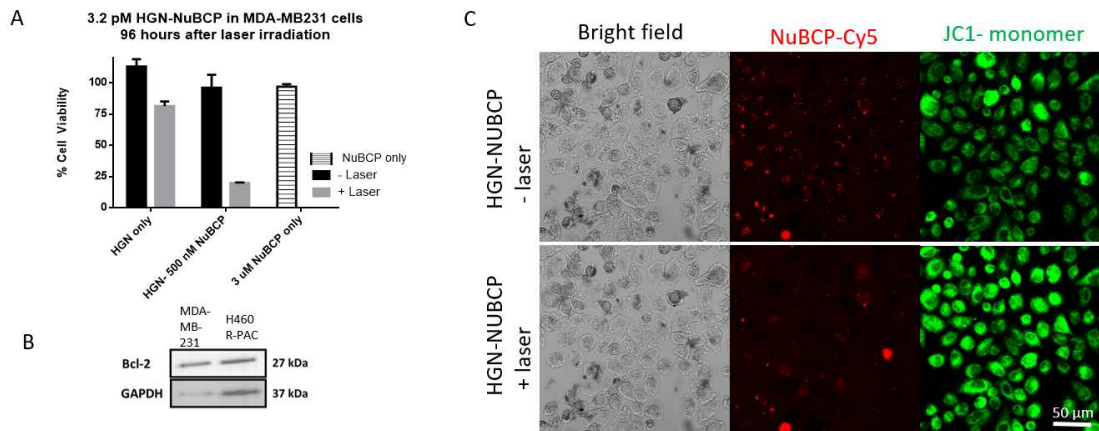


Figure II-4. (a) MDA-MB-231 cells were treated with 3.2 pM HGN, 3.2 pM HGN-NuBCP and were then irradiated with an 800 nm 5 kHz laser at 1 W as cells flowed through a borosilicate microcapillary tube at 100 μ L/min. 500 nM and 3 μ M NuBCP indicate the final concentration of NuBCP delivered in cell media via HGNs or in media alone for NuBCP only. Note the NuBCP only control was not treated with laser. Cell viability of MDA-MB231 cells was observed 96 hrs after laser irradiation. **(b)** Bcl-2 is expressed in both MDA-MB-231 and H460 R-PAC cells. Western Blot analysis of MDA-MB-231 and H460 R-PAC indicates levels of Bcl-2 and GAPDH is used as a loading control. **(c)** Laser dependent release of NuBCP-Cy5 in H460 cells with JC-1 assay shows mitochondrial destabilization as green fluorescence increases from the JC-1 monomer upon irradiation with two-photon 800 nm laser

To verify the cause of viability loss in cells expressing high levels of Bcl-2 was due to the induction of apoptosis, we tested the efficacy of the system in H460 lung cancer cells using the JC-1 mitochondrial stain to test for mitochondrial destabilization after irradiation of HGN-NuBCP particles (Figure II-4c). In cellular studies, aggregated JC-1 dye disassociates into a green fluorescing monomeric form when the mitochondrial membrane depolarizes. Mitochondrial depolarization can be an early indicator of cell death due to apoptosis. Confocal images show release of the NuBCP from HGN and the increase in green fluorescence form of the JC-1 monomers 30 minutes after irradiation with NIR light and release of NuBCP from the HGN (Figure II-3B). Only in areas with laser irradiation was an increase in green fluorescence observed, confirming the mitochondrial membrane becomes destabilized after irradiation of cells with HGN-NuBCP. There is no effect of HGN alone

with laser on mitochondrial health (Figure II-5). These findings show NuBCP can be delivered into human cancer cells where release of the NuBCP from the gold particles leads to a compromised mitochondria membrane.

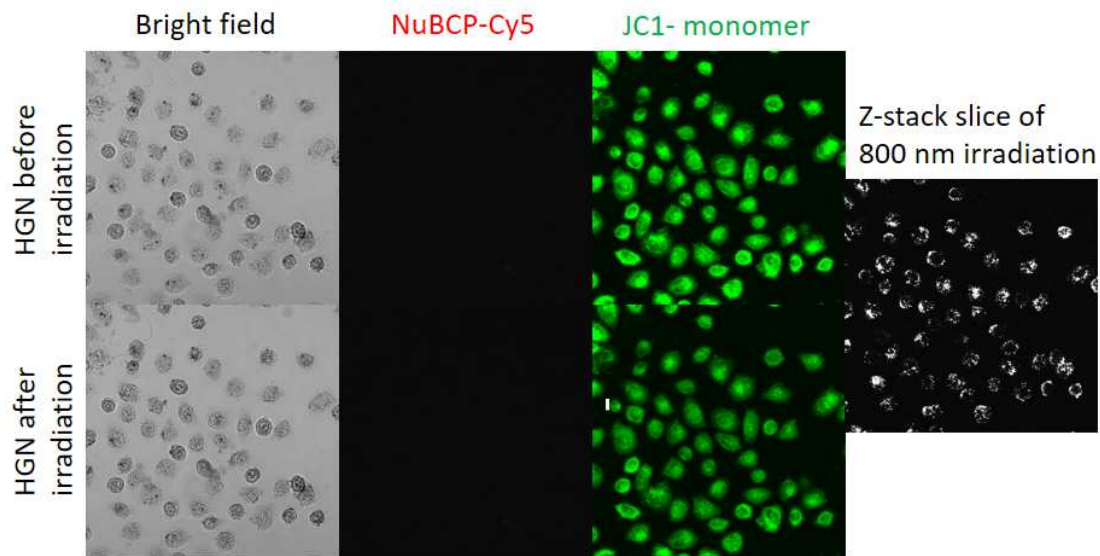


Figure II-5. Irradiation of H460 cells without NuBCP in the presence of HGN does not cause mitochondria depolarization. Irradiation of HGN in H460 cells with JC-1 assay does not show an increase in green fluorescence from the JC-1 monomer upon laser irradiation with 800 nm laser equipped 2 photon microscope indicating the mitochondria membranes remain intact post laser irradiation without NuBCP on the HGNs. No fluorescence is observed in the Cy5 channel due to no peptide on the HGNs. Confirmation of particles in cells through Z-stack slice of 800 nm irradiation which shows the surface resonance light scattering produced by the HGN internalized in the H460 cells. The white resonant light scattering is demonstrated through the white puncta visualized throughout the cells in the Z-stack slice during 800 nm irradiation.

To determine any potential toxicity of HGN-NuBCP-9 to normal cells we performed Zebrafish toxicity and survival assay (Figure II-6a). Exposure of HGN-NuBCP did not impact survival or development of abnormalities of zebrafish embryos. To demonstrate the in vivo efficacy of this HGN-NuBCP approach, we exposed paclitaxel resistant (PacR) H460 cells to either vehicle, HGN, or HGN-NuBCP and transplanted them into zebrafish embryos (Figure II-6). H460 cells were systematically exposed to low doses of paclitaxel, resulting in

increased Bcl-2 expression and resistance to paclitaxel (PacR H460 cell line) [4]. The H460 paclitaxel PacR cells derived from H460 parental cells are 10 fold less sensitive to paclitaxel than the parental cells at 10 nM paclitaxel, which is a clinically achievable concentration (Figure II-6b). The transplanted cells were imaged before and 3 days after two-photon NIR laser irradiation to measure loss of PacR H460 cells within the zebrafish. Half the zebrafish from each group were withheld from irradiation as controls. NIR irradiation had no effect on zebrafish survival as 98.3% and 96.6% of non-irradiated and irradiated zebrafish survived respectively. Laser irradiation of HGN-NuBCP treatment group had the greatest effect on the growth of PacR H460 cells inside zebrafish. Three days after laser irradiation, average PacR H460 xenograft tumor growth was reduced by 56.4% compared to the non-laser control for HGN-NuBCP treated groups (Figure II-6 g and h). PacR H460 xenograft growth was not significantly affected by the media used for delivery (Figure II-6 c and d) nor HGN alone (Figure II-6 e and f). Laser induced cell reduction with HGN exposure is similar to what was seen in vitro experiments where HGN irradiation may be generating localized heating.

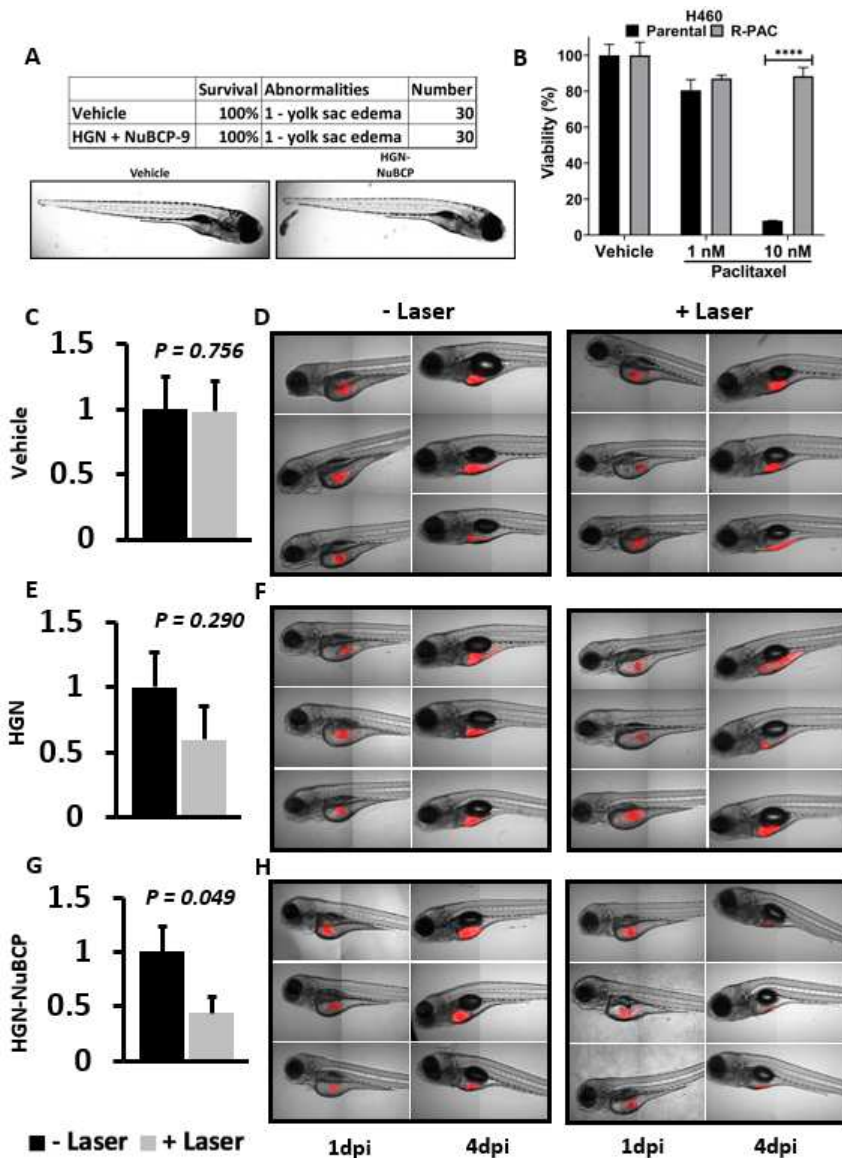


Figure II-6. (a) Effect of HGN-NuBCP-9 on survival and development of Zebrafish embryos. Treatment with vehicle (PBS-Tween 0.01%) and HGN-NuBCP-9 10 μ M in embryo media. Survivorship was assessed by counting the number of live versus dead fish in each group (n=30 all groups). **(b) H460 derived paclitaxel line is resistant to 10 nM paclitaxel treatment.** Percentage viability is calculated relative to vehicle treatment. Data is representative of three independent assays done in triplicate. Two-way ANOVA with Sidak's multiple comparisons post-test, ****P<0.0001. Log2 fold change of cell area for vehicle **(c)**, HGN **(e)** and HGN-NuBCP **(g)** exposed H460 PacR cells in xenografts after no exposure (-Laser) or exposure (+Laser) to two-photon NIR laser. Data normalized to no laser control; Vehicle (- Laser) N = 20, (+ Laser) N = 20; HGN: (- Laser) N = 20, (+ Laser) N = 19. HGN-NuBCP: (- Laser) N = 19, (+ Laser) N = 20. Representative figures zebrafish xenografts for vehicle **(d)**, HGN **(f)** and HGN-NuBCP **(h)** treatment groups at 1 and 4 day post injection (dpi) with transplanted H460 PacR cells (Red); 10x magnification.

E. DISCUSSION

Our primary interests were the induction of apoptosis in resistant cancer cells with NIR light control and to limit the amount of peptide required in therapeutic applications. Successful cancer therapies rely significantly on both the selectivity for cancer cells as well as creating a reasonable therapeutic window for in vivo studies. The Nur77 derived peptide, NuBCP targets Bcl-2 and converts it into a pro-apoptotic protein as well as inhibits the pro-survival function of Bcl-xl [17,18]. Therefore, delivery of NuBCP with hollow gold nanoshells would not only allow for control over release with light but the peptide itself would affect the cells that are resistant to traditional Bcl-2 targeting therapeutics [17,18]. Earlier studies using the Nur77 derived peptide, NuBCP required high micromolar concentration of peptide in order to cause apoptosis which can translate to poor efficacy in vivo [19-21]. Our hypothesis was that addition of the NuBCP to hollow gold nanoshells would improve the delivery efficiency since peptides delivered solely via targeting peptides are often caught in endosomes [5].

Our research demonstrates the release of the NuBCP peptide from our HGN construct with 800 nm light control (Figure II-4a). In Figure II-3a the power dependence of release is observed after different laser intensities are applied to the HGN containing NuBCP with a Cy5 dye. This suggests that the peptide is not released from the particle until a certain power of excitation is obtained. Since up to 20% of the loaded peptide was released from the HGN after laser irradiation, this would convert to a maximum of 50 nM NuBCP delivered in cellular studies. Furthermore, NuBCP laser dependent release from the HGN in cells is visualized by the diffusion of the dye attached to the peptide after laser irradiation (Figure II-

3c). Tracking of the DNA also attached to the particle is seen through the FAM fluorescence channel and shows that cells that release NuBCP also show the dispersion of DNA-FAM confirming that the NuBCP peptide is attached to the particle via the NTA-Cu-His interaction originally hypothesized.

Release of the NuBCP peptide from HGN not only showed significant cell death in MDA-MB231 breast cancer cells (Figure II-6a) but also that the overall peptide quantity required with HGN-NuBCP is 30 fold less than those previously delivery methods of NuBCP [19]. Active mitochondria can give insight to early apoptosis through the JC-1 assay, which detects membrane depolarization of the mitochondria. Our data in Figure II-4c suggests that only upon irradiation with NIR light does the HGN-NuBCP cause disruption of the mitochondria membrane, via enhancement of the green fluorescence overtime. Control studies with NIR light and HGN without the NuBCP peptide showed no change in the mitochondria health (Figure II-5). The JC-1 assay studies were conducted in the H460 (PacR) cell line. Bcl-2 is highly expressed in Non-Small Cell Lung cancer and Triple Negative Breast cancer (Figure II-4b), therefore NuBCP-9 targeting of Bcl-2 is not limited to one cancer type but will be effective in cancer subtypes expressing Bcl-2.

Finally, these results were translated to in vivo efficacy studies with HGN-NuBCP in zebrafish embryos. Embryo-larval zebrafish are highly sensitive to environmental factors during development. Zebrafish have been successfully used as model for assessing potential human toxicity with high sensitivity, including nanoparticles and therefore are uniquely qualified for initial testing to assess the safety of developing new drugs [25,26]. Moreover, the excellent transparency of the larval zebrafish allowed elucidation of the proper laser

power as visualization of HGN resonant light intensity was used to confirm that the proper laser power was reaching the cancer cells within the zebrafish [27,28]. Paclitaxel resistant (PacR) H460 cells were exposed to HGN-NuBCP and transplanted into zebrafish embryos, which were treated with NIR light. The NIR light allowed for release of the Bcl-2 targeting NuBCP and reduced the tumor growth in these samples by 56.4% compared to the non-laser control for HGN-NuBCP (Figure II-6 g and h). This indicates not only that the HGN-delivery method can be used for peptide delivery in vivo, but also that the release of the NuBCP from the HGN is light controlled in this system as well.

F. CONCLUSION

In conclusion, we report the use of HGN for the delivery of a Bcl-2 functional converting apoptotic peptide, NuBCP, to therapeutic resistant cells. Laser controlled HGN delivery of NuBCP not only drives down the therapeutic dose required of NuBCP to induce apoptosis by 30-fold, it also provides a means to target tumor-specific regions. Laser release was shown to be safe and effective for reducing chemotherapy resistant tumor growth in zebrafish xenografts. Our results suggest the light control of NuBCP with HGN not only increased efficacy in vitro but the efficiency in vivo demonstrates the potential application of HGN-NuBCP as a therapeutic to treat cancers that express Bcl-2.

G. REFERENCES

1. Allen TM. Ligand-targeted therapeutics in anticancer therapy. *Nat Rev Cancer*. 2002 Oct;2(10):750–63.
2. Holohan C, Van Schaeybroeck S, Longley DB, Johnston PG. Cancer drug resistance: an evolving paradigm. *Nat Rev Cancer*. 2013 Oct;13(10):714–26.
3. Gupta D, Kumar M, Tyagi P, Kapoor S, Tyagi A, Barman TK, et al. Corrigendum to ‘Concomitant delivery of paclitaxel and NuBCP-9 peptide for synergistic enhancement of

cancer therapy' NANO 14 (2018) 1301-1313. *Nanomedicine Nanotechnol Biol Med*. 2018 Oct;14(7):2129.

4. Pearce MC, Gamble JT, Kopparapu PR, O'Donnell EF, Mueller MJ, Jang HS, et al. Induction of apoptosis and suppression of tumor growth by Nur77-derived Bcl-2 converting peptide in chemoresistant lung cancer cells. *Oncotarget*. 2018 May 25;9(40).

5. Li H, Nelson CE, Evans BC, Duvall CL. Delivery of intracellular-acting biologics in pro-apoptotic therapies. *Curr Pharm Des*. 2011;17(3):293–319.

6. Hughes J, Rees S, Kalindjian S, Philpott K. Principles of early drug discovery: Principles of early drug discovery. *Br J Pharmacol*. 2011 Mar;162(6):1239–49.

7. Czabotar, P. E.; Lessene, G.; Strasser, A.; Adams, J. M. Control of Apoptosis by the BCL-2 Protein Family: Implications for Physiology and Therapy. *Nat. Rev. Mol. Cell Biol*. 2014, 15 (1), 49–63.

8. Yip KW, Reed JC. Bcl-2 family proteins and cancer. *Oncogene*. 2008;27(50):6398–406.

9. Bouchalova K, Svoboda M, Kharaishvili G, Vrbkova J, Bouchal J, Trojanec R, et al. BCL2 is an independent predictor of outcome in basal-like triple-negative breast cancers treated with adjuvant anthracycline-based chemotherapy. *Tumour Biol J Int Soc Oncodevelopmental Biol Med*. 2015 Jun;36(6):4243–52.

10. Honma N, Horii R, Ito Y, Saji S, Younes M, Iwase T, et al. Differences in clinical importance of Bcl-2 in breast cancer according to hormone receptors status or adjuvant endocrine therapy. *BMC Cancer*. 2015 Oct 15;15(1):698.

11. Giuliano M, Hu H, Wang Y-C, Fu X, Nardone A, Herrera S, et al. Upregulation of ER signaling as an adaptive mechanism of cell survival in HER2-positive breast tumors treated

with anti-HER2 therapy. *Clin Cancer Res Off J Am Assoc Cancer Res.* 2015 Sep 1;21(17):3995–4003.

12. Real PJ, Sierra A, De Juan A, Segovia JC, Lopez-Vega JM, Fernandez-Luna JL. Resistance to chemotherapy via Stat3-dependent overexpression of Bcl-2 in metastatic breast cancer cells. *Oncogene.* 2002 Oct 31;21(50):7611–8.

13. Choudhary GS, Al-harbi S, Mazumder S, Hill BT, Smith MR, Bodo J, et al. MCL-1 and BCL-xL-dependent resistance to the BCL-2 inhibitor ABT-199 can be overcome by preventing PI3K/AKT/mTOR activation in lymphoid malignancies. *Cell Death Dis.* 2015 Jan 15;6(1):e1593.

14. Yecies D, Carlson NE, Deng J, Letai A. Acquired resistance to ABT-737 in lymphoma cells that up-regulate MCL-1 and BFL-1. *Blood.* 2010 Apr 22;115(16):3304–13.

15. Lin B, Kolluri SK, Lin F, Liu W, Han Y-H, Cao X, et al. Conversion of Bcl-2 from Protector to Killer by Interaction with Nuclear Orphan Receptor Nur77/TR3. *Cell.* 2004 Feb 20;116(4):527–40.

16. Kolluri SK, Zhu X, Zhou X, Lin B, Chen Y, Sun K, et al. A Short Nur77-Derived Peptide Converts Bcl-2 from a Protector to a Killer. *Cancer Cell.* 2008 Oct 7;14(4):285–98.

17. Bodo J, Zhao X, Durkin L, Souers AJ, Phillips DC, Smith MR, et al. Acquired resistance to venetoclax (ABT-199) in positive lymphoma cells. *Oncotarget.* 2016 Sep 20;7(43):70000–10.

18. Huang, S.; Jiang, C.; Guo, H.; Wang, J.; Liu, Y.; Li, C.; Lopez, E.; Zhang, H.; Lorence, E. A.; Merolle, M.; et al. Resistance Mechanisms Underlying Venetoclax Resistance in Mantle Cell Lymphoma. *Blood* 2017, 130 (Suppl 1), 2749.

19. Kapoor S, Gupta D, Kumar M, Sharma S, Gupta AK, Misro MM, et al. Intracellular delivery of peptide cargos using polyhydroxybutyrate based biodegradable nanoparticles:

Studies on antitumor efficacy of BCL-2 converting peptide, NuBCP-9. *Int J Pharm.* 2016 Sep 25;511(2):876–89.

20. Kumar M, Gupta D, Singh G, Sharma S, Bhat M, Prashant CK, et al. Novel polymeric nanoparticles for intracellular delivery of peptide Cargos: antitumor efficacy of the BCL-2 conversion peptide NuBCP-9. *Cancer Res.* 2014 Jun 15;74(12):3271–81.

21. Kumar M, Singh G, Sharma S, Gupta D, Bansal V, Arora V, et al. Intracellular delivery of peptide cargos using iron oxide based nanoparticles: studies on antitumor efficacy of a BCL-2 converting peptide, NuBCP-9. *Nanoscale.* 2014 Nov 6;6(23):14473–83.

22. Prevo B, Esakoff S, Mikhailovsky A, Zasadzinski J. Scalable routes to gold nanoshells with tunable sizes and response to near-infrared pulsed laser irradiation. *Small.* 2008;4:1183–95.

23. Kimmel CB, Ballard WW, Kimmel SR, Ullmann B, Schilling TF. Stages of embryonic development of the zebrafish. *Dev Dyn.* 1995 Jul;203(3):253–310.

24 Schindelin J, Arganda-Carreras I, Frise E, Kaynig V, Longair M, Pietzsch T, et al. Fiji: an open-source platform for biological-image analysis. *Nat Methods.* 2012 Jul;9(7):676–82

25 Wehmas LC, Tanguay RL, Punnoose A, Greenwood JA (2016) Developing a Novel Embryo–Larval Zebrafish Xenograft Assay to Prioritize Human Glioblastoma Therapeutics. *Zebrafish* 13:317–329.

26 Chakraborty C, Sharma AR, Sharma G, Lee S-S (2016) Zebrafish: A complete animal model to enumerate the nanoparticle toxicity. *Journal of Nanobiotechnology* 14.

27 Liu J, Liu Y, Bu W, et al (2014) Ultrasensitive Nanosensors Based on Upconversion Nanoparticles for Selective Hypoxia Imaging in Vivo upon Near-Infrared Excitation. *Journal of the American Chemical Society* 136:9701–9709.

28 Liu H-Y, Wu P-J, Kuo S-Y, et al (2015) Quinoxaline-Based Polymer Dots with Ultrabright Red to Near-Infrared Fluorescence for In Vivo Biological Imaging. *Journal of the American Chemical Society* 137:10420–10429.

III. VIPER^{nano} : IMPROVED LIVE CELL INTRACELLULAR PROTEIN TRACKING

A. Abstract

Tracking intracellular proteins in live cells has many challenges. The most widely-used method, fluorescent protein fusions, can track proteins in their native cellular environment and has led to significant discoveries in cell biology. Fusion proteins add steric bulk to the target protein and can negatively affect native protein function. The use of exogenous probes such as antibodies or protein labels is problematic since these cannot cross the plasma membrane on their own and thus cannot label intracellular targets in cells. We developed a labeling platform, VIPER^{nano} (Versatile Interacting Peptides E and R with hollow gold nanoshells), for live cell imaging of intracellular proteins using a peptide fusion tag (CoilE) to the protein of interest and delivery of a fluorescently labeled probe peptide (CoilR). CoilR and CoilE forms an α -helical heterodimer with the protein of interest, rendering a labeled protein. Delivery of CoilR into the cell is done using a hollow gold nanoshell (HGN). The technology relies on the conjugation and light activated release of the CoilR peptide on the surface of the HGNS. We demonstrate light-activated VIPER^{nano} delivery and labeling with two intracellular proteins, localized either in the mitochondria or the nucleus. This technology has the ability to study intracellular protein dynamics and spatial tracking while lessening the steric bulk of tags associated with the protein of interest.

B. Introduction

Chemical biology tools can interrogate protein function within live cells and provide high resolution spatial and temporal information. In particular, visualizing and tracking proteins through fluorescence microscopy has transformed cell biology¹. Antibody-based methods form the basis of many such studies, yet these methods require specific reagents and many

proteins are not amenable to this approach. The reliance on cell fixation forms another barrier^{2,3}.

Fluorescent protein (FP) fusion tags provide an enormous improvement over immunolabeling by allowing the tracking of proteins in live cells for bioimaging and protein tracking⁴⁻⁷. However, FP fusion tags rely on proteins that in many cases are larger than the protein of interest (see Figure 1), which have been shown to alter protein function, trafficking, stability, and localization^{8,9}. More recently, smaller peptide epitopes consisting of ~10 amino acids (e.g., FLAGTM) have been explored as alternatives¹⁰. However, these methods still require membrane permeabilization, fixation and incubation with anti-FLAG antibodies which limits their capabilities for live cell imaging.

An alternative labeling strategy uses coiled-coil interactions as a basis for protein tagging. In this method, an endogenous protein-peptide fusion is labeled by incubation and dimerization with a second peptide conjugated to a fluorophore as shown in Figure 2a¹¹⁻¹⁴. We recently developed VIP (versatile interacting peptide) tags, which use a heterodimeric coiled-coil between two peptides as seen in Figure 2a^{11,12}. In the latest variation, VIPER, a fusion peptide tag (CoilE) binds with reporter-conjugated peptide (CoilR) and is used to label both extracellular and intracellular proteins. While the VIP tags are small (~5 kDa) and highly specific, the delivery of the probe peptide to cytosolic targets requires permeabilization and fixation of the cells^{11,12}. Here we sought to improve the VIP tags by introducing a technology for accessing intracellular targets in living cells^{11,13,14}.

VIPER^{nano} combines the VIPER technology with our hollow gold nanoshell (HGN) protein delivery platform¹⁵⁻¹⁷. We previously used HGNS to deliver siRNA, therapeutic peptides and gene editing enzymes into human cells and animal models with spatiotemporal

control^{16,18,19}. This delivery strategy relies on orthogonal linkers attached to the HGN surface, one for internalization using a cell penetrating peptide and the other for CoilR attachment. Particle internalization via endocytosis results in endosomal entrapment until irradiation with NIR light. For many nanoparticle delivery strategies, endosomal entrapment is a major obstacle^{20,21}. Our technology allows for controlled release of the HGNS from the endosome²² as well as release of the CoilR from the HGN surface with near infrared light.

Herein we describe a proof of concept co-localization study of intracellular targets on cellular components (mitochondria and histone H2B). Target proteins are expressed as a genetic fusion with the Coile peptide and the complementary, CoilR, conjugated to a Sulfo-Cy5 dye (CoilR-Cy5), is delivered using the HGNS. Expansion of this technology will allow for the study of dynamic protein tracking in live cells with less impact on the protein function.

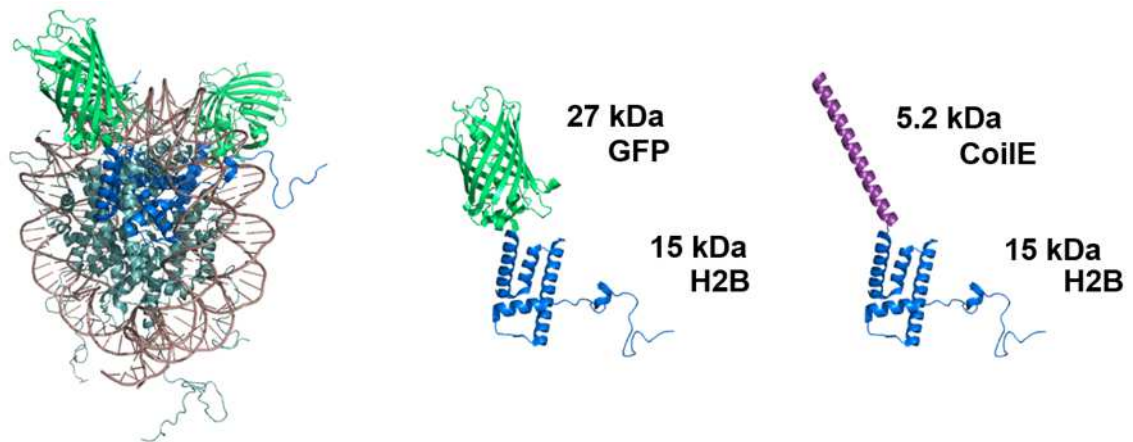
C. Results and Discussion

Particle Design, Characterization and Internalization

VIP tags were previously developed to enable cellular proteins to be labeled and imaged without the need to add a large protein fusion, such as green fluorescent protein. VIPER was used to distinctly label the histone protein H2B and an inner membrane mitochondrial protein (using a COX8 fragment encoding a localization sequence: “Mito”) with a significantly smaller tag¹². The Coile tag lessened the steric bulk around the protein of interest, which allows for the use of fluorescent labels with a more accurate representation of protein dynamics.

For example, a nucleosome core particle consists of a histone octamer wrapped with DNA²³ (Figure III-1a). The GFP fusion to H2B creates steric bulk at the site where the DNA wraps around the histone proteins. Our model of this interaction suggests that the size of the

GFP barrel would impact the structural role of histones in regulating transcription and in assembling specialized chromatin domains²³. Prior studies of fluorescent proteins such as GFP have shown unanticipated issues with protein dynamics^{8,9}. A comparison of H2B fused to a GFP (Figure III-1b) to CoileE (Figure III-1c) shows the size variation between the two tags. Notably, GFP is double the size of H2B whereas CoileE is just one-third the size of H2B. Our study relies on the use of protein FP fusions involving both coiled coil tags as well as FPs to enable a direct comparison of the localization as revealed by our technology; future applications of VIPER^{nano} will be used to track proteins without fluorescent protein fusions.



(A) Nucleosome with H2B-GFP (B) H2B-GFP fusion (C) H2B-CoileE fusion

Figure III-1. VIPER^{nano} relies on much smaller fluorescent protein tags. (A) Nucleosome (PDB ID: 1kx5) with H2B-GFP (GFP PDB ID: 2yog) shows the DNA (tan) wrapped around the octamer of histone proteins (light blue) including the two H2B proteins (dark blue) fused to GFP (green). (B) H2B-GFP fusion monomer with size markers for GFP (27 kDa) and H2B (15 kDa) (C) H2B-CoileE fusion monomer with size markers for CoileE (5.2 kDa) and H2B (15 kDa). Structure prediction for CoileE peptide model with PEPFOLD3^{24,25}.

Our HGN functionalization strategy relies on the robust affinity of the hexahistidine-tagged CoilR to nitrilotriacetic acid (NTA) in the presence of copper, which is attached to a thiolated PEG (polyethylene glycol) linker assembled on the surface of the HGN¹⁶. Cellular

internalization of the HGNs is guided by the transactivating transcriptional activator (TAT) peptide attached via streptavidin to a biotinylated PEG linker orthogonal to our CoilR component (Figure III-2b). The two different thiolated PEG strands were loaded onto the HGN in equimolar amounts to allow for proper loading of the internalization peptide, TAT, as well as the CoilR-Cy5. The final HGN particle size was ~150 nm (Figure III-2c). The Cy5 fluorophore is a red-fluorescent probe that is bright and pH insensitive, which makes it compatible with observing proteins in lysosomes and other acidic organelles²⁶.

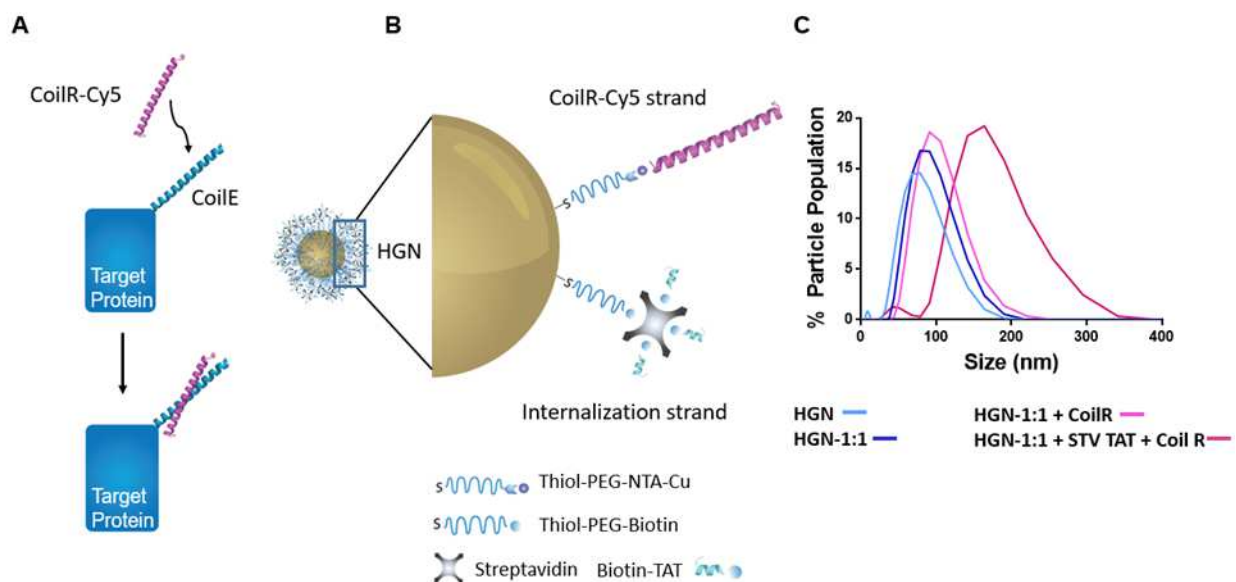


Figure III-2. Particle assembly strategy and size analysis (a) VIPER technology strategy. A target protein is genetically tagged with the CoilE peptide. The tagged protein can then be labeled by dimerization with a CoilR peptide conjugated to a fluorescent dye delivered with a HGN. (b) Illustration of HGN construct with 1:1 loading of thiol-PEG-NTA (CoilR-Cy5 strand): Thiol-PEG-biotin (Internalization strand). The biotin terminated PEG was labeled with streptavidin TAT for internalization while the orthogonal NTA terminated strand allowed for CoilR-Cy5 loading. (c) Dynamic light scattering size distribution of nanoparticles at different stages of synthesis and conjugation steps.

We previously demonstrated that the CoilR peptide alone, as well as gold particles without the TAT cell penetrating peptide, do not enter cells through passive diffusion^{12,27}. To

confirm the internalization of PEGylated HGN-CoilR-Cy5 particles, HeLa cells (100,000 cells) were incubated with 3.2 pM HGN-CoilR-Cy5 for two hours and visualized using both fluorescent and darkfield microscopy. The Cy5 fluorescent puncta within the HeLa cells indicated internalization of HGN-CoilR-Cy5 while the scattered light from the HGN surface in the darkfield microscopy image (orange puncta) demonstrated internalization of the HGN (Figure III-3b).

We controlled the internalization of the HGN construct into human cells by using the TAT peptide^{18,19}. The modular design of the HGN construct allows for the use of other targeting peptides depending on the target cell application (Figure III-2).

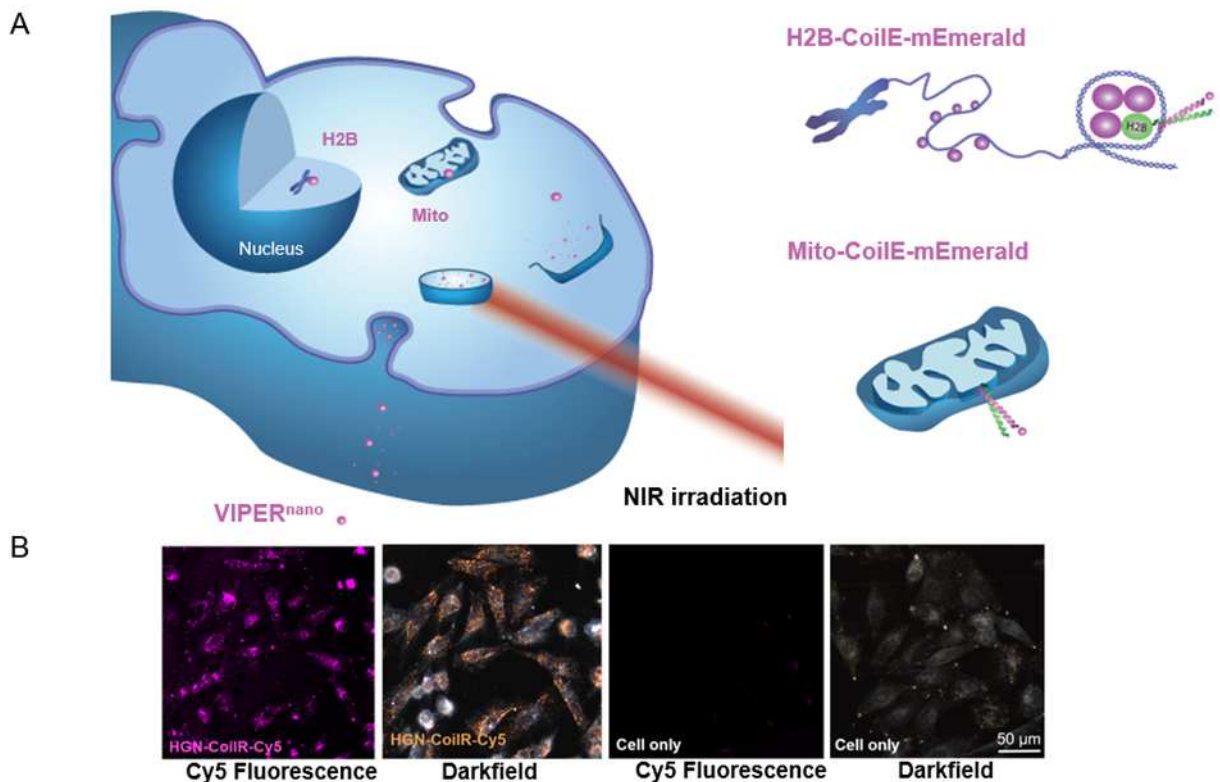


Figure III-3. (a) Schematic of HGN-CoilR-Cy5 (magenta) internalization and release from the endosome with NIR light colocalizes with cellular targets (e.g., H2B-CoilE-mEmerald and Mito-CoilE-mEmerald). (b) Streptavidin-TAT coating on nanoparticles allows for internalization of HGN-CoilR-Cy5 into HeLa cells observed by Cy5 fluorescence and light scattered from the gold nanoparticles with dark field microscopy (orange puncta).

Load and release characterization

Quantification of peptide load and release was determined in a cell free environment through analysis of the fluorescent Cy5 label on the CoilR peptide. HGNs (32 pM) were incubated with 1 μM CoilR and then washed to remove the excess CoilR-Cy5 via centrifugation. The particles were then exposed to a pulsed 800 nm laser at 300 mW for 15 seconds to release the loaded peptide from the surface of the particle. The particles were concentrated via centrifugation and the supernatant was analyzed using a Tecan M200

fluorescent plate reader and compared to a titration curve of known Cy5 fluorescence and CoilR concentration. The HGN-CoilR-Cy5 samples that were not irradiated with NIR light were treated with a buffer containing KCN to dissolve the gold particles and therefore chemically released the bound peptide for total loading quantification of the CoilR-Cy5 peptide. We determined that 10,000 CoilR-Cy5 peptides were loaded per particle, which is comparable to the HGN-DNA-NTA construct previously reported²⁷. Comparison of the supernatants in Figure III-4a demonstrates the release of 63% of the loaded CoilR peptide only upon NIR irradiation which agrees with previous PEG release studies using HGNS¹⁵.

Further release studies were conducted to demonstrate the release capabilities of CoilR-Cy5 from HGN once internalized into HeLa cells. Samples were irradiated with a commercial two-photon confocal microscope equipped with a scanning, tunable NIR laser set to 800 nm and 240 mW. Comparison of images taken before and after irradiation show release of CoilR-Cy5 from puncta upon irradiation with NIR light (Figure III-4b,c). Diffusion of the Cy5 dye upon irradiation is visualized in a low magnification image in Figure III-4b. Individual cells were isolated and compared for their overall intensity and distribution of Cy5 dye using the Image J Plot Profile analysis tool (Figure III-4b,c). Pixel plot profiles of 4 selected cells (in blue boxes shown in Figure III-4b) were analyzed before and after laser irradiation to demonstrate the overall increase in both intensity and distribution of Cy5 throughout the cells before (black trace) and after (magenta trace) laser irradiation (Figure III-4d). The gray value demonstrates the overall intensity of pixels at a given location in the box (distance, pixels).

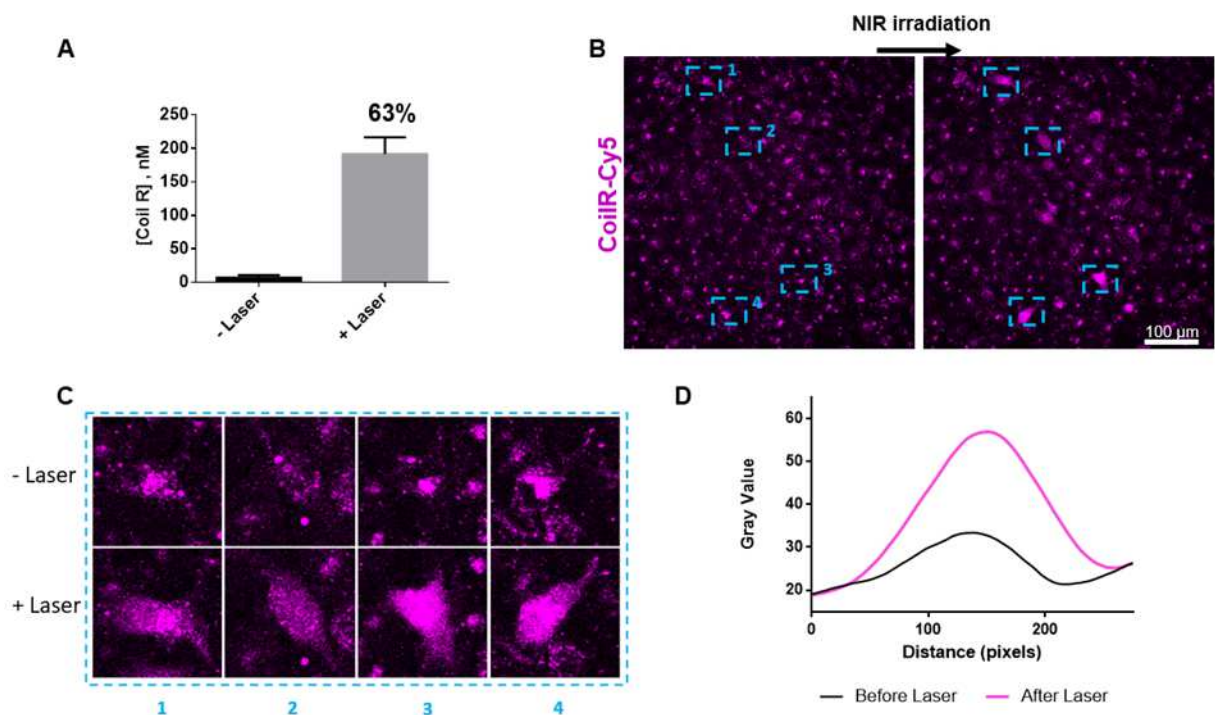


Figure III-4. Light activated release of CoilR-Cy5 from HGN is NIR light activated. (a) Release of CoilR-Cy5 from 32 pM HGNs quantified by fluorescence intensity observed in the supernatant solution after NIR irradiation and centrifugation. Samples were centrifuged and their pellets were analyzed for total peptide loading with KCN etch and fluorescence detection. (b) HeLa cells were treated with HGN-CoilR-Cy5 and irradiated using a two-photon microscope at 800 nm. Release of CoilR-Cy5 upon NIR irradiation is demonstrated by the diffusion of CoilR-Cy5 across HeLa cells as the peptide was released from the endosomal membrane into the cytosol. The blue boxes indicate region of interests (ROIs) selected to demonstrate CoilR-Cy5 diffusion through pixel distribution plots. (c) Magnification of selected ROIs demonstrating CoilR-Cy5 peptide diffusion from fluorescent puncta after NIR laser irradiation. (d) Smoothed pixel distribution plot (2nd order, 80 neighbors) where an increase in gray value demonstrates the increase in Cy5 fluorescence observed in an averaged plot from N = 4 before laser irradiation (black trace) and N = 4 after laser irradiation (magenta trace)

Colocalization of CoilR with Subcellular Targets is Laser Dependent and Allows for Dynamic protein tracking in Live Cells

Many labeling strategies that use endogenous tags lack the ability to control how much of the labeled target is released²⁸. The delivery of CoilR with HGN provides a means to tune the amount of CoilR delivered through changing the NIR laser power used to release the CoilR.

To demonstrate this feature, we plated HeLa cells on a gridded ibidi culture dish (60 μ -Dish, High Grid 500) to allow us to relocate the irradiated areas using a two-photon confocal microscope. HeLa cells transfected with Mito-CoilE-mEmerald were incubated with HGN-CoilR-Cy5 and subjected to NIR irradiation at different laser powers (0, 168, 240 mW). The samples were later visualized on a Leica SP8 resonant scanning confocal microscope to assess colocalization between the green fluorescent mitochondria target and the delivered red fluorescent Coil-Cy5 peptide (Figure III-5a). An increase in protein labeling was observed with higher laser powers and no mitochondrial protein label is observed in samples that were not irradiated with NIR light. Cells that do not express the CoilE fusion protein still internalized the CoilR-Cy5; however the mitochondria in these cells were not labeled due to the lack of CoilE fusion peptide (Figure III-5a).

Super-resolution microscopy can track single molecules in live cells and reveal details of cellular structures²⁹. We used the Bruker/Vutara 352 super-resolution microscope to observe HeLa cells expressing H2B-CoilE-mEmerald and treated with HGN-CoilR-Cy5 after laser irradiation and tracked the migration of CoilR-Cy5 over 10 seconds using the Vutara 2D particle tracking module³⁰. The software was able to track the movement of CoilR peptide through analysis of Cy5 dye movement in the selected cell demonstrating release of the CoilR after laser irradiation. The Cy5 dye was stationary in non-irradiated samples (Figure III-5b). From this tracking experiment, we conclude that VIPER^{nano} colocalization can be used for super resolution tracking of target protein movement in live cells in a laser power dependent manner.

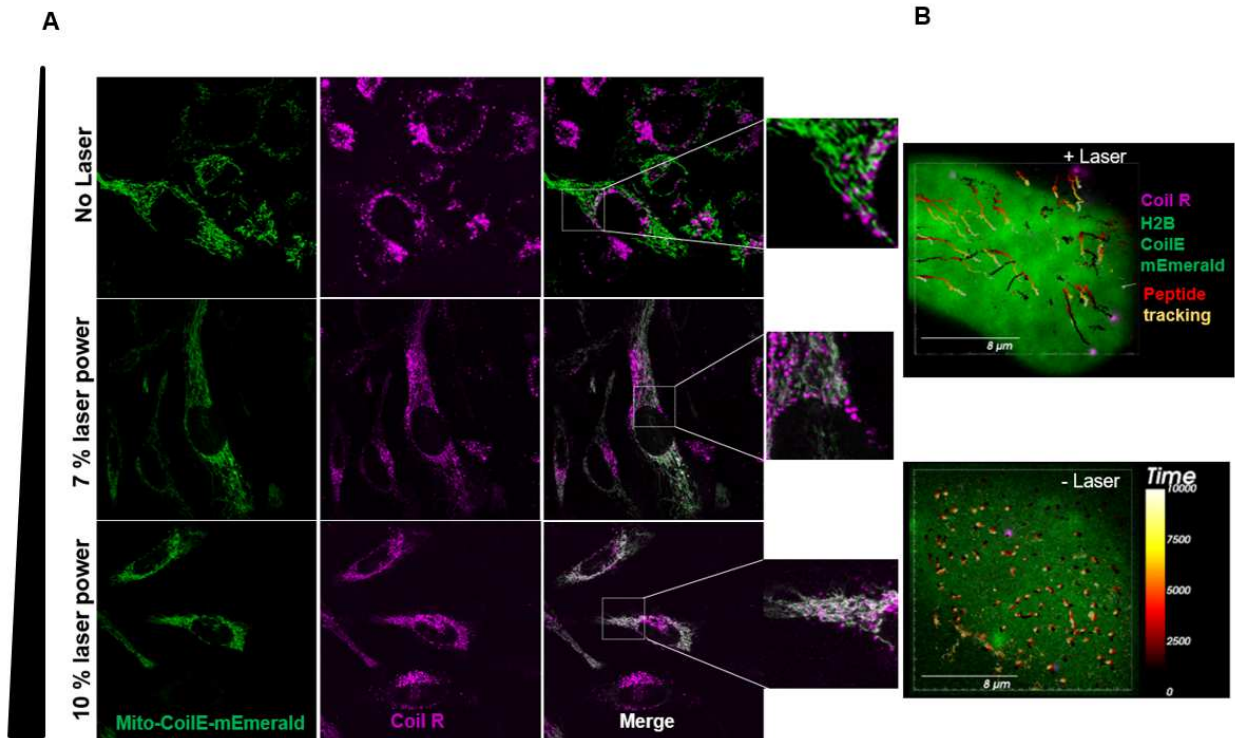


Figure III-5. (a) Confocal imaging of HeLa cells transfected with Mito-CoilE-mEmerald 24 hours post laser irradiation of a region of interest (ROI) with internalized HGN-CoilR shows specific labeling (white merge) of cellular mitochondria (Mito-CoilE-mEmerald in green) with CoilR-Cy5 (magenta) increases with higher laser irradiation power. Two-photon NIR excitation at full power was 2.4 W. (b) Overlay of mEmerald and Cy5 in high resolution fluorescence microscopy of CoilR-Cy5 in HeLa cells with H2B-CoilE-mEmerald over 10 seconds shows peptide movement only in irradiated samples (top image) and little to no movement in non-irradiated samples (bottom image) N=3 for both laser conditions.

We tracked protein labeling of the mitochondria and H2B targets over the course of hours and days to visualize protein movement in specific cells that were relocated using the gridded tissue culture plates. Time-lapse images were collected over a period of 2.5 hours for the mitochondria CoilR Cy5 labels to demonstrate the dynamic movement of the mitochondria overtime validated by simultaneously tracking mEmerald movement (Figure III-6a,c). A super resolution microscopy (SRM) technique, Super-Resolution Radial Fluctuations (SRRF), was used to extract sub-diffraction information from a quick, short burst of 100

images taken in time-lapse on a confocal fluorescent microscope³¹. The SRRF analysis allows for long term SRM time lapse acquisition using lower intensity illumination to prevent photo toxicity during the live cell microscopy analysis³². A SRRF time-lapse was acquired over the period of 2.5 hours showing the movement of mitochondria over a short period of time (Figure III-6c).

For H2B protein labeling we imaged at two time points 24 hrs apart to observe the longevity of the VIP tags in a system undergoing cellular division. Similar to previous histone-mEmerald fusion protein analysis of histone dynamics³³, chromatin bridges formed can be visualized during certain stages of mitosis³⁴. The same cells were located ~24 hours later using the gridded culture dish and imaged to show proper division into two individual cells (Figure III-6b). The CoilR and mEmerald co-localization demonstrates the capability of VIPER^{nano} for longer term protein dynamics analysis.

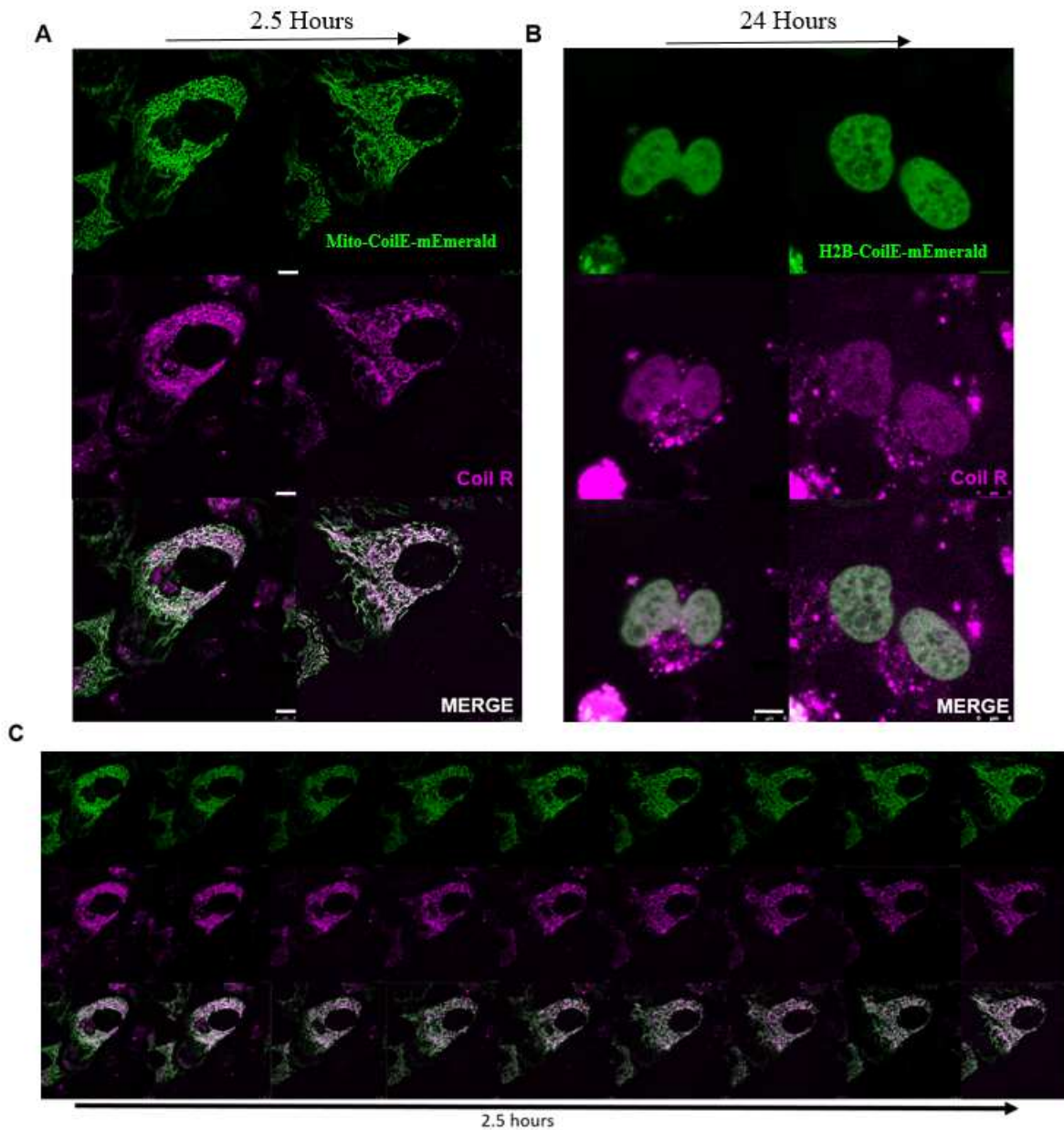


Figure III-6. Live tracking of cellular dynamics using HGN-CoilR (a) HeLa cells transfected with Mito-CoilE-mEmerald were treated with 3.2 pM HGN-CoilR and irradiated using a two-photon microscope at 800 nm. 24 hours post laser irradiated images were collected over a period of 2.5 hours to demonstrate the ability to track mitochondria movement over time. Each photo is a combination of 100 images taken as a time lapse to generate one NanoJ-SRRF high resolution image. (b) HeLa cells transfected with H2B-CoilE-mEmerald were treated with 3.2 pM HGN-CoilR and irradiated. The cells were later re-localized using gridded culture dishes 24 and 48 hours post laser irradiation to observe the separate of two nuclei using the CoilR peptide. (c) Time lapse imaging of (a) demonstrating dynamic movement of mitochondria with both CoilR and mEmerald. White scale bar in images corresponds to 8 μ m.

D. Conclusions

Our results suggest the light activated delivery of CoilR using HGN unleashes a way to study intracellular protein dynamics and tracking while lessening the steric bulk of tags associated with the protein of interest. This development provides a new strategy to track proteins without the introduction of large fusion proteins. We demonstrate VIPER^{nano}, which utilizes HGN for protein tagging of intracellular targets with the addition of a small tag, a peptide less than 6 kDa to the protein of interest. The HGN construct design for delivery is advantageous as it can be modulated to allow for particle internalization into diverse cell lines using an alternative cell penetrating peptide motif on the particle. For example, substitution of the TAT peptide for a biotinylated RPARPAR peptide lends to specific cell targeting to PPC-1 cells that overexpress the neuropilin-1 receptor^{15,35}. We demonstrated the light controlled capability of the technology that allows for control over when the labeling of intracellular targets occurs, how much of the CoilR peptide is released and cellular specification of peptide release.

E. Materials and Methods

PEG adsorption onto HGN

HGNs were synthesized using sacrificial silver template in a previously described protocol^{27,36}. The particles were then dialyzed overnight in sodium citrate buffer (500 mM) with 0.03% diethyl pyrocarbonate (DEPC) (Biochemica) in dialysis cassettes (MWCO 20kDa).

To coat the particles with the 1:1 PEG layer, HS-PEG-biotin (5K) and HS-PEG-NTA (3.4K) 1mM stocks were incubated with 12.5 mM TCEP for 10 minutes to reduce dithiols in solution. A final concentration of 10 μ M PEG (5 μ M SH-PEG-NTA and 5 μ M SH-PEG-biotin) was added to 64 pM HGNs, incubated on a rocker overnight at room temperature, and

washed 3x in PBS with 0.01% Tween 20 (PBST) at 20,000 g for 20 minutes to remove excess PEG.

Streptavidin and biotin-TAT functionalization

For particle internalization, streptavidin- biotin-TAT was added to the SH-PEG-biotin strands on the 1:1 PEG particles. A 2mg/mL streptavidin stock in PBST was added in equal volume to 64 pM pegylated particles and quickly sonicated and vortexed. After a 1 hour incubation period, excess streptavidin was removed with three washes in PBST at 10,000 g for 10 min. A final concentration of 20 μ M biotin-TAT (Anaspec) was achieved through two equal volume additions with a 30 minute incubation at room temperature after each addition. The particles were then washed another three times with PBST to remove any excess biotin-TAT and stored at 4 °C.

Quantification cell-free CoilR-Cy5 load and release

In brief, the Coil R peptide was previously expressed in *E. coli* BL21 (DE3) cells (thermofisher) using a pET28b(+)_CoilR plasmid and purified under denaturing conditions¹². The purified CoilR peptide was labeled with Cy5 dye for peptide tracking with a maleimide dye which reacted with the single reactive cysteine residue on the CoilR peptide¹².

CoilR-Cy5 (1 μ M initial) was loaded onto 32 pM HGNs incubated with 500 μ M CuCl₂ for 20 minutes on ice. Excess CoilR-Cy5 was removed with three washes in PBST via centrifugation at 10,000 g for 10 min. Total peptide loading per particle was determined using a previously described KCN etch procedure where 32 pM particles were incubated in a KCN solution [0.1 M KCN, 1mM K₃Fe(CN)₆] to dissolve the gold particles and release the labeled peptide²⁷. Concentration of the released peptide was quantified using a standard linear calibration curve between the concentration of CoilR-Cy5 and the corresponding fluorescence intensity detected using the Tecan M200 plate reader. HGN loaded with CoilR-

Cy5 were irradiated with NIR light using a pulsed laser generated from a femtosecond Ti:sapphire regenerative amplified (Spectraphysics Spitfire) running at 1 kHz repetition rate for 15 seconds at 500 mW laser power (power determined using a thermopile power meter). Quantification of peptide released was determined after centrifugation of the samples and removal of the supernatant. The supernatant was plated on a 96 well plate for Cy5 fluorescence analysis and the pellets were then etched to determine the amount of peptide retained on the particle.

Cell culture and transfection

VIPER^{nano} Imaging experiments were conducted in transiently transfected HeLa cells cultured at 37°C in 5% CO₂. To create the plasmid constructs for transfection, the CoilE gene was inserted into fusion protein mEmerald constructs obtained from Addgene (Michael Davidson's Collection): Mito-7-mEmerald (Addgene #54160) and H2B-mEmerald (Addgene #54111)¹². To generate the cell lines expressing the CoilE peptide, HeLa cells were plated in a 6 well tissue culture plate seeded at 3x10⁵ cells per well 48 hours prior to transfection. Each plasmid transfection was performed using lipofectamine 2000 (ThermoFisher Scientific) according to the manufacturer's protocol. Each transfection mixture included 1.4 µg plasmid DNA and 7 µL lipofectamine reagent in 400 µL Opti-MEM. The cells were washed after 2 hours and the transfection media was replaced with DMEM +10% FBS.

Darkfield and fluorescence microscopy for internalization analysis

HeLa cells were plated in an 8-well chambered glass slide (Millipore) at 4x10⁵ cells per well in 400 µL DMEM +10% FBS approximately 24 hours prior to particle internalization. HGN loaded with CoilR-Cy5 were suspended in DMEM + 10% FBS (3.2 pM) and incubated with plated HeLa cells for 2 hours at 37°C at 5% CO₂. Cells were washed with PBS twice and then one drop of PBS was added to each well before a cover glass was applied to the

glass slide containing the HeLa cells. Samples were observed on an Olympus BX51 upright compound microscope with a dark field condenser and a 20x objective lens.

Cellular release using two-photon microscope and analysis with Image J

Transfected cells were plated on Ibidi μ -Dish (35 mm, high Grid-50) at 100,000 cells 2-3 days post transfection and 24 hours prior to laser excitation. HGN were loaded with CoilR-Cy5 in the previously described method and filtered using a 0.22 μ m filter to remove any large particle contaminants prior to incubation with HeLa cells. 4 pM particles were incubated in 400 μ L DMEM with 10% FBS at 37°C at 5% CO₂ in ibidi culture dish. After 2 hours the samples were washed with PBS three times to remove excess particles and then suspended in 2 mL of DMEM, high glucose, HEPES, no phenol red supplemented with 10% FBS. Samples were focused using a Olympus Fluoview 1000MPE two-photon and confocal microscope equipped with a 25 x water immersion objective lens and irradiated using a mode locked Ti:sapphire tunable femtosecond pulsed laser (100 fs pulse duration, 80 MHz repetition rate, Mai Tai HP, Newport Spectra Physics). The cells were kept in a humidified chamber at 37°C and 5% CO₂ through the duration of the two-photon microscopy experiment. The NIR laser irradiation was set to irradiate at 800 nm in 0.69 nm slices through the cell volume at varying NIR power percentages to get to 168 and 240 mW. Images capturing mEmerald and Cy5 fluorescence were collected before and after laser irradiation to confirm release of the CoilR peptide and these images were later analyzed using (Fiji Is Just) ImageJ for diffusion of the Cy5 dye. Single cells were selected and analyzed using the pixel plot profile analysis tool. The data was later visualized in GraphPad Prism using 2nd order smoothing with 80 neighbors for qualitative analysis of pixel distribution with and without laser.

The cell samples were later analyzed for colocalization using a Leica SP8 resonant scanning confocal microscope or the Vutara 352 Superresolution microscope for particle tracking analysis.

Super resolution particle tracking

Post NIR irradiation, samples were imaged on the Vutara 352 super resolution microscope for analysis of Cy5 localization with and without laser irradiation. HeLa cells transfected with H2B-CoilE-mEmerald previously incubated with HGN-CoilR-Cy5 were initially visualized by focusing on the green fluorescence in the nucleus. Once a single cell was located, a 10,000 ms time lapse was obtained on both the mEmerald and Cy5 fluorescence channels. The peptide location was later analyzed using the SRX software capable of high resolution single molecule tracking for the Cy5 movement through the duration of the time-lapse. Cy5 movement in cells irradiated with NIR light were compared to the movement in those that were not irradiated with NIR light.

Confocal imaging for co-localization analysis

Confocal microscopy was conducted on a Leica SP8 resonant scanning confocal microscope with a 63x oil objective lens in a live cell chamber which kept the cells at 37°C and 5% CO₂ throughout the data collection. Excitation source for mEmerald and Cy5 fluorescence was a white light laser at 488 nm and 633 nm respectively. Time-lapse images (100 frames) for Mito co-localization for later SRRF analysis were collected using the xyt function for 10 minutes per final SRRF image. SRRF analysis was conducted using the NanoJ-SRRF plug-in for (Fiji Is Just) Image J. All images were false-colored using standard lookup tables: mEmerald (green) and Cy5 (magenta). These two colors when merged in Image J create white for co-localization analysis.

F. REFERENCES

- (1) Sigal, Y. M.; Zhou, R.; Zhuang, X. Visualizing and Discovering Cellular Structures with Super-Resolution Microscopy. *Science* **2018**, *361* (6405), 880–887. <https://doi.org/10.1126/science.aau1044>.
- (2) Jensen, E. C. Use of Fluorescent Probes: Their Effect on Cell Biology and Limitations. *Anat. Rec. Adv. Integr. Anat. Evol. Biol.* **2012**, *295* (12), 2031–2036. <https://doi.org/10.1002/ar.22602>.
- (3) Nagarkar-Jaiswal, S.; Lee, P.-T.; Campbell, M. E.; Chen, K.; Anguiano-Zarate, S.; Cantu Gutierrez, M.; Busby, T.; Lin, W.-W.; He, Y.; Schulze, K. L.; et al. A Library of MiMICs Allows Tagging of Genes and Reversible, Spatial and Temporal Knockdown of Proteins in *Drosophila*. *eLife* **2015**, *4*. <https://doi.org/10.7554/eLife.05338>.
- (4) Wang, Y.; Shyy, J. Y.-J.; Chien, S. Fluorescence Proteins, Live-Cell Imaging, and Mechanobiology: Seeing Is Believing. *Annu. Rev. Biomed. Eng.* **2008**, *10* (1), 1–38. <https://doi.org/10.1146/annurev.bioeng.010308.161731>.
- (5) Pakhomov, A. A.; Martynov, V. I. GFP Family: Structural Insights into Spectral Tuning. *Chem. Biol.* **2008**, *15* (8), 755–764. <https://doi.org/10.1016/j.chembiol.2008.07.009>.
- (6) Wu, B.; Piatkevich, K. D.; Lionnet, T.; Singer, R. H.; Verkhusha, V. V. Modern Fluorescent Proteins and Imaging Technologies to Study Gene Expression, Nuclear Localization, and Dynamics. *Curr. Opin. Cell Biol.* **2011**, *23* (3), 310–317. <https://doi.org/10.1016/j.ceb.2010.12.004>.
- (7) Frommer, W. B.; Davidson, M. W.; Campbell, R. E. Genetically Encoded Biosensors Based on Engineered Fluorescent Proteins. *Chem. Soc. Rev.* **2009**, *38* (10), 2833. <https://doi.org/10.1039/b907749a>.

(8) Costantini, L. M.; Snapp, E. L. Fluorescent Proteins in Cellular Organelles: Serious Pitfalls and Some Solutions. *DNA Cell Biol.* **2013**, *32* (11), 622–627. <https://doi.org/10.1089/dna.2013.2172>.

(9) Huang, L.; Pike, D.; Sleat, D. E.; Nanda, V.; Lobel, P. Potential Pitfalls and Solutions for Use of Fluorescent Fusion Proteins to Study the Lysosome. *PLoS ONE* **2014**, *9* (2), e88893. <https://doi.org/10.1371/journal.pone.0088893>.

(10) Kanca, O.; Bellen, H. J.; Schnorrer, F. Gene Tagging Strategies To Assess Protein Expression, Localization, and Function in *Drosophila*. *Genetics* **2017**, *207* (2), 389–412. <https://doi.org/10.1534/genetics.117.199968>.

(11) Zane, H. K.; Doh, J. K.; Enns, C. A.; Beatty, K. E. Versatile Interacting Peptide (VIP) Tags for Labeling Proteins with Bright Chemical Reporters. *ChemBioChem* **2017**, *18* (5), 470–474. <https://doi.org/10.1002/cbic.201600627>.

(12) Doh, J. K.; White, J. D.; Zane, H. K.; Chang, Y. H.; López, C. S.; Enns, C. A.; Beatty, K. E. VIPER Is a Genetically Encoded Peptide Tag for Fluorescence and Electron Microscopy. *Proc. Natl. Acad. Sci.* **2018**, *115* (51), 12961–12966. <https://doi.org/10.1073/pnas.1808626115>.

(13) Kawano, K.; Yano, Y.; Omae, K.; Matsuzaki, S.; Matsuzaki, K. Stoichiometric Analysis of Oligomerization of Membrane Proteins on Living Cells Using Coiled-Coil Labeling and Spectral Imaging. *Anal. Chem.* **2013**, *85* (6), 3454–3461. <https://doi.org/10.1021/ac400177a>.

(14) Wang, J.; Yu, Y.; Xia, J. Short Peptide Tag for Covalent Protein Labeling Based on Coiled Coils. *Bioconjug. Chem.* **2014**, *25* (1), 178–187. <https://doi.org/10.1021/bc400498p>.

- (15) Morales, D. P.; Wonderly, W. R.; Huang, X.; McAdams, M.; Chron, A. B.; Reich, N. O. Affinity-Based Assembly of Peptides on Plasmonic Nanoparticles Delivered Intracellularly with Light Activated Control. *Bioconjug. Chem.* **2017**, *28* (7), 1816–1820. <https://doi.org/10.1021/acs.bioconjchem.7b00276>.
- (16) Morales, D. P.; Morgan, E. N.; McAdams, M.; Chron, A. B.; Shin, J. E.; Zasadzinski, J. A.; Reich, N. O. Light-Triggered Genome Editing: Cre Recombinase Mediated Gene Editing with Near-Infrared Light. *Small* **2018**, *14* (30), 1800543. <https://doi.org/10.1002/sml.201800543>.
- (17) Morales, D. P.; Braun, G. B.; Pallaoro, A.; Chen, R.; Huang, X.; Zasadzinski, J. A.; Reich, N. O. Targeted Intracellular Delivery of Proteins with Spatial and Temporal Control. *Mol. Pharm.* **2015**, *12* (2), 600–609. <https://doi.org/10.1021/mp500675p>.
- (18) Huang, X.; Hu, Q.; Lai, Y.; Morales, D. P.; Clegg, D. O.; Reich, N. O. Light-Patterned RNA Interference of 3D-Cultured Human Embryonic Stem Cells. *Adv. Mater.* **2016**, *28* (48), 10732–10737. <https://doi.org/10.1002/adma.201603318>.
- (19) Huang, X.; Hu, Q.; Braun, G. B.; Pallaoro, A.; Morales, D. P.; Zasadzinski, J.; Clegg, D. O.; Reich, N. O. Light-Activated RNA Interference in Human Embryonic Stem Cells. *Biomaterials* **2015**, *63*, 70–79. <https://doi.org/10.1016/j.biomaterials.2015.06.006>.
- (20) Li, H.; Nelson, C. E.; Evans, B. C.; Duvall, C. L. Delivery of Intracellular-Acting Biologics in pro-Apoptotic Therapies. *Curr. Pharm. Des.* **2011**, *17* (3), 293–319.
- (21) Pearce, M. C.; Gamble, J. T.; Kopparapu, P. R.; O'Donnell, E. F.; Mueller, M. J.; Jang, H. S.; Greenwood, J. A.; Satterthwait, A. C.; Tanguay, R. L.; Zhang, X.-K.; et al. Induction of Apoptosis and Suppression of Tumor Growth by Nur77-Derived Bcl-2 Converting Peptide in Chemoresistant Lung Cancer Cells. *Oncotarget* **2018**, *9* (40). <https://doi.org/10.18632/oncotarget.25437>.

- (22) Huang, X.; Lai, Y.; Braun, G. B.; Reich, N. O. Modularized Gold Nanocarriers for TAT-Mediated Delivery of siRNA. *Small* **2017**, *13* (8), 1602473. <https://doi.org/10.1002/sml.201602473>.
- (23) Luger, K. Nucleosomes: Structure and Function. In *Encyclopedia of Life Sciences*; John Wiley & Sons, Ltd, Ed.; John Wiley & Sons, Ltd: Chichester, 2001. <https://doi.org/10.1038/npg.els.0001155>.
- (24) Shen, Y.; Maupetit, J.; Derreumaux, P.; Tufféry, P. Improved PEP-FOLD Approach for Peptide and Mini-protein Structure Prediction. *J. Chem. Theory Comput.* **2014**, *10* (10), 4745–4758. <https://doi.org/10.1021/ct500592m>.
- (25) Lamiable, A.; Thévenet, P.; Rey, J.; Vavrusa, M.; Derreumaux, P.; Tufféry, P. PEP-FOLD3: Faster *de Novo* Structure Prediction for Linear Peptides in Solution and in Complex. *Nucleic Acids Res.* **2016**, *44* (W1), W449–W454. <https://doi.org/10.1093/nar/gkw329>.
- (26) Rostad, C.; Currier, M.; Moore, M. Fluorescent and Bioluminescent Reporter Myxoviruses. *Viruses* **2016**, *8* (8), 214. <https://doi.org/10.3390/v8080214>.
- (27) Morgan, E.; Gamble, J. T.; Pearce, M. C.; Elson, D. J.; Tanguay, R. L.; Kolluri, S. K.; Reich, N. O. Improved in Vivo Targeting of BCL-2 Phenotypic Conversion through Hollow Gold Nanoshell Delivery. *Apoptosis Int. J. Program. Cell Death* **2019**. <https://doi.org/10.1007/s10495-019-01531-1>.
- (28) Klein, A.; Hank, S.; Raulf, A.; Joest, E. F.; Tissen, F.; Heilemann, M.; Wieneke, R.; Tampé, R. Live-Cell Labeling of Endogenous Proteins with Nanometer Precision by Transduced Nanobodies. *Chem. Sci.* **2018**, *9* (40), 7835–7842. <https://doi.org/10.1039/C8SC02910E>.

- (29) Coltharp, C.; Xiao, J. Superresolution Microscopy for Microbiology: Superresolution Microscopy for Microbiology. *Cell. Microbiol.* **2012**, *14* (12), 1808–1818. <https://doi.org/10.1111/cmi.12024>.
- (30) Vutara Brochure. Bruker Nano Surfaces Division, Middleton, WI, USA Version B2006.
- (31) Laine, R.; Tosheva, K.; Gustafsson, N.; Gray, R. D. M.; Almada, P.; Albrecht, D.; Risa, G. T.; Hurtig, F.; Lindås, A.-C.; Baum, B.; et al. NanoJ: A High-Performance Open-Source Super-Resolution Microscopy Toolbox. *bioRxiv* **2018**. <https://doi.org/10.1101/432674>.
- (32) Wäldchen, S.; Lehmann, J.; Klein, T.; van de Linde, S.; Sauer, M. Light-Induced Cell Damage in Live-Cell Super-Resolution Microscopy. *Sci. Rep.* **2015**, *5* (1). <https://doi.org/10.1038/srep15348>.
- (33) Kanda, T.; Sullivan, K. F.; Wahl, G. M. Histone–GFP Fusion Protein Enables Sensitive Analysis of Chromosome Dynamics in Living Mammalian Cells. *Curr. Biol.* **1998**, *8* (7), 377–385. [https://doi.org/10.1016/S0960-9822\(98\)70156-3](https://doi.org/10.1016/S0960-9822(98)70156-3).
- (34) Pampalona, J.; Roscioli, E.; Silkworth, W. T.; Bowden, B.; Genescà, A.; Tusell, L.; Cimini, D. Chromosome Bridges Maintain Kinetochores–Microtubule Attachment throughout Mitosis and Rarely Break during Anaphase. *PLOS ONE* **2016**, *11* (1), e0147420. <https://doi.org/10.1371/journal.pone.0147420>.
- (35) Teesalu, T.; Sugahara, K. N.; Kotamraju, V. R.; Ruoslahti, E. C-End Rule Peptides Mediate Neuropilin-1-Dependent Cell, Vascular, and Tissue Penetration. *Proc. Natl. Acad. Sci.* **2009**, *106* (38), 16157–16162. <https://doi.org/10.1073/pnas.0908201106>.

(36) Prevo, B.; Esakoff, S.; Mikhailovsky, A.; Zasadzinski, J. A. Scalable Routes to Gold Nanoshells with Tunable Sizes and Response to Near-Infrared Pulsed Laser Irradiation. *Small* **2008**, *4*, 1183–1195.

IV. CONTROLLING THE GENOME: UP AND DOWN-REGULATION WITH GOLD NANORODS AND NEAR INFRARED LIGHT

A. ABSTRACT

Using light to control cellular events has enormous potential to improve our understanding of cellular processes. Nanoparticle-based methods remain largely unexplored as a means to simultaneously up and down regulate genes with light. We developed a robust gold nanorod platform to controllably deliver regulatory proteins and nucleic acids, relying on benign near infrared light. We relied on GNRs with peak absorbances at 800 nm (GNR) and nanobones (NB) at 1150 nm to release the gene-editing enzyme Cre recombinase and siRNA respectively. In cell free studies the GNRs showed ~50% release of loaded cargo when irradiated with 800 nm pulsed laser, and negligible release when irradiated with 1150 nm pulsed laser. The NBs showed similar release, but only at the desired 1150 nm wavelength. Release of functional Cre recombinase was demonstrated after irradiation of GNRs with 800 nm NIR light by using a gene knock-in reporter system with green fluorescent protein (GFP) in HeLa cells. Control over gene knockdown was demonstrated after release of siRNA from NBs with 1150 nm NIR light causing a 75 % reduction in cells expressing GFP. These results show that we can selectively release distinct cargoes while allowing for both up and down regulation of target genes.

B. INTRODUCTION

Light control of cellular processes has enormous potential. In 2005, the field of neuroscience was transformed by the development of optogenetics for non-invasive, spatially and temporally resolved control of neural activity[1]. Other subfields of biology have followed suit, adopting optogenetic methods to interrogate fundamental questions such as

protein localization during vascularization and engineering tools to control gene expression, cell differentiation, and tissue morphogenesis [2, 3]. A key drawback of current optogenetic approaches is the reliance on short wavelengths of light with poor tissue penetration and which are potentially harmful to cells [3]. Current optogenetic approaches lack a single platform to invoke both gain-of-function (GOF) and loss-of-function (LOF) methods, a feature which is critical to classic cell biology [3].

Gold nanoparticles (GNPs) are of potential interest due to their unique ability to absorb longer wavelengths of light in the tissue-penetrating optical near infrared window of 650-1300 nm [4]. Also, this excitation window does not overlap with those of typical fluorophores used in imaging, which is an issue with optogenetic approaches that rely on short wavelength light. Further, GNP's can be functionalized with surface modifications, providing an avenue for targeting specific cell types by decorating the particles with specific peptides that induce receptor-mediated endocytosis [5–7]

The advantageous merging of optogenetics and nanotechnology began in neuroscience, where the aforementioned features have resolved many drawbacks of traditional optogenetic approaches [8]. However, the union has not been fully extended into cell biology. In order to allow for light activated release of biomolecules, we previously developed NIR light-activated gold-nanoparticle delivery techniques capable of delivering siRNA, peptides, and gene editing proteins such as Cre recombinase [9, 10]. Our previous work utilized hollow gold nanoshells (HGN) to deliver biomolecules with a single wavelength of near infrared light, were as here we sought to deliver two independent cargos to enable a system capable of interrogating both GOF and LOF experiments. We rely on a two-particle system such that each particle responds to a wavelength of light distinct from the other to eliminate the possibility of off-target release. Gold nanorods (GNR) have well resolved absorbance spectra

whose peaks have minimal overlap at maximum absorbance and are defined by unique aspect ratios [11]. In theory, each particle would release its cargo when excited by the peak excitation wavelength without impacting the cargo attached to the partner particle.

We relied on GNRs with a peak absorbance at 800nm (GNR) and nanobones (NB) with a peak absorbance at 1150 nm that release Cre recombinase or siRNA, respectively. Excitation with 800 nm light excites GNR-containing Cre recombinase, activating conditional expression of GFP in Hela cells engineered with loxP sites flanking a promoter for the GFP gene. Subsequently, these cells are irradiated with 1150 nm light to release GFP siRNA to silence GFP expression. This system expands upon current delivery methods to offer a platform capable of delivering both an upregulating protein and siRNA independently of one another to achieve spatial and temporal control over up and down regulation of a gene product.

C. RESULTS AND DISCUSSION

C.1. Characterization of GNRs and NBs

In order to determine their surface plasmon resonance peaks, the GNRs and NBs were characterized using UV-vis spectra. Initial experiments attempted to use HGNs for a two wavelength release approach yet were unsuccessful due to broad peak distribution which is common for HGN [14]. The GNRs had a longitudinal surface plasmon (LSPR) at ~750 nm as well as a second transversal plasmon peak at ~550 nm (Figure IV-2a) [12]. The NBs had a LSPR at ~ 1150 nm and a second transversal plasmon peak at 600 nm [12]. The sharp and well separated peaks demonstrated allow for excitation of the GNRs carrying the Cre recombinase upon irradiation with 800 nm NIR light while the NBs containing the siRNA do not release until irradiated with 1150 nm NIR light (Figure IV-1).

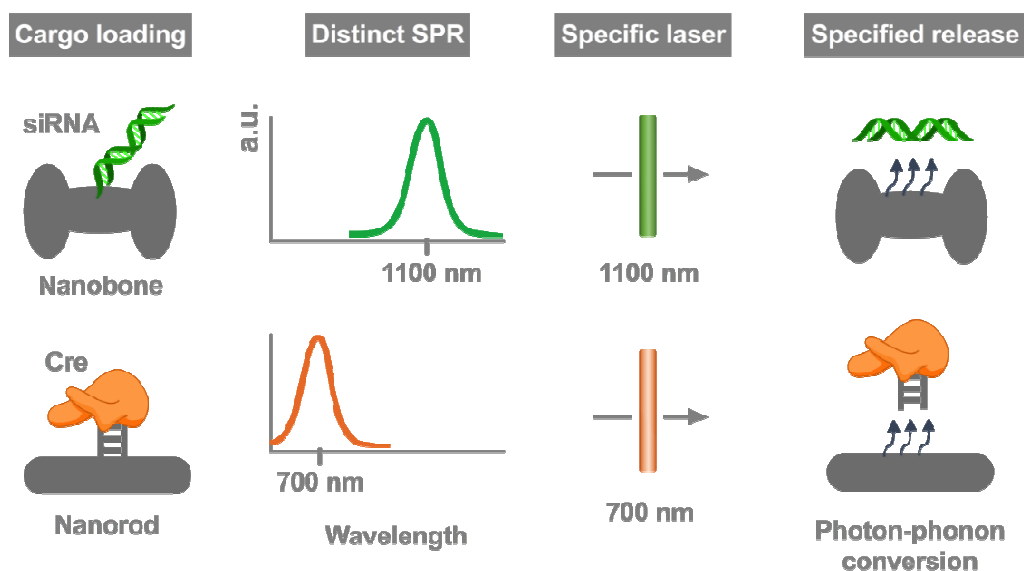


Figure IV-1. Illustration of the mechanism of the selective release. Upon irradiation with a 700 nm laser the GNR releases the Cre recombinase on the surface while the siRNA stays bound on the NBs. Upon irradiation with a 1100 nm laser, the NBs release siRNA targeting GFP from the surface of the particle.

To track cell-free release of cargo loaded on the particles a FAM labeled dsDNA (FAM-DNA) was attached to the surface. After laser irradiation at the specified wavelength, FAM fluorescence in the supernatant was measured. Once irradiated with 800 nm NIR light, only the GNRs released the FAM-DNA demonstrating control over release at this wavelength (Figure IV-2c). At 1150 nm NIR light the NBs release the loaded cargo upon irradiation however, the GNRs release a small amount of FAM-DNA at this wavelength as well (Figure IV-2d). We therefore released Cre recombinase from the GNRs and siRNA targeting GFP from the NBs to ensure that knockdown for GFP will not occur prematurely. This small amount of release from the GNRs did not affect the overall function of the up and down regulation of GFP see Figure IV-3b and IV-3cI.

An additional cell based experiment tested the release of FAM-DNA from GNR once internalized into HeLa cells. HeLa cells were plated on a gridded culture dish (ibidi) at 100,000 cells per dish and treated with 4 pM particles for 2 hours. Once internalized, the sample was irradiated using a commercial two-photon microscope equipped with a tunable, scanning NIR laser that can be set to wavelengths from 690 nm to 1020 nm. A region of interest (ROI) in orange (Figure IV-2d) was selected for excitation with 800 nm light and photos were collected before and after irradiation. Another ROI was selected for irradiation at 1020 nm (blue) and photos were taken before and after irradiation. Diffusion of the FAM-DNA from green puncta was observed only in the orange ROI indicating release of the GNR is dependent on irradiation with 800 nm NIR irradiation and does not release at 1020 nm (Figure IV-2d).

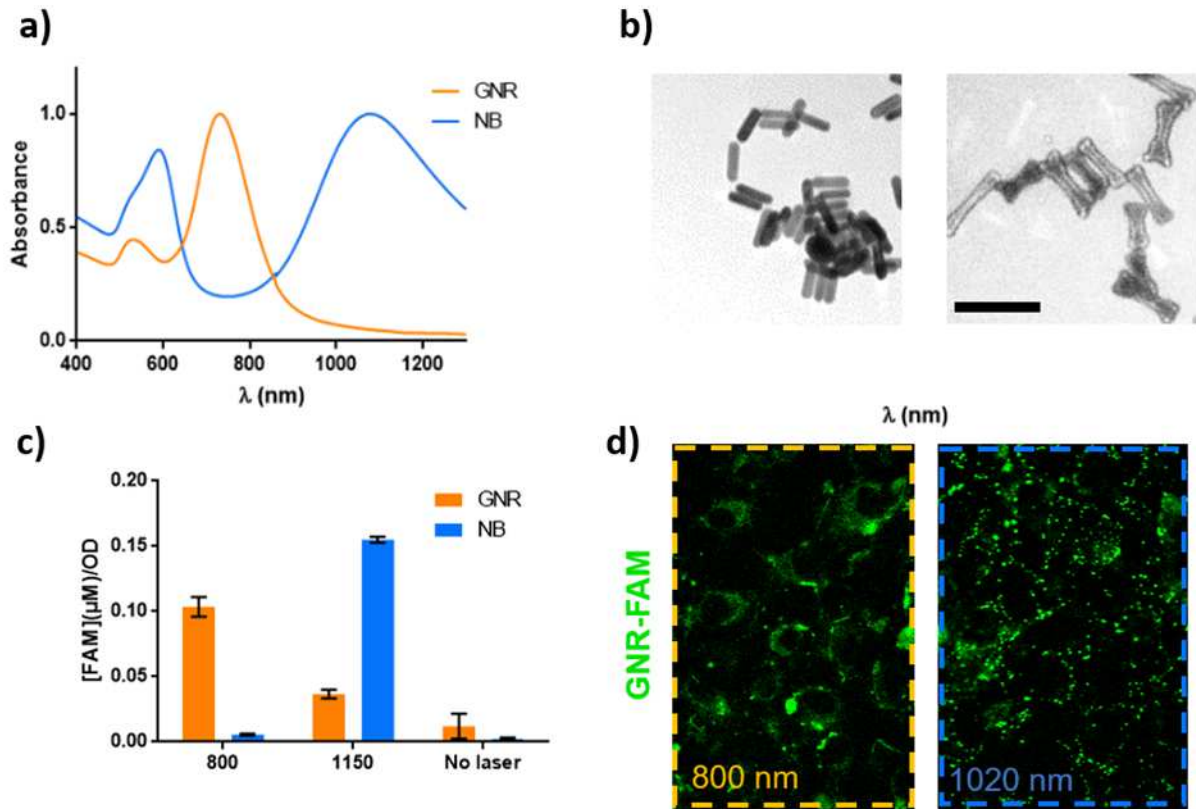


Figure IV-2. Selective release of gold nanoparticle cargo. a) UV-vis absorbance spectra show different absorbance peaks for both types of particles. b) TEM images of GNR and NB. Scale bar represents 100 nm. c) cell free experiment with GNR and NB displays a selective release of FAM-DNA cargo dependent on the wavelength of NIR excitation. d) Selective release of FAM-DNA from GNR internalized in HeLa cells where focused cells were irradiated with 800 nm (orange box) and another set was irradiated with 1020 nm (blue box) using two-photon excitation. Diffusion of the puncta shown in area irradiated with 800 nm only.

C.2. Flow cytometry analysis shows GFP upregulation with NIR excitation

To demonstrate the ability of this approach for both up and down regulation of a particular gene, we relied on a GFP reporter system in HeLa cells. HeLa cells were stably transfected with a GFP fluorescent reporter (CALNL-GFP) that knocks-in GFP expression upon recombination [15]. The Cre recombinase delivered via GNRs excises an interrupting sequence between the GFP promoter and gene by acting upon the Lox P sites flanking either side of the deleterious sequence allowing for GFP expression (Figure IV-3a). The GFP

knockdown occurs upon delivery of siRNA molecules released from the NBs after irradiation with 1150 nm (Figure IV-3a). The results of the knockdown were measured via flow cytometry and fluorescence microscopy (Figure IV-3b and Figure IV-3c).

Quantification of GFP fluorescence measured with flow cytometry showed that 48 hours after irradiation with 800 nm light GFP expression increased by 12.2% demonstrating successful delivery of Cre recombinase with GNRs (Figure IV-3b). This upregulation is similar to the previously demonstrated results using a lipofectamine transfection of a positive control plasmid containing Cre recombinase gene [10]. A sample that was irradiated with 800 nm to allow for GFP expression was irradiated 48 hours later with 1150 nm to release the siRNA from the NBs and caused a 75% decrease in GFP expression compared to the samples irradiated only with 800 nm NIR light (Figure IV-3b). Samples containing both particles and not irradiated with NIR light showed no major change in GFP expression (1%, Figure IV-3b).

C.3. Fluorescence Microscopy indicates control over release of cargo with NIR irradiation

The light activated control of GFP expression using dual wavelength NIR release with GNRs and NBs is demonstrated in Figure IV-3c using fluorescence microscopy. Figure IV-3cI shows the experimental and expected result when the GNRs and NBs are both incubated with the cells; GFP expression indicated by the presence of green fluorescent cells 48 hours after 800 nm irradiation demonstrates proper release of Cre recombinase from the GNRs. Two days after irradiation with 1150 nm, the previously fluorescent cells are no longer fluorescent, demonstrating release of the GFP siRNA from the NBs and proper knockdown of GFP (Figure IV-3cI). Control over siRNA release from the NBs is demonstrated in Figure IV-3cII when both particles are incubated with the cells, irradiation only occurs at one

wavelength (800 nm), and the cells remain fluorescent. Furthermore, when the NBs containing siRNA are not incubated with the cells, a similar level of fluorescence is observed 5 days later (Figure IV-3cIII). Finally, NIR control over Cre recombinase release is observed when both particles are incubated with the cells, no laser excitation occurred, and no GFP fluorescence was observed (Figure IV-3cIV).

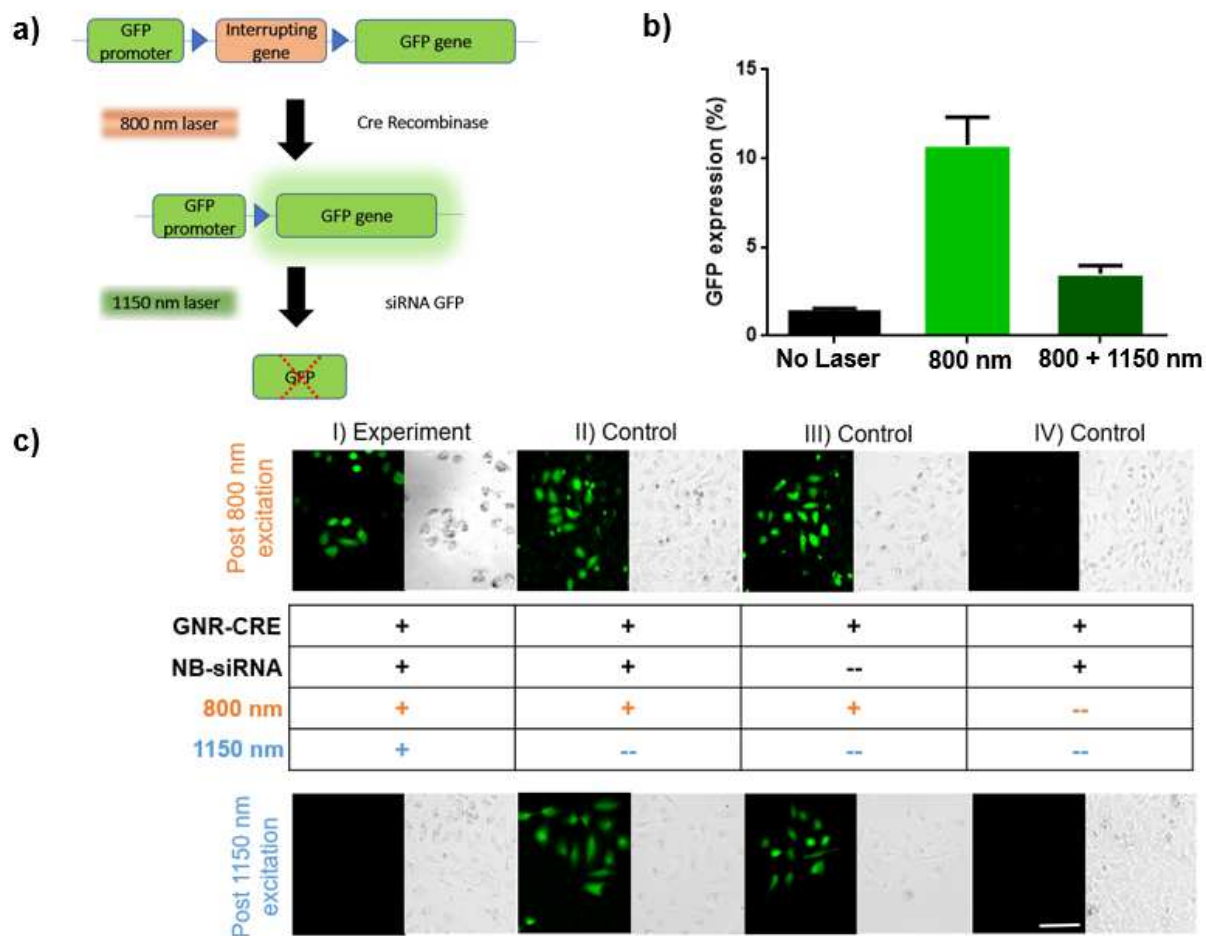


Figure IV-3. a) Gene editing by the Cre recombinase after release from the GNRs followed by the knockdown effect after release of the GFP siRNA from the NBs. b) Up and down regulation of GFP as measured by flow cytometry compared to 1 % in cell only control. HeLa reporter cells with both sets of particles but with no laser irradiation, 1.4 % ; 48 hours after 800 nm treatment, 11.2 % ; and 96 hours after 800 nm and 48 hours after 1150 nm, 3.2 %. c) Up and down regulation of GFP visualized by fluorescent microscopy. I) Cells containing both particles and irradiated with both laser wavelengths show efficient Cre release after 800 nm laser and almost total down regulation after 1150 nm laser as demonstrated by GFP fluorescence. II) Cells containing both GNR and NB and irradiated with only 800 nm light retain green fluorescence III) Cells with only GNR particles and irradiated only with 800 nm light show green fluorescence IV) Cells containing both particles and are not irradiated with either NIR wavelengths remain non fluorescent. Scale bar represents 100 μ m.

D. CONCLUSIONS

GNRs and NBs were prepared to have separate and distinct absorption maxima to allow for control over release of their cargo at separate wavelengths. We demonstrate release of the

gene-editing enzyme, Cre recombinase from GNRs with 800 nm NIR light using a reporter as well as the independent release of siRNA from NBs with 1150 nm NIR irradiation. This is a demonstration of gain and loss of function control with particles of distinct wavelengths and achieved by controlled delivery of protein and nucleic cargoes. We show that upon irradiation with 800 nm the GNRs release Cre recombinase, resulting in expression of GFP 48 hours later. Due to the ease of attachment to the particle via divalent cation affinity, this approach is suitable for any his tagged protein of interest including other gene editing proteins such as Cas9. Similarly, the control over siRNA release with 1150 nm NIR light can be expanded to other target genes. This approach should enable sophisticated manipulation of gene activity using NIR light.

E. EXPERIMENTAL SECTION

E.1 GNR and NBs seed synthesis

Gold nanoparticles were synthesized by a seed-mediated growth protocol [12]. To prepare the gold seed solution, 100 μL of 25 mM chloroauric acid tetrahydrate (HAuCl_4) was added to 10 mL of 0.15 M cetyl trimethylammonium bromide (CTAB) in a 25 mL glass vial under magnetic stirring. The solution turned orange and 600 μL of 0.01 M ice-cold sodium borohydride (NaBH_4) was added and the solution was stirred vigorously for 2 min, turning light brown, and left undisturbed at room temperature until use in GNR and NB synthesis.

E.2 NB growth and synthesis

For the NB synthesis, 294 μL of 25 mM HAuCl_4 was added to a solution containing 6 mL of 0.15 M CTAB solution and 9 mL of a 0.15 M benzyldimethylhexadecylammonium chloride under gentle magnetic stirring in a 25 mL glass vial until the solution turned orange.

Under the same conditions, 11.8 μL of a 0.1 M silver nitrate (AgNO_3) solution was added to the solution followed by 88.2 μL of a 0.1 M ascorbic acid solution which turns the solution colorless. Then, 14.9 μL of the previously prepared gold seed solution was added to the solution and left covered and undisturbed overnight at room temperature. Overnight the color of the solution turned pale pink and then 272 μL of 0.1 M ascorbic acid solution was added. The reaction was left undisturbed for 3 h resulting in a dark blue solution[12].

E.3 GNR growth and synthesis

For the GNR synthesis, 160 μL of 25 mM HAuCl_4 was added to 10 mL of 0.15 M CTAB in a 25 mL glass vial with slow stirring until the solution turned orange. Then, 8 μL of 0.1 M AgNO_3 was added under the same conditions followed by 50 μL of a 0.1 M ascorbic acid. The previously prepared gold seed solution (17 μL) was injected into the mixture and left undisturbed overnight at room temperature to initiate the growth of GNRs [12].

E.4 Preparation of GNR with NTA and Biotin

Single stranded DNA (C6-S-S-PEG18-ACCCTGAAGTTCATCTGCACCACCG-NH₂) (100 μM) (Biosearch Technologies) was deprotected with the treatment of 12.5 mM tris(2-carboxyethyl)phosphine hydrochloride (TCEP) for 30 minutes and extracted from 1 mL of chloroform to remove the C6 disulfide-protecting group 4 times. The TCEP-treated DNA was added first to the rapid modification at low pH (RMLP) buffer 1 (0.02 % SDS, 1X TBE, 500 mM NaCl, pH=3) to a final DNA concentration of 6 μM . The GNRs were added to a final concentration of 64 pM and left undisturbed overnight at room temperature. Subsequently, the modified particles were washed with centrifugation at 10,000 rpm for 10 minutes and then resuspended in RMLP buffer 2 (1x TBE, 100 mM NaCl) to remove excess DNA, and the wash step was repeated twice. The last resuspension was in a high salt hybridization buffer (10 mM MgCl_2 , 600 mM NaCl).

A previously determined ratio of 1:9 for complementary DNA (strand containing biotin: strand without biotin) allows for sufficient particle internalization and protein loading onto the particle [10]. Therefore, the complementary-biotin strand (Biotin-CGGTGGTGCAGATGAACTTCAGGGT) was added to a final 0.2 μ M concentration and the complementary strand without biotin (CGGTGGTGCAGATGAACTTCAGGGT) was added to a final concentration of 1.8 μ M to the previous GNR solution. The solution was then vortexed and sonicated briefly, incubated at 70 °C for 2 minutes, cooled to 45°C for 30 minutes, and brought to room temperature. The resulting GNRs were washed three times in PBST (phosphate-buffered saline, 1X, pH 7.4, 0.01 % Tween-20) via centrifugation. The last resuspension was in conjugation buffer (0.01 % Tween-20, 600 μ M Mg²⁺, 10 mM HEPES).

N-hydroxysuccinimide (NHS)-PEG4-Maleimide was added to the solution of GNRs to a final concentration of 1 mg/mL. The solution was incubated at room temperature for 20 minutes then washed three times with conjugation buffer at 4 °C via centrifugation. Thiolated N-[N, N-bis(carboxymethyl)-L-lysine]-12-mercaptododecanamide (Thiol-NTA) (Sigma Aldrich) which allows for attachment of the His-tagged Cre was added to a final concentration of 120 μ M and incubated for 3 hours at room temperature. Then the particles were centrifuged at 10,000 rpm for 10 minutes at 4 °C, washed three times and resuspended in PBST.

E.5 Preparation of NB with siRNA and biotin

The C6 disulfide protecting group on the sense strand of siRNA targeting GFP [13] (C6-S-S-PEG18-ACCCUGAAGUUCAUCUGCACCACCG-NH₂) was removed by incubating 100 μ L of 100 μ M RNA with 12.5 mM TCEP for 30 minutes, then extracted with chloroform four times. The TCEP-treated RNA was added first to RMLP buffer 1 to a final siRNA

concentration of 6 μM . Next, NBs were added to a final concentration of 64 pM, and left undisturbed overnight at room temperature. Subsequently the modified particles were centrifuged at 10,000 rpm for 10 minutes and resuspended in RMLP buffer 2 to remove excess siRNA, the wash steps were repeated twice. The last resuspension was in hybridization buffer and the NB concentration was adjusted to 32 pM in hybridization buffer.

The GFP antisense strand [13] (CGGUGGUGCAGAUGAACUUCAGGGU) was added to the previous NB solution to a final concentration of 2 μM . The solution was sonicated briefly, incubated at 70°C for 2 minutes, cooled to 45 °C for 30 minutes, and brought to room temperature. The resulting NBs were centrifuged at 10,000 rpm for 10 minutes and resuspended in PBST three times and the final resuspension was in conjugation buffer.

NHS-PEG4-Biotin was added to the NB solution to a final concentration of 1 mg/mL. The solution was incubated at room temperature for 1 hour then centrifuged at 10,000 rpm for 10 minutes at 4 °C and the pellet was washed in PBST three times.

E.6 Addition of streptavidin (STV) and Biotin-TAT to both NBs and GNRs

TAT-mediated internalization was achieved through the addition of STV to GNR and NB followed by addition of biotin-TAT. STV acts as a linker between the biotin on the DNA or RNA strand attached to the particle and the biotin-TAT. A final STV concentration of 1 mg/mL was added to a final volume of 500 μL of particles (32 pM) in PBST. The solution was sonicated briefly and incubated at room temperature for 1 hour then centrifuged at 10,000 rpm for 5 minutes and resuspended in PBST three times. Biotin-TAT was added twice to achieve a final concentration of 40 μM after brief sonication and 30 minutes of incubation at room temperature. The resulting nanoparticle solution was washed three times with PBST to remove excess biotin-TAT and stored at 4 °C until use.

E.7 Preparation of GNR with CRE

Approximatively 1 hour prior to cell treatment, the Cre recombinase (3 μ M) was loaded onto the GNRs (100 μ L) of 32 pM GNRs with 620 μ M CuCl₂ and incubated for 30 minutes on ice. Finally, the particles were centrifugated at 4°C at 10,000 rpm twice for 5 minutes and resuspended in 100 μ L of DMEM (Dulbecco's Modified Eagle Media) with 10% (v/v) FBS (Fetal Bovine Serum).

E.8 GNR release of FAM-DNA in HeLa cells

HeLa cells were plated on ibidi μ -Dish (35 mm, high Grid-50) at 100,000 cells 24 hours prior to particle internalization. GNR loaded with FAM-DNA and streptavidin-TAT (4 pM) were incubated in 400 μ L DEMEM with 10 % FBS at 37°C at 5% CO₂ for 2 hours. After incubation, cells were washed with PBS twice and the media was replaced with 2 mL of DMEM, high glucose (4500 mg/L), HEPES, no phenol red supplemented with 10% FBS. Samples were irradiated using an Olympus Fluoview 1000MPE two-photon and confocal microscope equipped with a mode locked Ti:sapphire tunable femtosecond pulsed laser (100 fs pulse duration, 80 mHz repetition rate, Mai Tai HP, Newport Spectra Physics). The cells were focused using a 25 x objective lens and bright field and green fluorescence images were collected before and after laser irradiation. A region of interest (ROI) was selected for irradiation with 800 nm in 0.69 nm slices through the cell volume at 240 mW power. After irradiation at 800 nm, images were collected for release analysis and the laser was set to 1020 nm. A second ROI was selected for irradiation with 1020 nm NIR irradiation. The laser was set to the same settings and images of green fluorescence and bright field were collected after irradiation. Images were false-colored using (Fiji is Just) ImageJ look up tables.

E.9 Addition of particles to cells and laser treatment

The HeLa reporter cell line [10] was cultured in DMEM with 10 % FBS at 37 °C in 5 % CO₂. 24 hours before laser irradiation the cells were plated in a 6 well tissue culture plate at 4 x 10⁵ cells per well. On the day of the experiment, the cells were incubated with cell dissociation buffer (Gibco) for 20 minutes at 37 °C then collected and washed twice with PBS through centrifugation at 500 rcf for 5 minutes. 1x10⁵ cells were incubated with 50 µL of 32 pM GNRs and 50 µL of 32 pM NBs for 2 hours for internalization. The cells were centrifuged at 500 xg for 5 minutes twice and resuspended in 100 µL of PBS. The cells were passed through a microcapillary device with a flow of 2 µl/s [10] and irradiated with pulsed NIR light from a femtosecond Ti:sapphire regenerative amplifier (Spectraphysics Spitfire) at 1 kHz repetition rate. Pulse duration was kept to 130 fs for the 800 nm (65 mW) GNR excitation. The cells were collected in a microcentrifuge tube and plated in 1 mL of DMEM with 10% FBS and 1% (v/v) penicillin streptomycin in a 24 well plate. After 48 hours the cells were observed on an Olympus IX70 inverted fluorescence microscope for GFP detection prior to irradiation with 1150 nm (300 mW) light for release of the siRNA from the NBs. 48 hours after release of the siRNA the GFP expression levels were observed via fluorescence microscopy and flow cytometry. Flow cytometry with the Accuri C6 flow cytometer was used to determine the quantity of GFP fluorescence after 10,000 cell counts were collected per sample. The samples were compared to a cell only control which was not treated with Cre recombinase from nanoparticle transduction and gave a baseline percent GFP for comparison.

E.10 Cell free controlled release of DNA-FAM

The DNA strand used for the GNR assembly was loaded onto 32 pM of both the GNR and NBs separately at a final concentration of 6 µM using the same TCEP, RMLP methods described previously. After washing, the complementary strand containing a fluorescein

(FAM) label on the 5' was added to the nanoparticle solutions at a final concentration of 2 μM . The solutions were sonicated briefly and incubated at 70 °C for 2 minutes, cooled to 45 °C for 30 minutes, then brought to room temperature. The resulting particles were centrifuged at 10,000 rpm for 10 minutes and resuspended in PBST three times to remove excess DNA-FAM and the final suspension was in PBST containing 0.1 mg/mL BSA for laser irradiation studies. The samples were then either irradiated with 800 nm (65 mW) or 1150 nm (300 mW) NIR light. The particles were then spun down at 10,000 rpm for 10 minutes and the supernatant was collected and plated on a 96 well plate for FAM fluorescence intensity measurements using a Tecan M200 plate reader. A calibration curve using the DNA-FAM oligonucleotide was used to determine the concentration of DNA-FAM loaded and released off the particles.

F. REFERENCES

1. Boyden ES, Zhang F, Bamberg E, et al (2005) Millisecond-timescale, genetically targeted optical control of neural activity. *Nature Neuroscience* 8:1263–1268. <https://doi.org/10.1038/nn1525>
2. Polstein LR, Juhas M, Hanna G, et al (2017) An Engineered Optogenetic Switch for Spatiotemporal Control of Gene Expression, Cell Differentiation, and Tissue Morphogenesis. *ACS Synthetic Biology* 6:2003–2013. <https://doi.org/10.1021/acssynbio.7b00147>
3. Johnson HE, Toettcher JE (2018) Illuminating developmental biology with cellular optogenetics. *Current Opinion in Biotechnology* 52:42–48. <https://doi.org/10.1016/j.copbio.2018.02.003>

4. Tromberg BJ, Shah N, Lanning R, et al (2000) Non-Invasive In Vivo Characterization of Breast Tumors Using Photon Migration Spectroscopy. *Neoplasia* 2:26–40. <https://doi.org/10.1038/sj.neo.7900082>
5. Delehanty JB, Boeneman K, Bradburne CE, et al (2010) Peptides for specific intracellular delivery and targeting of nanoparticles: implications for developing nanoparticle-mediated drug delivery. *Ther Deliv* 1:411–433
6. Giljohann DA, Seferos DS, Daniel WL, et al (2010) Gold Nanoparticles for Biology and Medicine. *Angewandte Chemie International Edition* 49:3280–3294. <https://doi.org/10.1002/anie.200904359>
7. Petros RA, DeSimone JM (2010) Strategies in the design of nanoparticles for therapeutic applications. *Nature Reviews Drug Discovery* 9:615–627. <https://doi.org/10.1038/nrd2591>
8. Mohanty SK, Lakshminarayanan V (2015) Optical Techniques in Optogenetics. *J Mod Opt* 62:949–970. <https://doi.org/10.1080/09500340.2015.1010620>
9. Huang X, Pallaoro A, Braun GB, et al (2014) Modular Plasmonic Nanocarriers for Efficient and Targeted Delivery of Cancer-Therapeutic siRNA. *Nano Letters* 14:2046–2051. <https://doi.org/10.1021/nl500214e>
10. Morales DP, Morgan E, McAdams M, et al Light-Triggered Genome Editing: Cre Recombinase Mediated Gene Editing with Near-Infrared Light
11. van der Zande BMI, Böhmer MR, Fokkink LGJ, Schönenberger C (2000) Colloidal Dispersions of Gold Rods: Synthesis and Optical Properties. *Langmuir* 16:451–458. <https://doi.org/10.1021/la9900425>

12. de Puig H, Cifuentes Rius A, Flemister D, et al (2013) Selective Light-Triggered Release of DNA from Gold Nanorods Switches Blood Clotting On and Off. *PLoS ONE* 8:e68511. <https://doi.org/10.1371/journal.pone.0068511>
13. Huang X, Hu Q, Lai Y, et al (2016) Light-Patterned RNA Interference of 3D-Cultured Human Embryonic Stem Cells. *Advanced Materials* 28:10732–10737. <https://doi.org/10.1002/adma.201603318>
14. Prevo B, Esakoff S, Mikhailovsky A, Zasadzinski J. (2008) Scalable routes to gold nanoshells with tunable sizes and response to near-infrared pulsed laser irradiation. *Small* 4:1183–1195
15. Matsuda T, Cepko CL (2007) Controlled expression of transgenes introduced by in vivo electroporation. *Proceedings of the National Academy of Sciences* 104:1027–1032. <https://doi.org/10.1073/pnas.0610155104>

V. SHAPE MATTERS: GOLD NANOPARTICLE SHAPE IMPACTS THE BIOLOGICAL ACTIVITY OF siRNA DELIVERY

A. Abstract

Plasmon-resonant nanoparticles provide unprecedented spatio-temporal control over the release of diverse cargoes into cells. Here we compare the loading, release and internalization efficiencies, and effectiveness of post transcriptional gene silencing of hollow gold nanoshells, hollow gold nanocages, and gold nanorods with plasmons tuned to absorb near-infrared light at 800 nm. The hollow gold nanoshells can be loaded with up to three times more siRNA cargo compared to nanocages and nanorods; however, nanorods exhibit the highest efficiency of release of attached siRNA strands when exposed to pulsed 800 nm laser excitation. In cellular treatments, all particles demonstrated efficient internalization into HeLa cells, but the nanoshells and nanocages display the highest downregulation of GFP expression 72 hours after treatment. These results provide novel insights into the relative efficiencies of three structurally distinct types of gold nanoparticles as siRNA carriers and examines different parameters that may influence their efficacy.

B. Introduction

Oligonucleotides, including small interfering RNA (siRNA), micro RNA (miRNA) antisense DNA and guide RNA (gRNA) are powerful technologies for gene regulation in basic cell research, cancer therapy, and regenerative medicine.¹⁻⁴ RNA silencing is a commonly used approach to knockdown specific target proteins⁵ like cyclin dependent kinases (CDKs), insulin growth factors (IGF), vascular endothelial growth factors (VEGF) and anti-apoptotic factors.⁶ However, functional siRNA requires an efficient delivery vehicle due to its bio-instability, inefficient accumulation in target tissues, and inability to cross cell

membranes to access the cytoplasm.⁷⁻⁹ Here we compare the relative effectiveness of three types of gold nanoparticles to deliver siRNA based gene knockdown in cancer cells.

Gold nanoparticles have attracted attention in biomedicine and basic science due to their relatively small size, biocompatibility, synthetic versatility, and ease of functionalization for targeting and delivery. Moreover, the ability for light controlled release makes gold nanoparticles a valuable tool for biological applications. By varying the size and the shape of the gold nanoparticles, their surface plasmon resonance (SPR) can be tuned to a desired wavelength. Previously, we demonstrated the attachment and controlled release of thiol labeled cargo from gold surfaces using near infrared (NIR) light following endocytotic uptake, providing a compelling platform for the delivery of peptides, proteins, and bioactive DNA and RNA.¹⁰⁻¹⁴ The ability to fine-tune optical properties of various gold nanoparticles is well documented,¹⁵⁻¹⁷ resulting in distinctive localized surface plasmons, with wavelengths ranging from the visible to the near infrared (NIR). The exposure of gold nanoparticles to femtosecond pulsed NIR laser irradiation generates an oscillation of electrons on the surface of the particle which cleaves the gold-thiol bond.¹⁸⁻²⁰ After cellular internalization of the particles with a cell-penetrating peptide (TAT)¹⁰, NIR light irradiation releases the double stranded siRNA from the nanoparticle's surface and facilitates endosomal escape to initiate gene silencing activity, with no detectable cell damage.^{11,21} The endosomal release arises through membrane disruption caused by a plasmonic heating of a nanometer sized shell of water surrounding the surface of the particles generating localized nanobubbles. These nanobubbles allow for disruption of the endosomal barrier without causing a bulk heating effect to the cell.^{12,13,21}

Prior characterization of gold nanorods and hollow gold nanoshells using continuous irradiation (rather than the pulsed laser used in this study) showed that light-triggered and

thermally-induced release are observed with nanoshell-based complexes whereas for nanorod complexes, no analogous release was detectable below the melting temperature of the DNA.²² Other studies have compared the physical and optical properties of different gold nanoparticles, the effect on photothermal therapy (PTT) and overall internalization.²¹ However, the effect of delivery of siRNA for knockdown applications beyond cytotoxicity by various nanoparticles has not been described.²¹ Christie et. al compared the effect of nanoparticle shape on PTT of gold nanorods and gold nanoshells and determined that even though gold nanorods were internalized more efficiently into macrophages, the gold nanoshells were more effective at PTT.²³ A recent study compared the cellular uptake and distribution of gold particles of different sizes and found that larger particles (40-50 nm) have greater potential as delivery vehicles for siRNA compared to smaller (15 nm) particles due to the quantity of particles internalized.²⁴ Lacking from prior studies is a comparison of particles of the same size yet different shapes in their ability to load and release their cargo, cellular uptake, and their ability to cause the desired biological change (e.g., post-transcriptional knockdown). The importance of shape has been studied for polymer based particles showing that co-block polymer nanoparticles with worm-like micelles allow for higher transfection efficiencies in rat liver.²⁵ Others have shown that a shape transformation from long worm and rod-like morphologies to more condensed nanoparticles with spherical and short-rod morphologies leads to improved transfection efficiency.²⁶ These studies lead us to investigate further the impact of shape on delivery efficiency of siRNA with gold nanoparticles.

We sought to determine which of the three ~45 nm diameter gold nanoparticles (hollow gold nanoshells (HGNS), hollow gold nanocages (HGNC) and gold nanorods (GNR)) is most suitable for gene regulation in mammalian cells. Selection criteria were based on loading capacity, release efficiency after laser irradiation, and efficiency of internalization into HeLa-

GFP cells as well as the subsequent knockdown of the green fluorescent protein (GFP) with siRNA upon treatment. To maintain uniformity using siRNA on different particle shapes, we used the same number of gold particles with the maximum amount of siRNA loaded in each experimental scenario.

C. Results and Discussion

Gold Nanoparticle Characterization

HGNS, HGNC, and GNR (45-50 nm diameter) were prepared (Figure V-1). UV-Vis spectroscopy was used to determine that each type of gold particle contains a characteristic surface plasmon peak at around 800 nm, optimal for NIR excitation and siRNA release. The HGNS exhibit a single yet broad resonance peak at ~750 nm due to size variations which can be seen in the transmission electron microscopy (TEM) image in Figure V-1. The HGNC also have a main resonance peak at 750 nm and display a hexagonal shape shown by the TEM image in Figure V-1. The hexagonal shape is due to truncation of the cube's corners and edges during the galvanic replacement reaction.²⁷ Finally, the GNR have a main longitudinal surface plasmon peak at ~750 nm as well as a second transversal plasmon peak at ~520 nm.^{28,29}

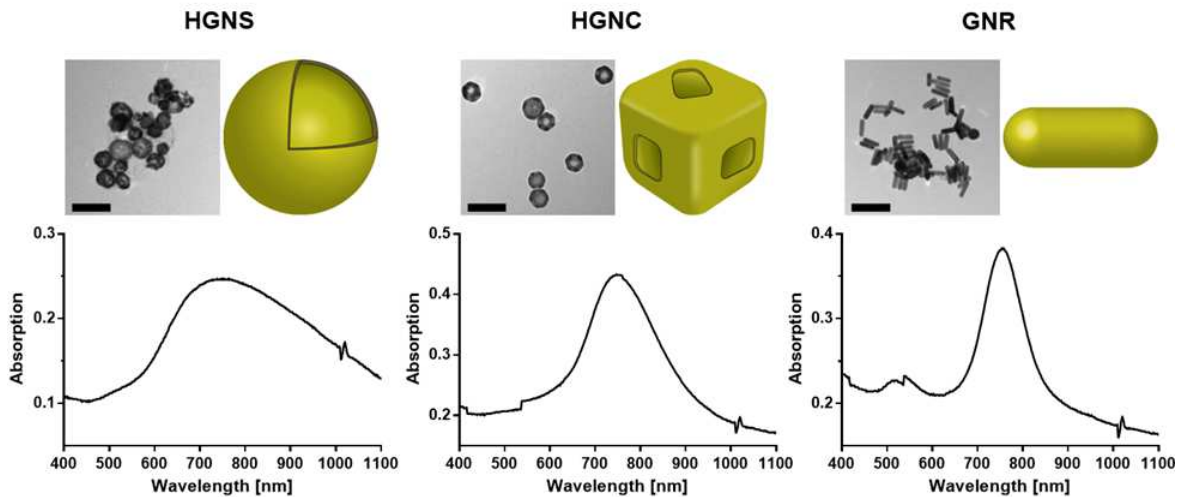


Figure V-1. Characterization of hollow gold nanoshells (HGNS), hollow gold nanocages (HGNC), and gold nanorods (GNR). Transmission electron microscope (TEM) imaging of gold nanoparticles depicts characteristic hollow structures of HGNS and HGNC as evidenced by the decreased electron density at the centers of the particles, while GNR are confirmed to be rod-like. TEM images (JEOL 1230 TEM) are accompanied by UV-Vis absorption spectra showing primary plasmon peaks at ~ 750 nm for each class of nanoparticle. Average size of each gold nanoparticle is ~ 45 nm (TEM scale bar is 100 nm, $n = 20$).

Load and Release of siRNA

A clear advantage of nanoparticle-based delivery of bio-active nucleic acids is that one particle can be loaded with many copies of the nucleic acid. Using thiol-modified oligonucleotides, two common assembly methods were tested and the oligonucleotide concentrations were increased to maximize the loading of each gold nanoparticle (Figure V-2). The loading of the thiolated oligonucleotides relied on a consistent use of 32×10^{-12} M particles, while the loading conditions for each particle were varied to ensure each particle shape had the maximum amount of siRNA on the surface. Each particle type was treated with either a low pH-induced adsorption followed by a buffer exchange where the particles were spun down and resuspended in HEPES buffer (assembly method 1) or a low pH-induced adsorption in combination with SDS (sodium dodecyl sulfate) and TBE (Tris, boric acid and

EDTA) (assembly method 2).^{16,28} Assembly method 1 appeared to be optimal for decorating siRNA onto HGNS only (Figure V-2).^{19,30} The GNR on the other hand exhibited instability after treatment, reflected by a blue-shift in the UV-vis spectra, indicative of flocculation of the particles (Figure V-2) and therefore was not used for GNR-siRNA assembly. Assembly method 2 delivered the best results for increasing siRNA loading on the GNR and HGNC but not for HGNS. Thus, buffer exchange with HEPES was used for further HGNS preparations, while SDS/TBE was employed for the GNR and HGNC. This would suggest that the initial capping agent used during the synthesis of the gold nanoparticles determines the optimum buffer for the exchange. Assembly method 1 worked best for the HGNS as they were initially capped with citrate during synthesis. However, the GNR and HGNC require capping agents such as CTAB and polyvinylpyrrolidone (PVP), respectively, which allows the use of stringent reagents such as SDS without particle flocculation. Figure V-3a shows the maximum ssRNA and dsRNA observed per particle for each of the three particle shapes quantified using a Qubit fluorescence assay (Invitrogen). Single stranded and double stranded RNA are presented in Figure V-3 to demonstrate the dsRNA quantitated in the loading experiment is solely due to the hybridization of the complement to the single strand attached to the particle rather than non-specific interaction with the particle surface. Loading of HGNS (~8,000 strands per particle) with both single and double stranded nucleic acids was significantly greater than for HGNC and GNR (~3,000 strands per particle for each). This is likely to impact various features of their delivery into cells (eg. stability of RNA, particle internalization and efficiency of knockdown).

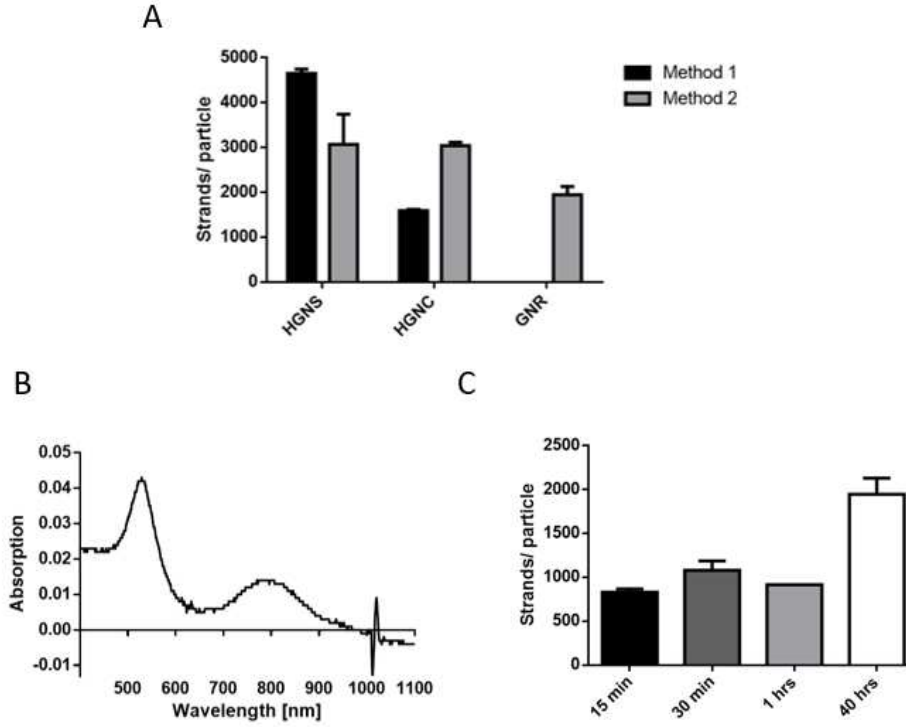


Figure V-2. Optimization of siRNA loading onto each kind of gold nanoparticle. (a) Total siRNA loaded onto 3.2 pM particles determined by KCN etch after Method 1 and Method 2. (b) Using method 1 for absorption of RNA onto GNR surface results in a UV-Vis spectrum where the 500 nm peak is much larger than the ideal surface plasmon peak at 800 nm. (c) Longer incubation times with RNA for GNR leads to a doubling in the amount of RNA loaded onto the surface of the particle

The siRNA release efficiency of each gold nanoparticle was determined by measuring the quantity of dsRNA in the supernatant of the sample after laser irradiation per gold nanoparticle (Figure V-3B). Against expectations, the high loading of siRNA onto the HGNS seen in Figure V-3A had lowest percentage (51%) of total dsRNA released with low laser power compared to HGNC and GNR (83% and 87% respectively). The low percentage of siRNA released from HGNS was increased dramatically (85%) when the laser power was increased while the other particles did not see as dramatic of an increase with an increase in laser power (Figure V-3B). The release percent for higher power laser excitation of HGNS (85%) is typical as seen by Braun et. al and Morales et. al.^{13,31}

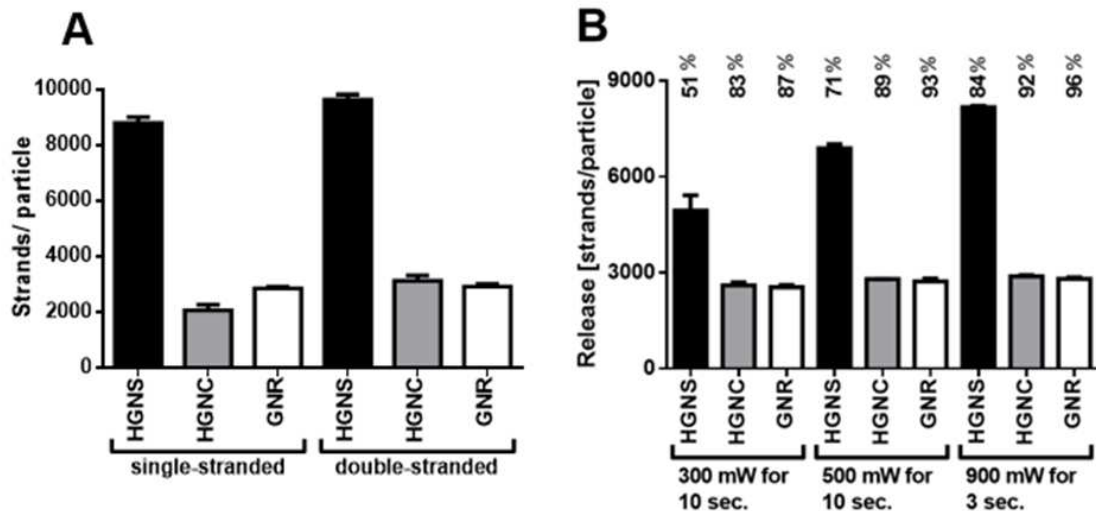


Figure V-3. HGNS show the highest level of loading and absolute quantity of siRNA release compared to HGNC and GNR with Qubit assay. (a) Total siRNA loaded onto 3.2 pM particles determined after dissolved with a solution containing KCN after initial loading of 3 μ M siRNA (1,000 X the max loading capacity of siRNA calculated). (b) Release of loaded siRNA from 3.2 pM gold nanoparticles after exposure to 800 nm femtosecond pulsed NIR laser light. Percent release from each particle is indicated above each bar (n = 6).

Influence of particle shape on TAT-mediated endocytosis.

Size, shape, and surface properties influence the internalization of particles into cells.³²⁻³¹ Previous studies lacked the comparison of the three different shapes of particles used in this study with similar dimensions. The influence of particle shape on internalization was determined quantitatively through flow cytometry (Figure V-4a) and qualitatively through fluorescence microscopy. (Figure V-5). For cellular studies, the adsorbed thiol oligonucleotides on the gold surfaces were hybridized at a 1:1 ratio with complementary sequences, one of which was labeled with a Cy3 dye for tracking, the other was labeled with a biotin tag for further functionalization with streptavidin and biotin-TAT. Note that in this case the Cy3 was added to the nanoparticles via the fluorescently labeled complement strand for the siRNA already attached to the particle whereas the quantification of dsRNA released from the particles was stated in Figure V-3b using the qubit assay (no fluorescent label). The qubit method is a standard for quantification of nucleic acid in a sample and was thus used to quantitate the amount of siRNA bound to each particle shape. Previous work conducted by Huang et. al. demonstrates the same amount of Cy3-siRNA is quantified using a fluorescence based assay on HGNS.¹⁰ Since these values are consistent for the HGNS across the two different quantification methods and the same complement sequence was used in this study.

The TAT peptide is well characterized to promote cellular uptake and our previous studies determined that a 1:1 ratio was optimal for internalization and sufficient for siRNA knockdown.¹³ HeLa cells were treated with HGNS, GNR and HGNC for two hours and then characterized by flow cytometry to measure the degree of gold nanoparticle uptake determined by the increase in cell population exhibiting Cy3 fluorescence (Figure V-4a). High incidence of Cy3 fluorescence was observed in 96 % of cells that were treated with

GNR, while 93 % of cells exhibited Cy3 when treated with HGNS. On the other hand, only 39 % of HGNC treated cells showed noticeable changes in fluorescence intensity.

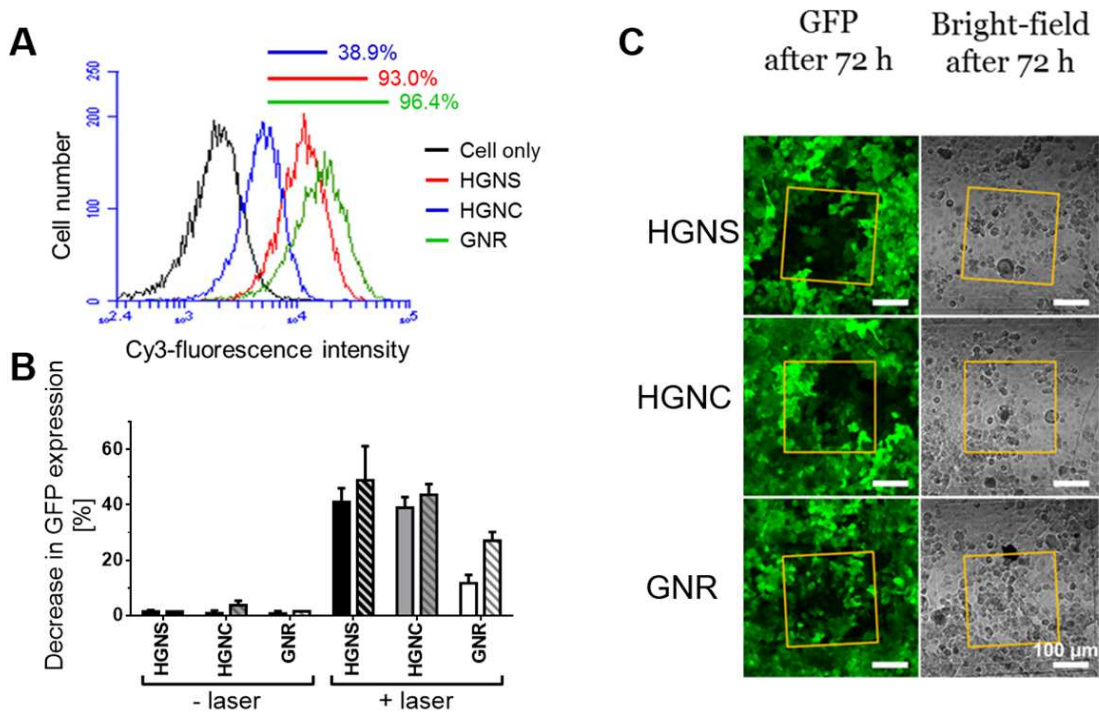


Figure V-4. HGNS and HGNC show comparable and superior gene knockdown efficiencies over GNR. (a) Flow cytometry histograms of internalization efficiencies of the different gold nanoparticles into HeLa cells as described by changes in fluorescence profiles due to Cy3 labeled particle uptake. Percentage of cells with Cy3 internalized shown for each type of gold nanoparticle was determined via flow cytometry. (b) Quantitative determination of the decreased GFP expression after knockdown in HeLa-GFP cells via flow cytometry. Percent decrease in GFP expression determined from number of cells not fluorescent three days after treatment of HeLa-GFP cells with a particle concentration of 3.8×10^{-12} M (solid bar) or 7.6×10^{-12} M (striped bar). (c) Spatially controlled knockdown of GFP using NIR excitation by confocal microscopy. GFP-fluorescence (green) and bright-field (grey) microscopy images of HeLa-GFP cells three days after siRNA release (yellow square) for GFP-knockdown treated with the different gold nanoparticles. Scale bar in the microscopy images is 100 μ m.

Internalization was also investigated by darkfield microscopy in which the gold nanoparticles are visible as bright, orange dots inside the HeLa cells due to light scattering (Figure V-5). Complementary fluorescence microscopy imaging mirrors the internalization results acquired through flow cytometry in Figure V-4a with GNR and HGNS internalized

best. However, dark field microscopy showed a discrepancy with the flow cytometry analysis in the amount of GNR internalized relative to the HGNS and reduced numbers of GNR were observed from imaging. The Cy3 fluorescence observed by flow cytometry (Figure V-4a) may be affected by the ability of gold nanoparticles to either quench or enhance fluorescent dyes close to particle surfaces.²⁶ GNR have been observed to enhance the fluorescence dyes on their surface and therefore lead to seemingly higher internalization as analyzed by cytometry.³³ The enhancement of the Cy3 dye on the surface of GNR as well as the dark-field microscopy data agree with the literature and indicates that less GNR are internalized into HeLa cells than HGNC and HGNS.

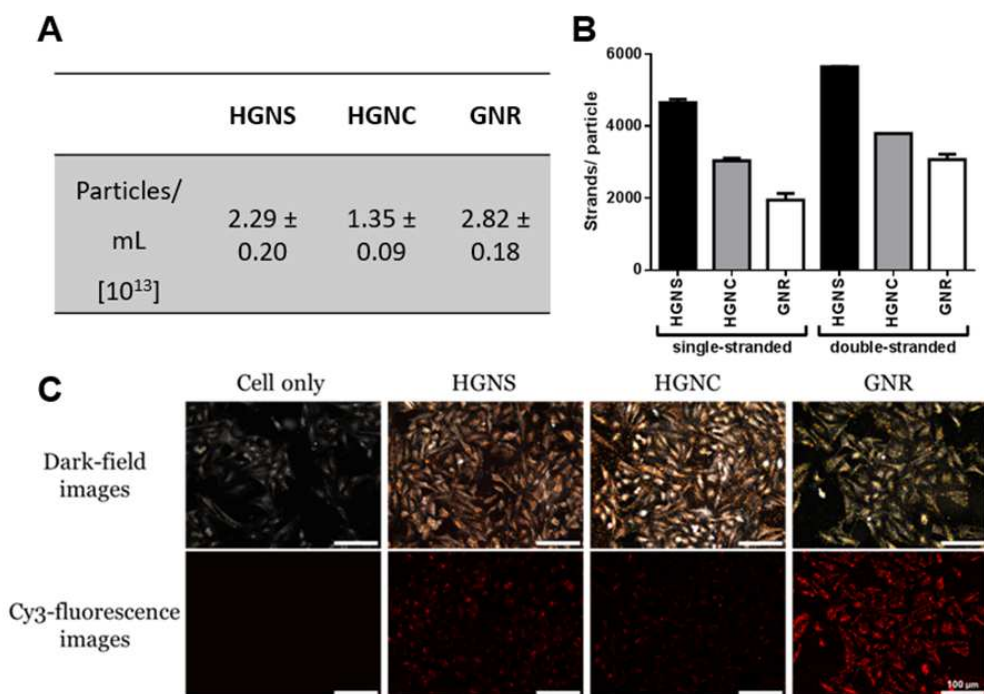


Figure V-5. Further characterization of different gold nanoparticles demonstrating DNA loading and enhancement effect of GNR on cy3 fluorescence. (a) Particle concentration of the different gold nanoparticles with double-stranded DNA attached onto the particle surface. All conversions shown in particles per mL are for samples where the maximum absorbance at 800 nm was 1 absorbance unit, as measured with a UV-vis spectrophotometer using a 1 cm pathlength cuvette. The variance is shown as standard error of the mean. The values were determined using the NanoSight NS300. (b) Loading of the different gold nanoparticles functionalized with DNA. (c) Dark-field microscopy images show the internalization of the gold nanoparticles from the orange colored light scattered from the gold nanoparticles. The cy3-fluorescence shows the internalization of the gold particles from the red fluorescence observed from the DNA strand attached to the gold nanoparticles. Scale bar in the microscopy images are 100 μm .

Efficiency of siRNA delivery for GFP knockdown in HeLa cells

A final comparison of the three gold nanoparticles tested the overall efficiency of gene knockdown, which includes all of the features tested independently up to this point (loading, release and, internalization). The number of particles used in the treatment was kept constant and two irradiation methods were used. The ensemble laser treatment relied on cells passed

through a capillary tube underneath the path of the NIR laser beam (Figure V-4b). The second set up used the two-photon microscope equipped with a mode-locked titanium-sapphire femtosecond (fs) tunable (690-1020 nm) pulsed laser to control when and where the gene knockdown occurs for qualitative knockdown studies (Figure V-4c). Experiments were conducted using both adherent and suspension cells. The two-photon irradiation method used adherent cells to demonstrate control over the area for knockdown (Figure V-4c). The suspension cell system used to determine the percent knockdown efficiency of each particle shape (Figure V-4b) allowed for bulk irradiation of the cells passed through a microfluidic device and later quantification of knockdown efficiency using flow cytometry.

GFP-knockdown was observed for the ensemble laser irradiation method with all three gold nanoparticle shapes via flow cytometry. The no laser control, which had particles internalized but which were not irradiated with NIR light, showed no GFP knockdown (Figure V-4b). GNR showed the smallest percent decrease in GFP knockdown. Both HGNS and HGNC had comparable knockdown efficiencies and each showed a slight increase in GFP knockdown efficiency with a higher particle concentration indicating the efficiencies were saturated with HGNS and HGNC. GNR showed a doubling in GFP knockdown with a doubling of particle concentration. Thus, more particles are required for GNR-induced GFP knockdown compared to HGNS and HGNC which agrees with the enhanced Cy3 dye effect of GNR observed in Figure V-5.

The two-photon microscope results in Figure V-4c used an Ibidi gridded cell culture dish that offers the opportunity to irradiate the HeLa-GFP cells in a specific area and relocate them 72 hours later. This experiment was used to complement the flow cytometry data and show the GFP knockdown. HeLa-GFP cells with internalized gold nanoparticles showed patterns

of GFP knockdown in areas of irradiation after 72 hours (Figure V-4c). Cell culture areas treated with HGNS or HGNC show clear non-fluorescent spots in the irradiation areas while the GNR samples exhibit only slightly less fluorescence in the area of irradiation with a lot of green fluorescent cells in between. Samples without gold nanoparticles showed no decrease in fluorescence after 72 hours (Figure V-6). The targeted knockdown using the two-photon microscope again confirms that the GNR do not exhibit the same knockdown capabilities as the HGNS and HGNC.

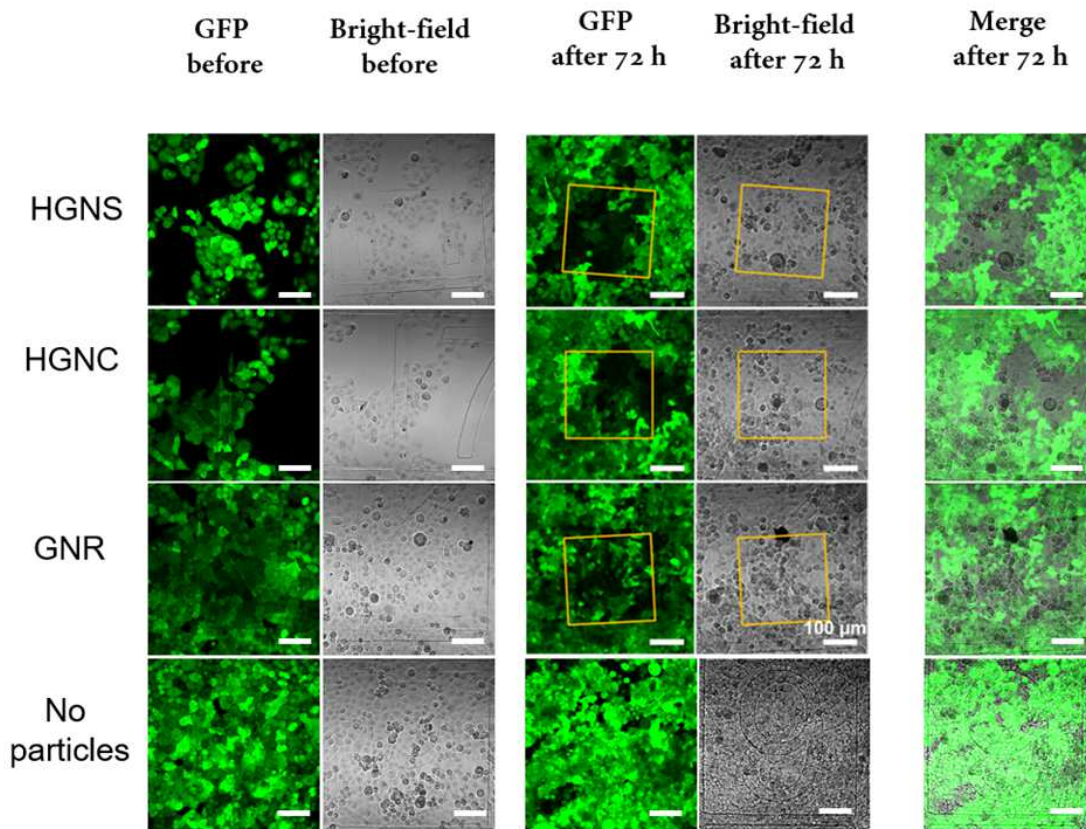


Figure V-6. Spatially controlled knockdown of GFP using NIR excitation by confocal microscopy. GFP-fluorescence (green) and bright-field (grey) microscopy images of HeLa-GFP cells before irradiation (two columns on the left) and three days after siRNA release (yellow square) for GFP-knockdown treated with the different gold nanoparticles (two columns on the right). Merged images used to show the GFP knockdown after 72 h. Scale bar in the microscopy images is 100 μm .

D. Conclusion

We observed the effect of gold nanoparticle shape on siRNA delivery through studying their loading and release efficiencies, internalization efficiencies and determined how these results affect the overall knockdown efficiency of GFP in HeLa cells. After maximizing the amount of siRNA loaded onto each type of gold nanoparticle, HGNS were found to load more than three times the amount of siRNA strands compared to HGNC and GNR. Despite the increase in siRNA loading on the HGN, the overall knockdown efficiency of the HGN compared to the HGNC was similar. In addition, we found that the shape of the particle strongly affected the internalization of the gold nanoparticles of similar size resulting in an observable change in the number of particles internalized to HeLa cells. When the HeLa cells were treated with a consistent number of gold nanoparticles across the different shapes, the final GFP knockdown results showed that GNR were the least efficient at GFP knockdown. This data in combination with the decrease in internalization seen for the GNR shows the importance of high particle internalization over loading/release for efficient gene knockdown using gold nanoparticles.

E. Experimental Procedures

Synthesis of the different gold nanoparticles

The HGNS are porous with a hollow core formed by a gold galvanic exchange initiating at the surface of silver precursor nanoparticles and were synthesized as described earlier³⁴. Porous and HGNC were made by synthesizing silver nanocubes and subsequent conversion into hollow gold nanocages by galvanic replacement reaction as described earlier³⁵. The synthesis and purification of the GNR was carried out with the rapid modification at low pH method, described before³⁶. For the experiments all working solutions had to be ribonuclease (RNase)-free. The HGNS as well as HGNC were dialyzed overnight in sodium citrate

dialysis buffer (500×10^{-6} M) with 0.03% diethyl dicarbonate (DEPC) with dialysis cassettes (molecular weight cut-off (MWCO) of 20,000). GNR were not synthesized in a RNase-free environment and afterwards purified with RNase-free solutions.

Functionalization of the nanoparticles

Deprotection of RNA/ DNA

The disulfide protecting group on each oligonucleotide (DNA/RNA) was removed by incubating 12.5×10^{-3} M tris (2-carboxyethyl)phosphine HCl (TCEP) with 100×10^{-6} M DNA/RNA strands at room temperature (RT) for 20 min followed by a chloroform extraction ($4 \times 1000 \mu\text{L}$). The freshly reduced thiol-modified RNA or DNA was afterwards added to the different shaped particles.

Attachment of RNA/ DNA

Assembly method 1: For the attachment onto the surface of HGNS 3×10^{-6} M deprotected RNA or DNA was added to HGNS with an optical density (OD) of 1 (correspond to $\sim 3.58 \times 10^8$ HGNS/mL) in the presence of 10×10^{-3} M sodium citrate-HCl ($\text{Na}_3\text{Cit-HCl}$), and incubated at RT for 20 min after brief sonication. Afterwards, the pH was neutralized by adding 130×10^{-3} M HEPES buffer, the solution was gradually salted to 1 M Na^+ within 20 min using 3.0 M sodium chloride (NaCl), 0.3 M sodium citrate (Na_3Cit) pH 7.0 (20x SSC), in the presence of 0.01% Tween-20 and 1×10^{-3} M magnesium chloride (MgCl_2). Unbound RNA/DNA strands were removed by washing the HGNS twice in washing buffer (1×10^{-3} M MgCl_2 , 0.01% Tween-20, 300×10^{-3} M NaCl and 30×10^{-3} M Na_3Cit pH 7). All washing steps were performed by centrifuging at $7000 \times g$ for 10 min followed by brief sonication. After the last centrifugation step, the particles were resuspended in the hybridization buffer (10×10^{-3} M MgCl_2 and 600×10^{-3} M Na^+).

For the attachment of RNA/ DNA onto the surface of HGNC and GNR first, 1x TBE buffer, 500 mM NaCl and 0.02% SDS were mixed together and inverted by hand. Hydrochloric acid (HCl) was used to adjust the mixture's pH to 3.0. To this solution both 3×10^{-6} M of deprotected RNA/ DNA as well as 1 OD of HGNC (correspond to $\sim 2.52 \times 10^8$ HGNC/mL) or GNR (correspond to $\sim 6.53 \times 10^8$ GNR/mL) were added and incubated in the dark for 40 hrs. Afterwards, unbound RNA/ DNA strands were removed by washing the HGNC and GNR twice in washing buffer followed by brief sonication. After the last centrifugation step, the particles were resuspended in the hybridization buffer.

Hybridization of complementary RNA/ DNA strand

Complementary RNA or DNA (1×10^{-6} M) were added to the single stranded RNA/ DNA assembled particle solution (1 OD HGNS, HGNC or GNR) in hybridization buffer followed by an incubation at 70 °C for 2 min and an immediate incubation at 45 °C for 30 min. Excess complementary RNA/ DNA strands were washed out by centrifuging 2x at 7000 x g for 10 min, using 0.1% Tween-20 in Dulbecco's phosphate-buffered saline (PBST).

For the particles with RNA assembled on the surface, an additional step was carried out to functionalize the 3'-end of the thiol- RNA with biotin. The particles were resuspended in conjugation buffer (10×10^{-3} M HEPES pH 7.5, 1×10^{-3} M $MgCl_2$, 0.01% Tween-20) after the last washing step. Afterwards, a large excess of 127×10^{-6} M NHS-PEG₄-Biotin (Thermo SCIENTIFIC) in dimethyl sulfoxide (DMSO) was added to the particles with RNA to complete the functionalization of the particle. The solution was sonicated briefly and incubated for 1 hr at room temperature followed by washing with conjugation buffer twice to remove excess biotin reagent.

Functionalization with Streptavidin and Biotin-TAT

Streptavidin was added at 2 mg/mL to 32×10^{-12} M gold nanoparticles in the presence of 0.5x PBST, 33.5×10^{-3} M HEPES buffer and 335×10^{-6} M MgCl_2 . To avoid self-aggregation of the particles caused by streptavidin bridging, the solution was vortexed and sonicated immediately upon the addition of streptavidin and incubated at RT for 1 hr. Afterwards, the gold nanoparticles were washed twice with PBST at 4 °C. 15×10^{-6} M of biotin-TAT (N-terminal biotin, YGRKKRRQRRR, GenScript) was added twice to 32 pM of nanoparticles in 0.5x PBST and 50×10^{-3} M HEPES buffer followed by brief sonication and 30 min of incubation at RT. The resulting functionalized gold nanoparticles were washed with PBST and stored at 4 °C prior to cell use.

UV-Vis absorbance spectra

For the absorbance spectra, the gold nanoparticles were diluted in water and the measurement was carried out with a UV-Vis spectrometer (PharmaSpec instrument with a UV-1700, Shimadzu) at a wavelength from 400 to 1100 nm for each different gold nanoparticle type.

TEM

For the detection of the different kinds of gold nanoparticles, 3×10^{-6} L of each particle sample (3.2×10^{-12} M) was pipetted onto a carbon-covered TEM copper mesh grid (SPI Supplies) and stored at RT until the whole solvent (water) was evaporated. Afterwards, the grids were brought into the JEOL JEM-1230 TEM (JEOL) to image the different kinds of gold nanoparticles with a voltage of 80 kV and a 150,000 x magnification.

Detection of DNA/RNA concentration

For the determination of the amount of oligonucleotides attached onto the surface of the different kinds of gold nanoparticles a KCN etch was performed. The particles were etched

by potassium cyanide (KCN) solution (20×10^{-3} M KCN, 200×10^{-6} M $K_3Fe(CN)_6$) to completely release the coated RNA/ DNA. Afterwards, the RNA/ DNA concentration can be determined with the Qubit ssDNA Assay Kit (Invitrogen). For these measurements, the ssDNA Reagent was diluted 1:200 in ssDNA Buffer (working solution). Then, the samples were diluted 1:10 in the working solution and afterwards measured at the Qubit 3.0 Fluorometer (Invitrogen).

Bulk pulsed NIR-laser irradiation for cell free release studies

Release experiments were carried out with gold nanoparticle solutions in the presence of 0.1×10^{-3} g/ 10^{-3} L bovine serum albumin (BSA). The samples were irradiated with a pulsed laser generated from a femtosecond Ti:sapphire regenerative amplifier (Spectraphysics Spitfire) running at 1 kHz repetition rate with a Gaussian beam diameter of 5 mm. Pulse duration was kept to 130 fs and the spectral full width at half maximum of the laser radiation was 12 nm centered around 800 nm. The laser was directed onto the sample by a series of mirrors, and no focusing optics were used. The laser power was measured with a thermopile power meter (Newport Inc.). After laser irradiation, the samples were centrifuged down to separate the released DNA/ RNA strands in the supernatant from the gold nanoparticle pellet.

Cell Culture

Both HeLa cells as well as HeLa-GFP cells (Huang et al. 2016), were cultured in Dulbecco's modified Eagle medium (DMEM) supplemented with 10% fetal bovine serum (FBS) at 37 °C in 5% CO₂ atmosphere. The cells were passaged every 3-4 days by cell dissociation with trypsin.

Internalization experiments with flow cytometry

HeLa cells were harvested by the incubation with non-enzymatic cell dissociation buffer (CDB-Thermo Scientific) at 37 °C in 5% CO₂ atmosphere for 10 – 15 min. Cells were centrifuged 2x at 500 x g for 5 min and resuspended in DMEM medium (supplemented with 10% FBS) to a final concentration of 5 x 10⁵ cells per mL. 7.6 x 10⁻¹² M of both biotin-TAT and Cy3 (ratio 1:2) functionalized gold nanoparticles were added to 200 µL of cell suspension and incubated in a 1.5 mL Eppendorf tubes at RT for 2 hrs on a rotator. Free gold nanoparticles were washed out by centrifugation 2x at 500 x g for 5 min. The cells were resuspended in 500 x 10⁻⁶ L PBS and stored on ice until injection into a BD Accuri C6 flow cytometer (BD Biosciences) with a flow rate of 14 µL/min. A gate area was selected from the forward versus side scatter plots and 10,000 events were collected for each sample.

siRNA GFP-knockdown

Microfluidic Excitation (Ensemble treatment)

A 64 x 10⁻³ m capillary tube with a 20 x 10⁻⁶ L capacity was fixed unto a large glass microscope slide with epoxy. Capillary tubing was then assembled unto the ends of the tube and sealed using commercial nail polish. The samples were loaded slowly into upstream tubing of the device using a 50 µL glass syringe (Hamilton). To flow samples through the microcapillary, the samples were pushed with a 1 mL plastic syringe. The cells were collected in an Eppendorf tube. Samples were irradiated with the same laser used in the cell free release studies.

HeLa-GFP cells were harvested with CDB and centrifuged twice at 500 x g for 5 min and resuspended in DMEM medium (supplemented with 10% FBS) to a final concentration of 1 x 10⁶ cells per mL. For each particle type, two concentrations of particles were tested: 7.6 x

10^{-12} M (2X) and 3.8×10^{-12} M (1X) of siRNA functionalized gold nanoparticles were added to 200 μ L of cell suspension and incubated at RT for 2 hrs on a rotator. Free gold nanoparticles were washed out by centrifugation twice at 500 x g for 5 min. The cells were resuspended in 50 x 10^{-6} L Hank's Balanced Salt Solution (HBSS) supplemented with 10% FBS and afterwards irradiated with 900 x 10^{-3} W for 30 seconds through the syringe and tubing system. After irradiation, the cells were transferred to a 6-well plate with DMEM supplemented with 10% FBS and incubated at 37 °C in 5% CO₂ atmosphere. After 72 hrs the cells are dissociated with trypsin, washed twice at 500 x g for 5 min. The cells were resuspended in 500 x 10^{-6} L PBS and stored on ice until injection into a BD Accuri C6 flow cytometer with a flow rate of 14 x 10^{-6} L/min. A gate area selection was determined from the forward versus side scatter plots and 10,000 events were collected for each sample. As a positive control of the GFP-knockdown in HeLa-GFP cells, a reverse transfection StealthTM (Invitrogen) siRNA was carried out. First, 6 pmol siRNA duplex were diluted in 100 x 10^{-6} L Opti-MEM[®] I Medium without serum in the well of a 24-well tissue well plate and mixed gently. 1 x 10^{-6} L of Lipofectamine[®] RNAiMAX was added to the diluted siRNA molecules, mixed gently, and incubated for 10-20 min at room temperature. The HeLa-GFP cells were diluted to 50,000 cells in 500 x 10^{-6} L in DMEM supplemented with 10% FBS and added to the siRNA duplex – Lipofectamine[®] RNAiMAX complexes. This leads to a final volume of 600 x 10^{-6} L and a final RNA concentration of 10 x 10^{-9} M. The samples were mixed gently and incubated for 72 hrs at 37 °C in 5% CO₂. After incubation the cells were dissociated, washed and measured at the flow cytometer as described before.

NIR Excitation Confocal Microscopy

24 hrs before the particles are added to the cells, HeLa-GFP cells were split onto Ibidi gridded petri dishes with 1 x 10⁵ cells for each sample and incubated at 37 °C in 5% CO₂.

The next day, cells outside the grid area of the petri dishes were scraped away and the cells were washed 2x with DPBS. Then, the HeLa-GFP cells were incubated with 7.6×10^{-12} M of siRNA functionalized gold nanoparticles in 200×10^{-6} L DMEM with 10% FBS supplemented at 37 °C in 5% CO₂ atmosphere for 2 hrs. After washing twice with PBS the cells were stored in 1×10^{-3} L of Hank's buffered saline solution (HBSS) supplemented with 10% FBS for the use at the 2-Photon microscope. To activate the siRNA release, the HeLa-GFP cells on gridded petri dishes were irradiated with a pulsed NIR laser, generated by a two-photon microscope (Olympus Fluoview 1000 MPE). The two-photon microscope was equipped with a 25x water immersion objective (numerical aperture 1.05), a mode-locked titanium-sapphire femtosecond (fs) tunable (690-1020 nm) pulsed laser (100 fs pulse duration, 80 MHz repetition rate, MaiTai HP, Newport-Spectra physics), 473/559/633 nm laser diodes, a transmitted light detection system, and a scan head controlled by Fluoview software. The MaiTai laser was tuned to 800 nm at 8% of the maximum power (≈ 2 mW) and exposed to z-stacks (1.4 μ M interval) of intended cells through line-by-line scanning (125 kHz) of selected pixels in each z-stack (512 x 512 pixels, 0.331 μ m per pixel) at 2 μ s per pixel. The sample was imaged in a single-photon confocal mode with the blue (for GFP) and green (for Quasar 570 on the siRNA) laser diodes at a scan speed of 80 kHz before and after the exposure to the MaiTai fs laser to compare the fluorescence signal difference caused by the laser treatment. Cells treated with laser and without laser were incubated for 72 h at 37 °C in 5% CO₂ environment and then relocated at the microscope according to the grid information on the bottom of the petri dish, and imaged in the single-photon confocal mode for GFP or Quasar 570 fluorescence, as well as bright-field images from the transmitted channel.

F. References

- (1) Esteller, M. Non-Coding RNAs in Human Disease. *Nat. Rev. Genet.* 2011, 12 (12), 861–874. <https://doi.org/10.1038/nrg3074>.
- (2) Forbes, D. C.; Peppas, N. A. Oral Delivery of Small RNA and DNA. *J. Controlled Release* 2012, 162 (2), 438–445. <https://doi.org/10.1016/j.jconrel.2012.06.037>.
- (3) Hemphill, J.; Borchardt, E. K.; Brown, K.; Asokan, A.; Deiters, A. Optical Control of CRISPR/Cas9 Gene Editing. *J. Am. Chem. Soc.* 2015, 137 (17), 5642–5645. <https://doi.org/10.1021/ja512664v>.
- (4) Riboldi, G.; Zanetta, C.; Ranieri, M.; Nizzardo, M.; Simone, C.; Magri, F.; Bresolin, N.; Comi, G. P.; Corti, S. Antisense Oligonucleotide Therapy for the Treatment of C9ORF72 ALS/FTD Diseases. *Mol. Neurobiol.* 2014, 50 (3), 721–732. <https://doi.org/10.1007/s12035-014-8724-7>.
- (5) Draz, M. S.; Fang, B. A.; Zhang, P.; Hu, Z.; Gu, S.; Weng, K. C.; Gray, J. W.; Chen, F. F. Nanoparticle-Mediated Systemic Delivery of SiRNA for Treatment of Cancers and Viral Infections. *Theranostics* 2014, 4 (9), 872–892. <https://doi.org/10.7150/thno.9404>.
- (6) Fire, A.; Xu, S.; Montgomery, M. K.; Kostas, S. A.; Driver, S. E.; Mello, C. C. Potent and Specific Genetic Interference by Double-Stranded RNA in *Caenorhabditis Elegans*. *Nature* 1998, 391 (6669), 806–811. <https://doi.org/10.1038/35888>.
- (7) Bumcrot, D.; Manoharan, M.; Koteliansky, V.; Sah, D. W. Y. RNAi Therapeutics: A Potential New Class of Pharmaceutical Drugs. *Nat. Chem. Biol.* 2006, 2 (12), 711–719. <https://doi.org/10.1038/nchembio839>.
- (8) Li, J.; Xue, S.; Mao, Z.-W. Nanoparticle Delivery Systems for SiRNA-Based Therapeutics. *J. Mater. Chem. B* 2016, 4 (41), 6620–6639. <https://doi.org/10.1039/C6TB01462C>.

- (9) Whitehead, K. A.; Langer, R.; Anderson, D. G. Knocking down Barriers: Advances in SiRNA Delivery. *Nat. Rev. Drug Discov.* 2009, 8 (2), 129–138. <https://doi.org/10.1038/nrd2742>.
- (10) Huang, X.; Lai, Y.; Braun, G. B.; Reich, N. O. Modularized Gold Nanocarriers for TAT-Mediated Delivery of SiRNA. *Small* 2017, 13 (8), 1602473. <https://doi.org/10.1002/sml.201602473>.
- (11) Huang, X.; Hu, Q.; Lai, Y.; Morales, D. P.; Clegg, D. O.; Reich, N. O. Light-Patterned RNA Interference of 3D-Cultured Human Embryonic Stem Cells. *Adv. Mater.* 2016, 28 (48), 10732–10737. <https://doi.org/10.1002/adma.201603318>.
- (12) Morales, D. P.; Braun, G. B.; Pallaoro, A.; Chen, R.; Huang, X.; Zasadzinski, J. A.; Reich, N. O. Targeted Intracellular Delivery of Proteins with Spatial and Temporal Control. *Mol. Pharm.* 2015, 12 (2), 600–609. <https://doi.org/10.1021/mp500675p>.
- (13) Morales, D. P.; Wonderly, W. R.; Huang, X.; McAdams, M.; Chron, A. B.; Reich, N. O. Affinity-Based Assembly of Peptides on Plasmonic Nanoparticles Delivered Intracellularly with Light Activated Control. *Bioconjug. Chem.* 2017, 28 (7), 1816–1820. <https://doi.org/10.1021/acs.bioconjchem.7b00276>.
- (14) Morales, D. P.; Morgan, E. N.; McAdams, M.; Chron, A. B.; Shin, J. E.; Zasadzinski, J. A.; Reich, N. O. Light-Triggered Genome Editing: Cre Recombinase Mediated Gene Editing with Near-Infrared Light. *Small* 2018, 14 (30), 1800543. <https://doi.org/10.1002/sml.201800543>.
- (15) Link, S.; El-Sayed, M. A. Spectral Properties and Relaxation Dynamics of Surface Plasmon Electronic Oscillations in Gold and Silver Nanodots and Nanorods. *J. Phys. Chem. B* 1999, 103 (40), 8410–8426. <https://doi.org/10.1021/jp9917648>.

(16) Link, S.; El-Sayed, M. A. Shape and Size Dependence of Radiative, Non-Radiative and Photothermal Properties of Gold Nanocrystals. In *International Reviews in Physical Chemistry*; 3; 2000; Vol. 19, pp 409–453.

(17) Daniel, M.-C.; Astruc, D. Gold Nanoparticles: Assembly, Supramolecular Chemistry, Quantum-Size-Related Properties, and Applications toward Biology, Catalysis, and Nanotechnology. *Chem. Rev.* 2004, 104 (1), 293–346.

(18) Dreaden, E. C.; Alkilany, A. M.; Huang, X.; Murphy, C. J.; El-Sayed, M. A. The Golden Age: Gold Nanoparticles for Biomedicine. *Chem Soc Rev* 2012, 41 (7), 2740–2779. <https://doi.org/10.1039/C1CS15237H>.

(19) Huang, X.; Pallaoro, A.; Braun, G. B.; Morales, D. P.; Ogunyankin, M. O.; Zasadzinski, J.; Reich, N. O. Modular Plasmonic Nanocarriers for Efficient and Targeted Delivery of Cancer-Therapeutic siRNA. *Nano Lett.* 2014, 14 (4), 2046–2051. <https://doi.org/10.1021/nl500214e>.

(20) Jain, P. K.; Qian, W.; El-Sayed, M. A. Ultrafast Cooling of Photoexcited Electrons in Gold Nanoparticle–Thiolated DNA Conjugates Involves the Dissociation of the Gold–Thiol Bond. *J. Am. Chem. Soc.* 2006, 128 (7), 2426–2433. <https://doi.org/10.1021/ja056769z>.

(21) Lukianova-Hleb, E. Y.; Belyanin, A.; Kashinath, S.; Wu, X.; Lapotko, D. O. Plasmonic Nanobubble-Enhanced Endosomal Escape Processes for Selective and Guided Intracellular Delivery of Chemotherapy to Drug-Resistant Cancer Cells. *Biomaterials* 2012, 33 (6), 1821–1826. <https://doi.org/10.1016/j.biomaterials.2011.11.015>.

(22) Huschka, R.; Zuloaga, J.; Knight, M. W.; Brown, L. V.; Nordlander, P.; Halas, N. J. Light-Induced Release of DNA from Gold Nanoparticles: Nanoshells and Nanorods. *J. Am. Chem. Soc.* 2011, 133 (31), 12247–12255. <https://doi.org/10.1021/ja204578e>.

- (23) Christie, C.; Madsen, S. J.; Peng, Q.; Hirschberg, H. Photothermal Therapy Employing Gold Nanoparticle- Loaded Macrophages as Delivery Vehicles: Comparing the Efficiency of Nanoshells Versus Nanorods. *J. Environ. Pathol. Toxicol. Oncol.* 2017, 36 (3), 229–235. <https://doi.org/10.1615/JEnvironPatholToxicolOncol.2017021545>.
- (24) Yue, J.; Feliciano, T. J.; Li, W.; Lee, A.; Odom, T. W. Gold Nanoparticle Size and Shape Effects on Cellular Uptake and Intracellular Distribution of SiRNA Nanoconstructs. *Bioconjug. Chem.* 2017, 28 (6), 1791–1800. <https://doi.org/10.1021/acs.bioconjchem.7b00252>.
- (25) Jiang, X.; Qu, W.; Pan, D.; Ren, Y.; Williford, J.-M.; Cui, H.; Luijten, E.; Mao, H.-Q. Plasmid-Templated Shape Control of Condensed DNA-Block Copolymer Nanoparticles. *Adv. Mater.* 2013, 25 (2), 227–232. <https://doi.org/10.1002/adma.201202932>.
- (26) Williford, J.-M.; Ren, Y.; Huang, K.; Pan, D.; Mao, H.-Q. Shape Transformation Following Reduction-Sensitive PEG Cleavage of Polymer/DNA Nanoparticles. *J Mater Chem B* 2014, 2 (46), 8106–8109. <https://doi.org/10.1039/C4TB00967C>.
- (27) Sun, Y.; Xia, Y. Mechanistic Study on the Replacement Reaction between Silver Nanostructures and Chloroauric Acid in Aqueous Medium. *J. Am. Chem. Soc.* 2004, 126 (12), 3892–3901. <https://doi.org/10.1021/ja039734c>.
- (28) Hong, Y.; Huh, Y.-M.; Yoon, D. S.; Yang, J. Nanobiosensors Based on Localized Surface Plasmon Resonance for Biomarker Detection. *J. Nanomater.* 2012, 2012, 1–13. <https://doi.org/10.1155/2012/759830>.
- (29) Zhang, X.; Chen, Y. L.; Liu, R.-S.; Tsai, D. P. Plasmonic Photocatalysis. *Rep. Prog. Phys.* 2013, 76 (4), 046401. <https://doi.org/10.1088/0034-4885/76/4/046401>.

(30) Zhang, X.; Servos, M. R.; Liu, J. Instantaneous and Quantitative Functionalization of Gold Nanoparticles with Thiolated DNA Using a PH-Assisted and Surfactant-Free Route. *J. Am. Chem. Soc.* 2012, 134 (17), 7266–7269. <https://doi.org/10.1021/ja3014055>.

(31) Braun, G. B.; Pallaoro, A.; Wu, G.; Missirlis, D.; Zasadzinski, J. A.; Tirrell, M.; Reich, N. O. Laser-Activated Gene Silencing via Gold Nanoshell–siRNA Conjugates. *ACS Nano* 2009, 3 (7), 2007–2015. <https://doi.org/10.1021/nn900469q>.

(32) Whitney, M.; Savariar, E. N.; Friedman, B.; Levin, R. A.; Crisp, J. L.; Glasgow, H. L.; Lefkowitz, R.; Adams, S. R.; Steinbach, P.; Nashi, N.; et al. Ratiometric Activatable Cell-Penetrating Peptides Provide Rapid In Vivo Readout of Thrombin Activation. *Angew. Chem. Int. Ed.* 2013, 52 (1), 325–330. <https://doi.org/10.1002/anie.201205721>.

(33) Xue, C.; Xue, Y.; Dai, L.; Urbas, A.; Li, Q. Size- and Shape-Dependent Fluorescence Quenching of Gold Nanoparticles on Perylene Dye. *Adv. Opt. Mater.* 2013, 1 (8), 581–587. <https://doi.org/10.1002/adom.201300175>.

(34) Prevo, B., Esakoff, S., Mikhailovsky, A., and Zasadzinski, J. (2008) Scalable Routes to Gold Nanoshells with Tunable Sizes and Response to Near-Infrared Pulsed Laser Irradiation. *Small* 4, 1183–1195.

(35) Skrabalak, S. E., Chen, J., Au, L., Lu, X., Li, X., and Xia, Y. (2007) Gold Nanocages for Biomedical Applications. *Adv. Mater.* 19, 3177–3184.

(36) Shi, D., Song, C., Jiang, Q., Wang, Z.-G., and Ding, B. (2013) A Facile and Efficient Method to Modify Gold Nanorods with Thiolated DNA at a Low PH Value. *Chem. Commun.* 49, 2533.

VI. DETAILED EXPERIMENTAL PROCEDURES

A. CONFOCAL AND TWO-PHOTON MICROSCOPY

AI. INTRODUCTION

One of the most crucial barriers in delivery of biomolecules using nanoparticles is endosome entrapment. Two-photon microscope experiments not only allow for visualization of endocytosed fluorescent cargo, it also allows for visualization of cargo release post NIR excitation. The Olympus fluoview 1000MPE 2-photon is equipped with a chamber that allows for 5% CO₂ and 37°C for live cell imaging applications. The two-photon microscope is equipped with a 25x water immersion objective lens (numerical aperture 1.05), a mode-locked titanium-sapphire femtosecond tunable (690-1020 nm) pulsed laser (100 fs pulse duration, 80 MHz repetition rate, MaiTai HP with a scan head controlled by the Fluoview software. This microscope can image a variety of fluorescent dyes using the three laser diodes (473/599/633 nm). The z-stack capability of the microscope allows for scanning of your sample from one determined set point to the next. Note that while the 25x objective lens allows for visualization of the fluorescently labeled cargo, two color systems can be problematic for co-localization experiments. There is an offset in Z-stack caused by the lower objective lens and therefore cannot be used for co-localization. See Figure VI-1 where a particle coated in two fluorescent dyes was imaged to determine location of the particle through z-stack scanning. The two dyes (Cy5 and GFP), loaded onto the same fluorescent bead should show up at the same location however, they are on separate focal planes. Similarly, HeLa cells expressing MITO-CoilE-GFP and CoilRCy5 are shown on separate focal planes. This is something to keep in mind when using the two-photon microscope for

imaging. The co-localization experiments shown previously in this thesis use the Leica SP8 confocal microscope with an inverted 100x objective lens. The 100x objective lens allows for the visualization of 2 or more dyes on the same focal plane.

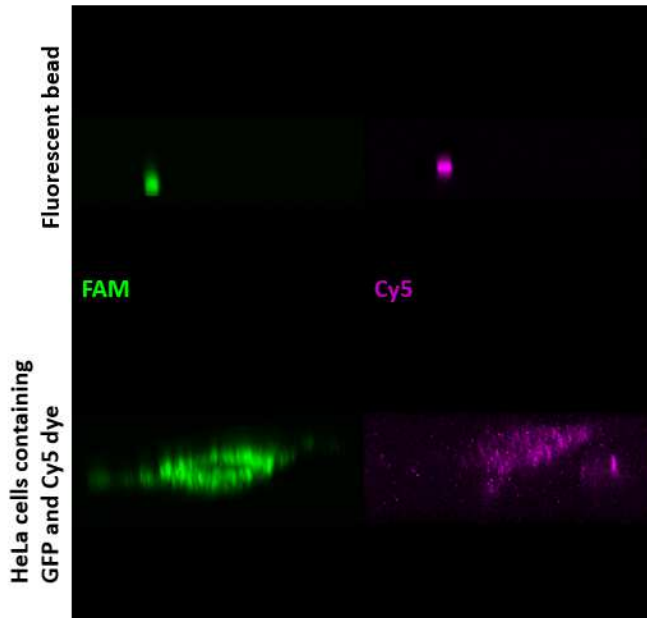


Figure VI-1. Cy5 and GFP Z-stack show optical focal planes separate depending on dye used. The fluorescent bead imaged had both FAM and Cy5 attached to the surface of the particle. In the bottom image, a single HeLa cell expressing MITO-CoilE-GFP with CoilR-Cy5 shows separate layers for the two dyes.

AII. INTERNALIZATION EXPERIMENTS

For small scale internalization experiments, the 8 well chambered glass slide will allow for fixation and visualization on the two photon microscope as well as the dark field microscope (for determination of gold particle internalization via scattered light). For these experiments, cells were plated 24 hours prior to visualization at 40,000 cells per well in an 8 well chambered class slide (Millipore) in 200 μ L of DMEM + 10% FBS. If the cells were needed 2 days after plating, the cells were plated at 30,000 cells per well. Particles (25 μ L of 1 o.d.)

were added to 200 μ L of DMEM +10% FBS and sonicated prior to addition to the wells and placed at 37°C in 5% CO₂ for 2 hours. For darkfield and internalization experiments, cell fixation was used to keep the cells for long-term storage and imaging. The remainder of the steps were conducted in the lab's fume hood. The cells were washed 2x with PBS, the chamber was removed, and 200 μ L of 4% formaldehyde was added to each well (formaldehyde ampules are a 16% solution and were diluted with water). The cells incubated at room temperature in the fume hood for 10-20 minutes with the formaldehyde, washed one more time with PBS and 1 drop of fluorogel (stored at 4 °C) was added to each well. A slide cover was added to the slide and sealed with clear nail polish.

For the darkfield microscope (Olympus BX51), the original microscope condenser was removed by lowering and loosening the screw on the right side. The dark field condenser was put in the same place and one drop of oil was added to the top. Once the slide is loaded onto the microscope the condenser is brought up to meet the slide from underneath. Once touching, the microscope should be set to "brightfield" mode and all ND filters are off. The condenser should be open all of the way and the ring is centered through the objective. Both fluorescence and darkfield can be used to track internalization using this microscope however it is necessary to check the filter cubes for each microscope to make sure the fluorescent tag being used can be visualized.

AIII. RELEASE EXPERIMENTS

For release experiments, the two-photon microscope is required for the NIR excitation source. Since the two photon is 25x water immersion you can either do the experiment as previously described however instead of fixation of the cells, simply place PBS and seal. The experiment done in this way is short term and cannot be used for more than 1-2 hours. For long term analysis a gridded Ibidi μ -Dish was used to track where the cells were located before and after irradiation. Cells were plated on the Ibidi dish at 100,000 cells 24 hours prior to laser excitation only in the center well of the dish (400 μ L DMEM with 10% FBS). 2 hours prior to laser excitation, 50 μ L of 1 o.d. particles were added to 350 μ L of DMEM +10% FBS, sonicated and added to the center of the dish with the cells for 2 hours at 37°C in 5% CO₂. After 2 hours the samples were washed with PBS three times to remove excess particles and the bottom of the whole Ibidi dish is covered in 2 mL of DMEM, high glucose, HEPES, no phenol red supplemented with 10% FBS and 1% penstrep (this is to prevent contamination during the imaging process). Media containing HEPES is important for these long-term imaging experiments because it balances the pH of the media during transport and irradiation. For two photon experiments (using the Olympus Fluoview 1000MPE) the cells were kept in a humidified chamber at 37°C and 5% CO₂ and focused using the 25x water immersion objective lens (dipped into the center of the dish). The fluoview software was used to turn on the NIR laser (this could be set from 690-1020 nm at a range of % power, usually 10% (~200 mW) to avoid cell death from higher powers). The correct dyes were selected (in single photon mode) and the dial was set to “1” on the microscope. Once the cells were located using the brightfield objective through the eye piece, the fluorescent cargo was found using the XY scan function in fluoview (512x512 pixels). The voltage next to each dye can be increased to give more signal however checking the cell only control for auto

fluorescence at this time was important (FAM dyes especially). Samples were imaged in single-photon confocal mode at 12 μs per pixel prior to, and after laser excitation. After the initial picture, the z stack was set to “0 μm ” to confirm the center point of irradiation (where the cells and fluorescent dye are in the best focus), set back to 1x and 2 μs per pixel for irradiation. The microscope was then switched to two-photon mode and the dial was set to “2” on the microscope. Z- stack scans can vary but typically the interval steps were set to 0.69 μm per slice ranging about 20 μm in thickness. It is important to make sure that all of the sample is irradiated. To ensure that the entire cell is irradiated while scanning, the image should show black, then dots where the particles scatter the light, back to black again. If this is not the case then the top and bottom z start and stop values should be altered. The microscope is then switched back to single photon mode for visualization of release. Note, all samples are kept in the incubator during imaging to ensure they remain at at 37°C and 5% CO₂. After irradiation they were returned to the cell culture incubator for later visualization.

AIV. VISUALIZATION USING THE LEICA SP8

The Leica SP8 confocal microscope is used for imaging of multiple dyes using the 63x oil immersion objective lens. The live cell imaging capability is due to the incubator stage that can be set to 5% CO₂ and 37°C. There are a variety of excitation sources, a 405 nm laser, an argon laser with several standard laser lines, and the white-light laser (WLL) that can supply up to 8 simultaneous laser lines (from 470- 670 nm). Within the WLL setting, there is a “dye assistant” which can give you excitation and emission suggestions for your selected dye. Note that these can be tuned and adjusted to give the most ideal signal to noise ratio. For sample with low signal, the pinhole size can be increased to allow for more excitation light, however note that this may reduce the overall resolution capability of the image. Super- resolution

radial fluctuations (SRRF) can be used to extract sub-diffraction information from a quick, short burst of 100 images taken in time-lapse on a confocal fluorescent microscope. The SRRF analysis allows for long term SRM time lapse acquisition using lower intensity illumination to prevent photo toxicity during the live cell microscopy analysis. For this analysis at least 100 images need to be taken using the xyt function for a total of 10 minutes for one final SRRF image. SRRF analysis was conducted using the NanoJ-SRRF plug-in for (Fiji Is Just) Image J with the following settings : ring radius, 2.94; radially magnification, 8; axes in ring, 5; frames per time point, 100. These settings can be altered to increase signal to noise ratio. All images were later false-colored using standard lookup tables.

B. CRIPSR CAS9 DELIVERY

BI. INTRODUCTION

As CRISPR/Cas9 systems continue to gain therapeutic potential for gene editing, a need for controlled and highly regulated methodology is increasingly important^{1,2}. This led to the development of light activation methods for controlled CRISPR/Cas9 delivery using light responsive domains that depend on complex modifications of the Cas9 enzyme³. We aimed to delivery CRISPR Cas9 in a variety of ways using hollow gold nanoshells activated by NIR light. Not only would this allow for targeted control over which cells were editing, it also allows for simplification in the modification of the Cas9 enzyme (just a 6xHis tag, which is used in the purification process). We developed three different platforms for the delivery of the CRISPR/Cas9 system in collaboration with Dr. Piyush K. Jain.

Jain et.al developed a method to photo cage the activity of the guide RNA called “CRISPR-plus” (CRIPSR-precise light-mediated unveiling of sgRNAs). In this work they designed “protectors” that were complementary ssDNA oligonucleotides of varying lengths and positions on the target region of the guide RNA, and had photocleavable groups throughout them⁴. The good protectors were designed with a high melting temperature (T_m) preventing the sgRNA from binding to the target DNA sequence until the protector is photolyzed, releasing it from the sgRNA allowing for it to bind to the target DNA sequence. The photolysis creates short fragments of the cleaved protector, reducing the melting temperature and allowing for CRISPR/Cas9 activation in cells already expressing Cas9. One of the major drawbacks of this technology is the lack of delivery of Cas9 as well as the use of potentially damaging UV irradiation for photolysis.

We plan to build off this technology to allow for NIR light activated delivery of both Cas9 enzyme and sgRNA. There are 3 constructs we designed for delivery of CRISPR/Cas9 (Figure VI-2). The first involves the delivery of sgRNA to HeLa-Cas9 cell line which includes a thiolated protector group (with no photocleavable groups) that would hybridize to the sgRNA for light triggered activation of the CRISPR/Cas9 system. The second, delivery of Cas9/sgRNA with thiol linker, works similarly to I however, the tight interaction of the ribonucleoprotein (RNP) complex is used for delivery of both Cas9 as well as the sgRNA. The final delivery method involves the delivery of Cas9/sgRNA using the His-Tagged Cas9 complexed to sgRNA. This method differs from II as it involves attachment of the 6xHis tag on Cas9 and association of the sgRNA with the Cas9 for delivery of the system.

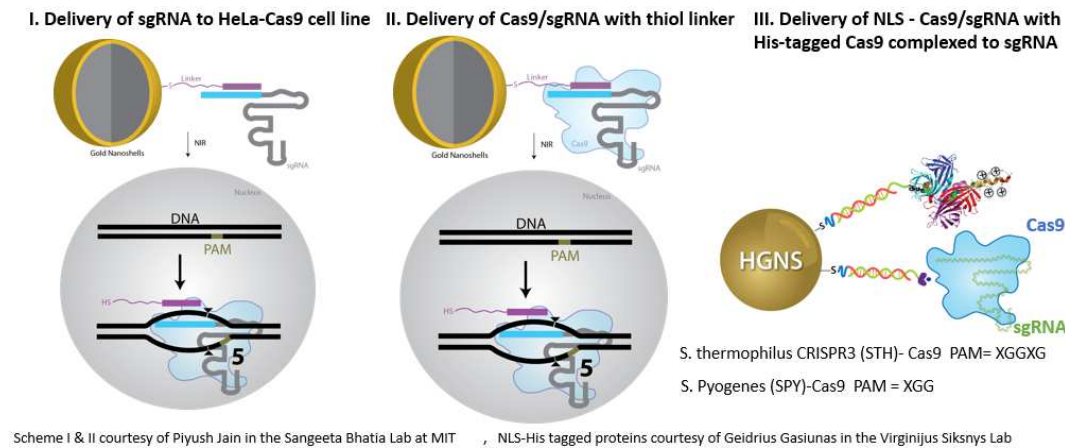


Figure VI-2. Three different particle constructs for Cas9/sgRNA delivery. I. Delivery of sgRNA to HeLa-Cas9 cell line involves a thiolated protector group that would hybridize to the sgRNA and later would be delivered into cells expressing Cas9 for light triggered activation of the CRISPR/Cas9 system. II. Delivery of Cas9/sgRNA with thiol linker works similarly to I however the ribonucleoprotein (RNP) complex is used for delivery of both Cas9 as well as the sgRNA. III. Delivery of NLS-Cas9/sgRNA with His-Tagged Cas9 complexed to sgRNA involves attachment of the 6xHis tag on Cas9 for delivery and association of the sgRNA with the Cas9 for delivery of the system.

The protectors for use in constructs I and II were selected using the diagrams provided by Piyush in Figure IV-3 which demonstrate the ability of certain protectors to prevent sgRNA from binding to DNA target. We chose to use “poor protectors” (indicated in blue) to allow for loading onto our HGN which in principle would still allow for the sgRNA to bind to the DNA target once delivered. A mix of complementary poor protectors (5 DNA and 6 RNA in Figure IV-3c) as well as crRNA and tracrRNA (1-4) were ordered to test for loading onto HGNs.

crRNA and tracrRNA are naturally occurring RNAs in the bacteria for CRISPR/Cas9 that were fused together to create a sgRNA (single chimeric guide RNA). The sgRNA is more commonly used than the crRNA/tracrRNA since the single RNA can be transcribed more easily. However, for our case crRNA could also work, is easily modified (42 nt).

Effect of length and position of protectors

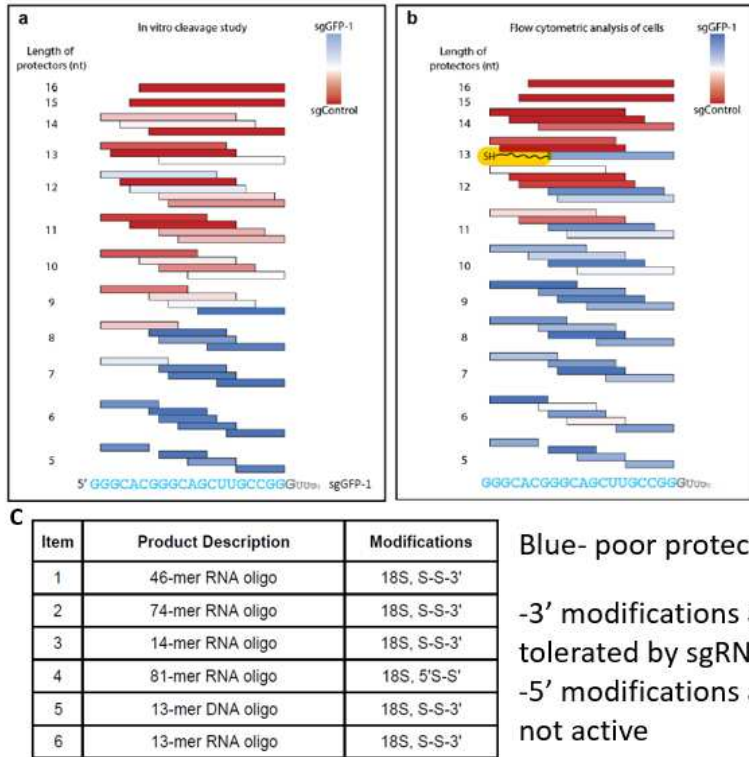


Figure IV-3. Modified figure from Jain et. al. A. Effect of length and position of protectors using the in vitro cleavage assay with Cas9 and target DNA strand described in Jain et. al. B. Effect of length and position of protectors using flow cytometry analysis of GFP fluorescence gene knockdown. The protectors highlighted in blue indicate “poor protectors” that allow for gene knockdown when hybridized to sgRNA. Red protectors do not allow for gene knockdown and are comparable to the control sgRNA that does not target the DNA template. C. a list of ordered thiolated oligos for testing loading onto the HGNs for delivery.

BII. INVITRO CLEAVAGE ASSAY

The in vitro cleavage assay is used to determine the activity of the CRISPR/Cas9 system in vitro through the incubation of Cas9, sgRNA and template DNA for cleavage. Briefly, 100 ng of DNA template, 60 ng of sgRNA, 1 μ g of BSA and 500 ng of Cas9 were incubated with 10 μ L of 1x Cas9 buffer (NEB) in RNase free water for 1 hours at 37°C. The reaction was then quenched with the addition of SDS containing loading dye (NEB) and the fragments were loaded onto a 1.5% agarose gel for 1 hour at 100 V and stained with Sybr Gold. The

uncleaved DNA would remain at 702 bp whereas the cleaved samples would have bands at 702 bp, 563 bp and 139 bp 4. This assay can be used to test the activity of the protein once released from the HGN, activity of the loaded cargo etc.

BIII. GFP KNOCKOUT STUDIES

GFP fluorescence can be used for analysis of successful delivery of the CRIPSR/Cas9 system. In our cell culture stocks we have a HEK-GFP cell line that already expresses Cas9. This cell line can be used to test successful delivery of sgRNA using our HGNs via flow cytometry post laser irradiation. A crucial control to have is delivery of the sgRNA using RNAi MAX, a common transfection reagent for siRNA delivery. We also have HeLa-GFP which could be used to test GFP knockout when Cas9 and sgRNA are delivered using the HGNs. Note- this has not been tested yet so a transfection control with sgRNA and Cas9 should be tested here.

BIV. INTERNALIZATION AND RELEASE STUDIES WITH CAS9-CY3

We have a powdered, Cy3 labeled, His tagged, Cas9 that can be used to study the load and release of Cas9 onto the HGN. Previously it was shown to have significant release in test tube release experiments however did not see release in two-photon experiments. This should be further tested since the results were not conclusive nor was the matter fully investigated.

BV. REFERENCES

(1) Jinek, M.; Chylinski, K.; Fonfara, I.; Hauer, M.; Doudna, J. A.; Charpentier, E. A Programmable Dual-RNA-Guided DNA Endonuclease in Adaptive Bacterial Immunity. *Science* 2012, 337 (6096), 816–821. <https://doi.org/10.1126/science.1225829>.

- (2) Doudna, J. A.; Charpentier, E. The New Frontier of Genome Engineering with CRISPR-Cas9. *Science* 2014, 346 (6213), 1258096–1258096.
<https://doi.org/10.1126/science.1258096>.
- (3) Konermann, S.; Brigham, M. D.; Trevino, A. E.; Joung, J.; Abudayyeh, O. O.; Barcena, C.; Hsu, P. D.; Habib, N.; Gootenberg, J. S.; Nishimasu, H.; et al. Genome-Scale Transcriptional Activation by an Engineered CRISPR-Cas9 Complex. *Nature* 2015, 517 (7536), 583–588. <https://doi.org/10.1038/nature14136>.
- (4) Jain, P. K.; Ramanan, V.; Schepers, A. G.; Dalvie, N. S.; Panda, A.; Fleming, H. E.; Bhatia, S. N. Development of Light-Activated CRISPR Using Guide RNAs with Photocleavable Protectors. *Angew. Chem. Int. Ed.* 2016, 55 (40), 12440–12444.
<https://doi.org/10.1002/anie.201606123>.